Review Paper

Ti_3C_2 MXene-Polymer Nanocomposites and Their Applications

Hossein Riazi[1], Srinivasa Kartik Nemani[2], Michael C. Grady[3], Babak Anasori[2], and Masoud Soroush[1*]

[1]Department of Chemical and Biological Engineering, Drexel University, Philadelphia, PA 19104, USA

[2] Purdue School of Engineering and Technology, Indiana University-Purdue University Indianapolis, IN 46202, USA

[3] Global Innovation Center, Axalta Coating System, Navy Yard, Philadelphia, PA 19112, USA

February 7, 2021

SECOND REVISED REVISION

Submitted for Publication in *Journal of Materials Chemistry A*

*Corresponding author: Soroushm@drexel.edu

Graphical Abstract

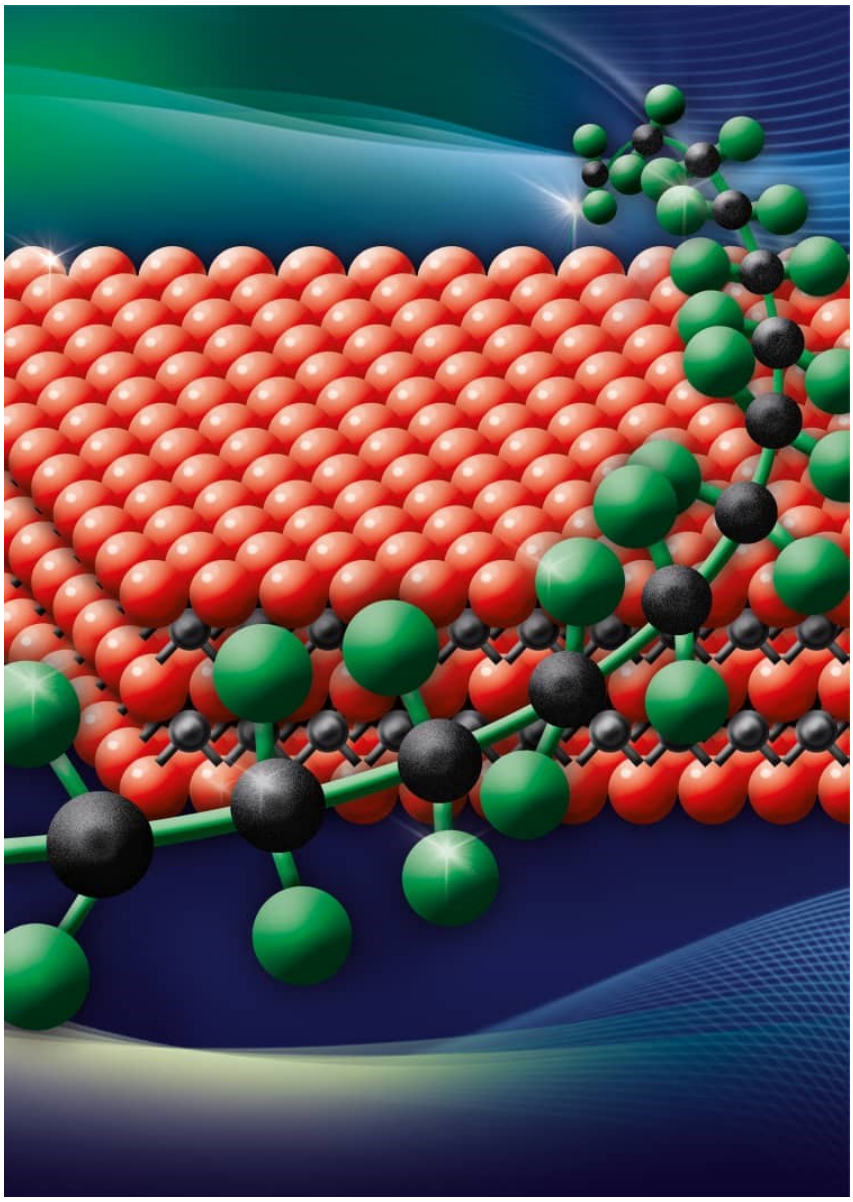

Favorable interactions between polymer chains and Ti_3C MXene flakes are essential to develop state-of-the-art MXene/polymer nanocomposite devices

Abstract

MXene/polymer nanocomposites simultaneously benefit from the attractive properties of MXenes and the flexibility and facile processability of polymers. These composites have shown superior properties such as high light-to-heat conversion, excellent electromagnetic interference shielding, and high charge storage, compared to other nanocomposites. They have applications in chemical, materials, electrical, environmental, mechanical, and biomedical engineering as well as medicine. This property-based review on MXene/polymer nanocomposites critically describes findings and achievements in these areas and puts future research directions into perspective. It surveys novel reported applications of MXene-based polymeric nanocomposites. It also covers surface modification approaches that expand the applications of MXenes in nanocomposites.

Contents

List of Acronyms:

2D: Two dimensional
AIBI: 2,2-Azobis[2-(2-imidazolin-2-yl)propane] dihydrochloride
BMI: Bis(4-maleimidophenyl) methane
CCG: Chemically converted graphene
CNC: Cellulose nanocrystals
CNF: Cellulose nanofiber
CTAB: Cetrimonium bromide
CVD: Chemical vapor deposition
DDAB: Didodecyldimethylammonium bromide
DGEBA: Diglycidylether of bisphenol A
DFT: Density functional theory
DI: Deionized water
DMF: Dimethyl formamide
DMSO: Dimethyl sulfoxide
DTAB: Decyltrimethylammonium bromide
EDX: Energy-dispersive X-ray
EG: Ethylene glycol
EM: Electromagnetic
EMI: Electromagnetic interference
EMW: Electromagnetic wave
FA: Furfurylamine
GO: Graphene oxide
HF: Hydrofluoric acid
ITO: Indium tin oxide
KPS: Potassium persulfate
LCST: lower critical solution temperature
LLDPE: linear low-density polyethylene
MILD: Minimally intensive layer delamination
MQD: MXene quantum dot
NMP: N-methyl-2-pyrrolidone
NMR: Nuclear Magnetic Resonance
NR: Natural rubber
OTAB: Octadecyl trimethylammonium bromide
PAA: Polyacrylic acid
PAAm: Polyacrylamide
PADC: Polydiallyldimethylammonium chloride

PAN: Polyacrylonitrile
PANI: Polyaniline
PC: Propylene carbonate
PCL: Polycaprolactone
PDMS: Polydimethyl siloxane
PDT: Decentralized conjugated polymer
PEDOT:PSS: poly(3,4-ethylenedioxythiophene):poly(styrene sulfonate)
PEG: Polyethylene glycol
PEO: Polyethylene oxide
PET: Polyethylene terephthalate
PI: Polyimide
PP: Poly(3,4 ethylenedioxythiophene)-poly(styrenesulfonate)
PPy: Polypyrrole
PVA: Polyvinyl alcohol
PVDF: Polyvinylidene fluoride
PVP: Polyvinyl pyrrolidone
PU: polyurethane
PUF: polyurethane foam
SA: Sodium alginate
SEM: Scanning electron microscope
SERS: Surface enhanced Raman scattering
TPU: Thermoplastic polyurethane
UHMWPE: Ultrahigh molecular weight polyethylene
UV: Ultraviolet
UV-Vis: Ultraviolet-visible
XRD: X-ray powder diffraction

1 Introduction

MXenes are a large family of electrically-conductive, hydrophilic, layered, two-dimensional (2D) nanomaterials made from transition metal carbides, nitrides, or carbonitrides with a range of aspect ratio and few atomic layer thickness[1]. More than 30 different compositions of MXenes have been synthesized to date[1, 2]. MXenes possess high electrical conductivity (~15,000 S cm^{-1} for Ti_3C_2 films), excellent solvent compatibility and stability, hydrophilicity, electrochemical behavior, and mechanical strength. A single-layer MXene is optically transparent (absorbing 3% of visible light) and can function as an electromagnetic interference shield[3, 4]. The general formula of MXenes is $M_{n+1}X_nT_x$, where M signifies an early transition metal such as Ti, X is carbon and/or nitrogen, T is a surface functional group such as OH, F, and O, and x is the number of functional groups. The value of n is an integer between 1 to 4. The most-studied MXene is Ti_3C_2, which was first reported in 2011[5]. From a morphological point of view, MXenes are similar to GO, as the sheet thickness of a single layer of a MXene is approximately 1 nm, while their lateral dimensions can vary from a few hundred nanometers to tens of microns[6]. MXenes usually appear in the form of stacked sheets and their properties strongly depend on their morphology, and the nature of chemical species that exist between their layers. Single-layer MXenes can be easily synthesized by sonication or sever hand shaking of the multilayer counterpart [7-10]. Colloidal single-layer Ti_3C_2 MXene has excellent dispersity in water and polar aprotic solvents[11].

Polymers have exceptional properties in terms of impact and tensile strengths, fatigue, abrasion, corrosion, fracture resistance and other bulk properties. Their solubility in organic solvents enhances their compatibility with nanoparticles and facilitates their incorporation into 2D material systems. Hybrid materials simultaneously benefit from properties of both polymers and the nanoparticles; this has motivated the addition of 2D nanoparticles such as clay[12], graphene[13] and GO[14] to polymer matrixes.

Graphene and Graphene Oxide have been widely explored as filler materials to develop polymer nanocomposites,[15, 16] with impregnation methods such as solution processing, in-situ polymerization, grafting, melt blending and other covalent, non-covalent modification techniques.[17-21] MXene and Graphene usually undergo identical processing routes due to their analogous surface morphologies. However, graphene and GO-based polymer nanocomposites have exhibited active adsorption of organic solvents into the graphene layers, which influences the properties of the material adversely and impacts their strength, surface chemical activity,

electronic, and thermal properties.[22, 23] Ti_3C_2 MXene on the other hand, exhibits excellent solvent stability with tailorable adsorption properties due to the presence of surface functional groups on the basal planes. This relative advantage of MXene over their close counterparts, enables greater synergy between the filler and polymer matrix that can be harnessed to develop highly robust composite materials. MXene's ability to disperse within the polymer matrix without the addition of dispersing agents further facilitates its ability to be introduced during the initial polymer synthesis steps that can be adapted into an existing production line. Processes such as in-situ polymerization induce strong interfacial interactions between the polymer and graphene but also affect viscosity of the system which inhibits subsequent processing and material-forming.[17] MXene can be incorporated via in-situ polymerization without the relative disadvantages of viscosity stabilizing agents, active agglomeration, and solution incompatibility as discussed in later sections of this review. Another advantage of MXene is its relatively defect-free processing and synthesis via top-down approaches with high yields when compared to other 2D filler materials. Certain sensitive applications such as gas sensors and electronics require low error-prone systems which are expensive to manufacture with graphene via bulk processing routes. The synthesis of defect-free large area graphene sheets has been achieved with methods such as chemical vapor deposition. However, from an economic standpoint, they are less viable for large scale synthesis and implementation in sensitive technological fields such as electronics and energy storage.[24] The size and morphology being important, a surfactant-free stabilization is still a challenge to overcome in graphene synthesis.[25] Robust synthesis routes to manufacture high-quality monolayer, defect-free graphene sheets are yet to be achieved[26].

In terms of properties, MXene, similar to GO is shown to exhibit size dependent variations which specially impacts its dielectric properties in polymer composites.[27, 28] Similar to graphene, the ratio of permittivity to the loss factor of large flake composites is higher to that of the composites with small filler flakes. In addition, a strong correlation with the charge accumulation at the surfaces between the two-dimensional flakes and the polymer matrix under an external applied electric field is also observed in MXene-polymer composites.[28] Graphene based composites have exhibited lesser conductivities specially when they are synthesized via melt processing, blending, solution casting, and CVD techniques. One reason of the latter can be the agglomeration of fillers in the matrix.[29-31] However, the diverse chemistry of surface modifications of graphene similar to MXene, continues to be an essential bridging tool, particularly in energy

and environmental technologies, which require good interfacing with other functional components such as polymers.[31]

Considering mechanical robustness of single-layer Ti_3C_2 MXene, there are not many studies, unlike graphene and its derivatives.[32-34] However, single-layer MXene has reportedly exhibited the highest young's modulus among all solution processed two-dimensional materials[32]. The effect and imbibement of MXene's mechanical properties in hybrids are yet to be evaluated in more details to derive direct comparison with other 2D fillers. MXene as the latest member of 2D nanoparticle family is mixed with many polymers to develop state-of-the-art materials for different applications[35-37]. Recently several review papers have been published on MXene/polymer nanocomposites[35, 38]. Unlike previously published reviews papers, this review focuses more on processing aspects of MXene/polymer systems and describes potential applications of MXene/polymer nanocomposites in terms of inherent properties of MXenes. It first describes the surface chemistry of MXenes, their oxidation stability, their interlayer distance and then the synthesis methods of MXene. Next, MXene/polymer nanocomposite fabrication methods are explained. This section covers surface modification approaches to improve the affinity of MXene for polymers and delinates the development of MXene-based polymeric hydrogels, foams and aerogels. Next, the review paper describes processing methods of the nanocomposites which includes topics like solvent selection criteria and solvent exchange techniques. In addition, techniques such as solution casting, vacuum filtration, spray coating, spin casting, dip-coating, latex blending, electrostatic assembly, wet spinning, and electrospinning are discussed. MXenes can be processed along with thermoplastic polymers in high-temperature conventional processes such as compression molding, extrusion, and melt blending, which are also covered herein. Different applications of MXene/polymer nanocomposites based on inherent properties of MXene are discussed. The 2D structure of MXenes is highlighted, as it renders these nanomaterials appealing for use in anti-corrosive coatings, nanocomposites with high electromagnetic interference shielding capability, gas separation membranes, wastewater treatment membranes, air filters, smart textiles, sensors, wearable heater, and self-healing coatings.

2 Ti_3C_2 MXeneSurface Chemistry

Properties of MXenes can be tuned by modifying the surface chemistry of MXenes [39]. MXenes inherently possess hydroxyl, fluorine, chlorine and oxygen groups on their surface depending on the synthesis protocol used for the etching of their precursor MAX phase [40]. The distribution of these functional groups on single-layer MXene surface is not uniform, and the functional groups are mobile enough to migrate[41]. The concentration of the etching agent (HF) during MXene synthesis affects the population of oxygen groups as well as atomic defects in both single-layer and multilayer MXenes[42, 43]. Around 26% of all functional groups on the surface of a single-layer MXene are hydroxyl groups that are dispersed randomly on the surface[44]. At the present time, the synthesis of a MXene with uniform surface distributions of these groups is a challenge. ^{1}H and ^{19}F NMR spectroscopy results have shown that the population of hydroxyl groups is much lower than those of oxygen and fluorine ones[45, 46]. However, it has been reported that the reaction of a single-layer MXene with an alkali changes the fluorine to hydroxyl groups[47]. Also, it has been verified that thermal annealing of a pristine single-layer MXene removes fluorine and hydroxyl groups from the surface of the MXene[48]. Oxygen-terminated MXenes are more stable than hydroxyl-terminated counterparts which eventually transform into oxygen-terminated ones[49]. Moreover, MXenes with more oxygen functional groups have stronger interactions with metal ions such as Li and possess higher mechanical strength compared with those MXenes containing fluorine or hydroxyl terminations[50, 51].

Several theoretical studies revealed that fluorine prefers to occupy the most thermodynamically stable sites of Ti_3C_2. The fluorine presence improves the stability of the MXene in aqueous electrolytes and simultaneously enhances its electron transport properties such as transmission/absorption[52-54]. In addition, DFT studies have shown that a higher population of fluorine facilitates the delamination of Ti_3C_2 into thinner sheets[55]. For single-layer Ti_3C_2 to work as an electrocatalyst for hydrogen evolution reaction, however, DFT and experimental results showed that high population of fluorine groups in the basal plane deteriorates Ti_3C_2 performance[1]. In applications where the presence of fluorine is not desirable, treating single-layer Ti_3C_2 with argon removes fluorine groups and generates hydrophilic functionalities instead[56]. When multilayer Ti_3C_2 is used for energy applications, optimizing surface functional groups facilitates the tailoring of energy band gap to enhance its performance[57]. When 2D nanoparticles such as GO

and Ti_3C_2 are used for wastewater treatment, the population of oxygen-containing groups on the surface affects water permeability, as these groups are capable of establishing transient hydrogen bonds[58]. So, to increase water permeance, it is necessary to decrease the population of such groups. On the other hand, for applications such as ethanol dehydration by MXene membranes, higher population of oxygen functional groups is favorable[59]. Removing heavy metal ions by a single-layer Ti_3C_2 film is another example where a high population of surface hydroxyl groups is favorable[60]. If single-layer Ti_3C_2 is used for air purification applications, surface functional groups of the Ti_3C_2 are important again as they can interact with air pollutants causing the adsorption of them on Ti_3C_2 surface and invariably cleaning the air molecules to deliver purified air [48]. It is imperative to control the nature and type of functional groups since their variable affinities may or may not be beneficial for the hybrid. In addition to inherently available surface functional groups (F, CL, OH, O), other functionalities can also be attached on MXene surface by electrostatic attraction forces, impregnation, reaction with silane coupling agents or grafting of polymer brushes. Surface functionalization of MXenes and its importance in the fabrication of hybrid materials will be discussed in the next sections in detail.

2.2 Oxidation Stability of Ti_3C_2

MXene colloidal dispersion in water is stable because of MXene's negative zeta potential. However, a potential impediment in the use of MXenes in an aqueous mixture is the relatively low shelf life of MXene flakes due to the oxidation of Ti layers, which leads to the formation of titanium oxide. The oxidation is a result of the interaction of the flakes with water. In the case of a non-aqueous mixture, the flakes can react with dissolved oxygen in the medium. MXene hydrolysis plays the main role in complete transformation of Ti_3C_2 MXenes into anatase (TiO_2) in aqueous media [61]. The degradation is indicated by a gradual change in the mixture color from black [colloidal solution] (Figure 1A) to light gray (3 days), off-white (14 days), and milky white (28 days) [62, 63].

The degradation of a single-layer MXene may be explained by exponential growth kinetics. Nucleation initiates from the flake edges, and the flake size plays a crucial role in the rate of degradation[11]. Smaller flakes deteriorate faster. Thus, the deterioration rate can be lowered by controlling the flake size during delamination steps or by altering the surface chemistries of the flakes. Multilayer MXenes with tailored surface moieties such as $Al(OH)^-_4$ have shown greater structural stability while exhibiting passivation against oxidizing reagents[64]. Moreover, altering surface moieties have also shown greater

stability for thinner and smaller flakes indicating the impact of lateral dimensions in-tandem to surface functional groups being vital for overall colloidal stability of MXene[64].

When the use of an aqueous medium is required, storing colloidal MXene in a hermitic Ar-sealed container, at lower temperatures (i.e., refrigeration), and in a dark environment can reduce the oxidation rate significantly[11]. Another potential route to develop MXenes with longer shelf life is by edge-capping MXene flakes with a polyanion such as a polyphosphate, polysilicate, or polyborate in a low concentration (< 0.12 M). Since MXene oxidation starts from the flake edges, edge capping prevents oxide nucleation and growth right at the source, thereby increasing shelf life[65]. More recently, it has been reported that the synthesis route of the MAX phase has a significant effect on Ti_3C_2 MXene aqueous colloidal stability [66]. When Ti_3AlC_2 MAX phase was synthesized by the use of excess aluminum; i.e., well above the required stoichiometric ratio (that is two moles of aluminum instead of one mole), MXene flakes showed stability up to 6 months after storage in an aqueous solution. The higher stability can be attributed to the lower concentration of defects (i.e., Ti vacancies) in the material. However, the reason for the increased stability has not been fully understood yet [66].

Water and oxygen are two main reasons of MXene degradation where this degradation is quicker in liquid media compared with solid counterparts[67]. To protect MXenes from degradation, at least one of them (oxygen or water) or preferably both of them should be eliminated[68]. De-aerating aqueous MXene colloids with an inert gas like argon is the first technique to remove oxygen. To remove water, one may think that the easiest way is the centrifugation of MXene colloid and then drying the sediment or filtration of the colloid to get MXene powder or film. However, for subsequent applications, the redispersion of these dried powders or films in a new solvent needs long sonication times. Sonication not only breaks down the flakes and impairs some good properties of MXene, but also rarely provides fully single-layer flakes again. Regarding MXene properties deterioration by sonication, it has been reported that despite similar inherent conductivity, smaller flakes compared with bigger counter parts have less chance to form a conductive network due to the higher number of resistive contact points in their network. Thus, sonication should be avoided to keep electrical conductivity of a MXene network high. Under these conditions, a solvent exchange method is favorable [62]. In such a method, water is replaced with another solvent without a need for drying a colloid and for MXene sonicating to redisperse[62]. The detrimental effects of oxygen on MXenes are much lower in an organic solvent compared with the water. Thus, a sonication-free solvent exchange method is an effective way for lowering

the degradation rate of MXenes, even more effective than de-aerating the colloid with a gas like argon or nitrogen[62].

Another motivation for solvent exchange is the immiscibility of water with many organic polymers. An aqueous colloidal MXene cannot be mixed with a polymer dissolved in a water-immiscible organic solvent for nanocomposite fabrication. To overcome this problem, exchanging the aqueous medium of MXene colloid with a solvent like DMF is a decent option. In addition, for MXene-based devices that are supposed to work in temperatures lower than 0 ℃, using an aqueous dispersion of MXene is not possible due to freezing of water in those temperatures. A good example is single-layer MXene-based hydrogels used as conductive motion sensors, working at sub-zero temperatures. By exchanging water with EG, which is a well-known anti-freezer material, the functionality of the sensors extends to temperatures as low as –40 ℃ (Figure 1B). This figure shows that a MXene-based nanocomposite containing EG keeps its twistability at temperatures as low as –40 ℃. However, the counterpart nanocomposite containing water shows brittleness at that temperature. In addition, replacing of water with EG prolongs the service life of the hydrogel sensor in room temperature as the evaporation rate of EG is much lower than that of water. The EG-containing hydrogel sensors keep their functionality for a longer time compared with water-containing counterparts (Figure 1C)[69].

Recently, Syedin et al.[62] proposed a solvent exchange procedure to replace water with other solvents without using sonication. Figure 1D shows this sonication-free solvent exchange procedure and compares it with another available solvent exchange method which needs sonication. According to Syedin's method[62], the first solvent which is usually water is separated from MXene flakes by centrifugation. The supernatant will be decanted and a new solvent, DMF for example, will be added. Vigorous handshaking or a mechanical shaker is used to re-disperse MXene sediment, deposited at the bottom of the centrifuge tube, into fresh DMF. Centrifugation is then repeated to separate the added DMF from MXene flakes and then be decanted. This cycle is repeated by adding fresh DMF, redispersion, centrifugation and supernatant decantation for three times to assure that there is no trace of initial solvent in the final solvent-exchanged colloidal MXene. As the Figure 1D-II shows, no sonication is needed in this novel solvent exchange technique.

Using the technique described in the previous paragraph, solvent-exchanged Ti_3C_2 has been dispersed in polar solvents like methanol, ethanol, isopropanol, acetone, DMF, and DMSO.

The DMF and DMSO colloids were found to be stable, similar to the original MXene in water colloid, without using any sonication. Figure 4B indicates that methanol is a poor solvent for Ti_3C_2. However, Ti_3C_2 forms a stable colloid in methanol when the sonication-free solvent exchange technique is applied. This points to the superiority of Syedin et al.'s method to other available methods[62]. Solvent-exchanged colloids prepared by Seyedin et al. showed dark color after 28 days meaning no oxidation happened in non-aqueous media. In addition, this method is capable of further delaminating MXene flakes even compared with original fresh single-layer MXene in water. In comparison with aqueous colloidal single-layer Ti_3C_2 purged by argon, shown in Figure 1D-I, dispersing solvent-exchanged Ti_3C_2 into ethanol, acetone, DMF, DMSO, and etc. downshifts the 002 peak in XRD spectrum. Moreover, this method allows for transferring MXene flakes from one medium to another sequentially. For example, one can start with a MXene colloid containing water as the dispersing medium, then exchange water with DMSO, DMSO with ethanol, ethanol with chloroform, and finally chloroform with acetone, to get a stable colloid in the last step of the solvent exchange process[62].

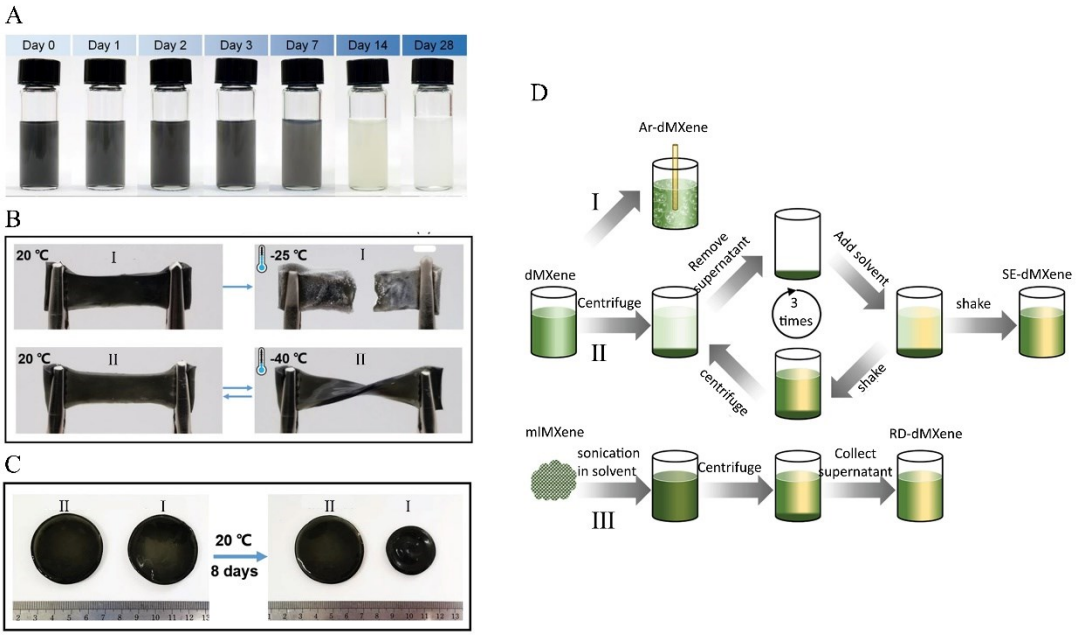

Figure 1. A) Color change of colloidal Ti_3C_2 due to degradation over time, Reproduced with permission from ref.[62] Copyright (2019), Wiley Online Library. B) Hydrogels containing (I) water and (II) ethylene glycol both show good flexibility at 20 ℃, but (I) turns into a brittle material at -40 ℃ due to freezing of the water. C) (II) Hydrogel containing ethylene glycol does not lose its solvent after 8 days of storage at 20 ℃ but (I) water-containing counterpart shrinks due to the evaporation of water, Reproduced with permission from ref.[69] Copyright (2019), Wiely Online Library. D) Three approaches to stop Ti_3C_2 degradation (I) de-aerating with an inert gas, (II) sonication-free solvent exchange process from water to an organic solvent, and (III) redispersion into an organic solvent by sonication, Reproduced with permission from ref.[62] Copyright (2019), Wiley Online Library.

2.3 MXene Interlayer Distance

Many experimental and theoretical studies have shown that properties of MXene-based devices depend on the interlayer distance between the hierarchically-layered individual atoms of the M and X elements. The interlayer distance of the sheets is affected by the composition of the etchant with which the A layers are selectively etched in the top-down synthesis process. In fact, the population of surface functional groups and consequently the population and strength of hydrogen bonds formed between MXene layers, which affect the interlayer distance, are dependent on the etchant type and composition[70]. The interlayer distance is also a pressure-dependent parameter which endows MXenes with piezoresistive properties[71]. Argon treatment and nitrogen doping are some approaches to increase distance between layers of a multilayer MXene [56, 72]. MXenes with enlarged interlayer distances have high capability for working as the anode of sodium-ion batteries[73].

Intercalation allows for adjusting the distance between MXene layers. MXenes with tuned interlayer distances are suitable for different post processes such as interlayer monomer diffusion and subsequent polymerization. For example, Ti_3C_2 intercalated by ε-Caprolactam undergoes ring opening polymerization to produce a MXene/Nylon nanocomposite that shows excellent water barrier properties[73]. In addition to monomers, many other chemicals such as surfactants and cationic solvents can be used for MXene intercalation. Each of these chemicals may affect interlayer distance and other inherent properties of MXene differently. For example, hydrazine can intercalate Ti_3C_2 at the expense of decreasing its water content and number of hydroxyl and fluorine groups[74]. In other cases, some cations like Li^+, $Na^+$and Mg^{2+} can intercalate Ti_3C_2 by replacing water molecules between layers causing contraction and consequent reduction in interlayer spacing[75]. Some contrary reports also mention that the intercalation of Na^+ between Ti_3C_2 layers in nonaqueous media increases the interlayer distance of Ti_3C_2 as they work as pillar [76]. These disagreements remain as a simulation paper reported that the intercalation of Ti_3C_2 with k^+ improves water stability between Ti_3C_2 layers[77]. These three seemingly contradictory reports point to a need for a careful selection of an intercalant and processing medium for Ti_3C_2 intercalation procedure [75-78]. Some cationic surfactants such as CTAB can also work as a spacer to increase the interlayer distance of Ti_3C_2 through pillaring[39, 75]. Moreover, using high valance cations like Al^{3+} for pre-intercalation is practiced to increase interlayer distance of Ti_3C_2 sheets [79].

As multilayer Ti_3C_2 is a conductive nanoparticle, its interlayer distance and the ion rejection capability of MXene-based membranes vary by applying a voltage. Thus, voltage is a tool to inhibit or enhance the rate of ion intercalation. The control of Ti_3C_2 interlayer distance and ion-rejection capability of MXene-based membranes by electrical potential are special features that distinguish MXene from other 2D nanomaterials[80].

To suppress self-restacking of MXene nanosheets and increase MXene inter-layer distance, electrostatic self-assembly between negatively charged Ti_3C_2 sheets and positively charged GO sheets is performed successfully[81]. Self-assembly between negatively charged pristine single-layer Ti_3C_2 MXene and positively charged amine-functionalized Ti_3C_2 MXene also increased MXene inter-layer distances[82]. To suppress restacking, it is also possible to insert another 2D nanoparticle between MXene sheets. For example, reduced graphene oxide is inserted between MXene sheets to suppress its self-restacking and to prevent from shrinkage in its interlayer distance. The latter hybrid structure is implemented in heavy metal ion removal processes[60].

Annealing of MXene sheets at high temperatures lets the adjustment of the interlayer distance in MXene thin films and membranes. Sintering usually decreases the interlayer distance due to loss of water and surface functional groups at high temperatures. In addition, annealing increases the risk of multilayer MXene oxidation and the formation of TiO_2 nanoparticles on the MXene flakes[83].

2.4 MXene Synthesis

MXenes have been synthesized using different approaches, leading to the production of MXenes with different qualities in terms of size[84], surface functional groups[45], and structural defects[43]. Details of single-layer MXene synthesis are described elsewhere thoroughly[85, 86]. Here, we limit our focus to general guidelines and the reactions that are involved. In general, there are two types of MXene synthesis approaches, top-down and bottom-up.

2.4.1 Top-down Synthesis

Top-down approaches involve an etchant addition to the parental material, MAX phase, or in-situ production of the etchant in the presence of a MAX phase. The etchant is usually HF or a mixture of HCl/HF. HF can be formed in-situ by mixing of a fluoride salt with HCl. Different

salts like LiF, NaF, KF, and NH_4F can be used. This in-situ production of HF is safer than the external addition. In the case of in-situ formation of HF, the cleanness of the surface of the synthesized MXene depends on the type of salt used, as the cations have different affinities for the surface of MXenes. For example, a single-layer MXene etched with a mixture of NaF/HCL contains less Na^+ on its surface compared with the one synthesized with LiF/HCL, as it is much easier to wash out Na^+ from the surface, compared with Li^+ [87]. Some other environmental-friendly, green HF-free methods like electrochemical etching in dilute HCl, anodic corrosion, and etching in Lewis acidic melts like $ZnCl_2$ are described in the literature[88].

MAX phase is a ceramic with a general formula of $M_{n+1}AX_n$, where M is a transition metal like Ti, A is an element from groups 13 and 14, and X is carbon and/or nitrogen. Ti_3AlC_2 is the most used MAX phase. The general formula of MXenes is $M_{n+1}X_nT_x$, which is obtained by the removal of A element. T represents OH, O, F, and CL surface functional groups, which are generated on the surface and edges of MXene during the etching process[5].

The synthesis of single-layer MXene consists of three steps including etching, washing, and delamination (Figure 2A). In the etching step, HF comes into contact with the MAX phase to remove its A element. The amount of HF should be adjusted accurately, otherwise an excessive amount of HF causes complete dissolution of the MAX phase which is unfavorable[88]. In the case of Ti_3AlC_2, Al will be removed by an etchant with a HF concentration between 10 to 50 wt.%. The required time for etching depends on HF concentration and temperature. For example, at room temperature, by using an etchant with HF concentration of 50 wt.%, just 2 hours is needed to remove Al from Ti_3AlC_2[85]. As the reaction is exothermic, MAX phase should be gradually added to the etchant to prevent from uncontrollable heat generation. In-situ formation of HF results in larger MXene flakes than direct addition of pure HF. The mole ratio of LiF to HCl significantly affects the quality of the resulting MXene. Two usual mole ratios of LiF to HCL are 5 M LiF: 6 M HCl and 7.5 M LiF: 9 M HCl. The most recent method is the addition of HF/HCl mixture to etch the MAX phase, which like the LiF/HCl etchant, allows for the production of large size single-layer MXene. [89]

Second step is washing which occurs after etching to remove etchant and some by-products like AlF_3 or LiF. Due to the presence of HF and possibly HCl, the reaction medium is extremely acidic. Thus, it is necessary to wash off acids to increase the pH of the medium to around ~6 and obtain a stable colloidal MXene. One cycle of washing consists of centrifugation, the decantation

of the supernatant which is an acidic water, the addition of fresh water, and the re-dispersion of MXene sheets that are settled down on the bottom of the centrifuge tube. This cycle is repeated until supernatant reaches a neutral pH. The product of this step is an aqueous colloidal multilayer MXene, where the layers are held to each other by hydrogen bonding or Van der Waals forces. If the purpose is the synthesis of multilayer colloidal MXene, the procedure finishes in this step. MXene dried powder or films can then be obtained from the colloid by filtration or casting of the colloid[85].

The third step is the delamination of the multilayer MXene to single-layer ones. This can be done by ultrasonication, hand shaking, the addition of intercalants or all/some of them together. The need for sonication or handshaking for the delamination is dependent on the etchant type. For example, MAX phases etched by 7.5 M LiF: 9 M HCl mixture or HCL/HF mixture usually do not need sonication for delamination. The approaches that do not need sonication for delamination are called MILD approaches. The advantage of MILD methods is that single-layer large flakes can be produced. Sound waves generated during the course of sonication usually break down MXene flakes. A large-flake MXene usually has better properties than small-flake counterparts. For example, although the conductivity of a large MXene flake is the same as that of a small flake of the same MXene, larger flakes form a more conductive network due to the lower total contact resistivity of larger flakes. To facilitate delamination, different materials are used as intercalant. LiCl, DMSO, tetraalkylammonium hydroxides, and lithium ions are a few to name. In the MILD approaches, after the addition of an intercalant like LiCl, the delamination of multilayer MXene is expected to happen after stirring the colloid for several hours and then vigorous handshaking. Next, the colloid undergoes another centrifuge cycle to separate single-layer from multilayer sheets and possibly remained unetched MAX phase. When delamination occurs, the sediment on the bottom of the centrifuge tube swells up significantly which is observable with a naked eye (Figure 2B). In addition, the existence of a dark supernatant after centrifugation is another sign of successful delamination. That dark supernatant contains single-layer MXene that should be collected as the final product[85].

To close this section, a few more points are worth to mention. XRD and EDX spectroscopies are the best characterization techniques to assure about the success of the etching. A peak at $2\theta \sim 39°$ in the XRD spectrum of MAX phase disappears after a successful etching (Figure 2C). Also 002 peak of Ti_3AlC_2 downshifts from 9.5° to 9° and then to ~ 6° upon etching and then

delamination. In addition, no trace of Al should be observed in the EDX spectrum. If a MXene with a large flake size, several microns, is required, etching of a MAX phase with large grain size has been recommended. Whenever sonication is needed for whatever reason, it is advised to purge colloidal MXene with an inert gas like argon or nitrogen and also keep it in an ice bath during the sonication. If MXene is not used immediately after production, it is recommended to store it in argon or nitrogen sealed vials and keep it in a refrigerator. This is important as it is shown that single-layer Ti_3C_2 MXene degrades by 42%, 85% and 100% after 5, 10 and 15 days of storage, respectively, in open vials[11]. Finally, if a person is suspicious to MXene degradation due to a long-time storage, a UV-Vis test can be used. Possible degradation changes the 700-800 nm peaks of Ti_3C_2 MXene[85].

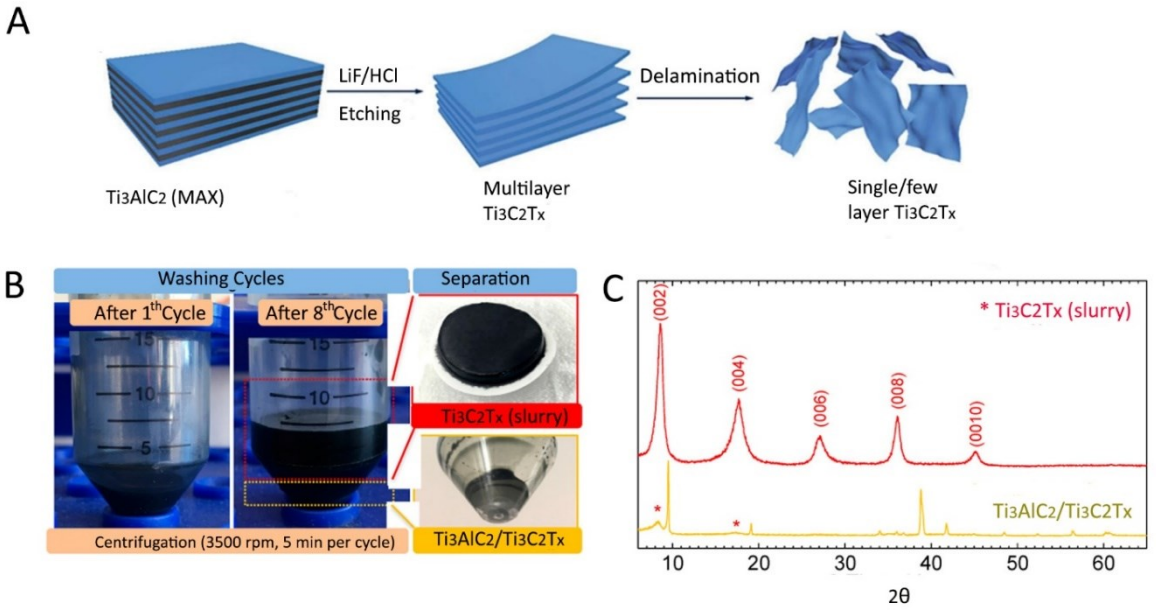

Figure 2. A) Schematic showing the synthesis of a MXene from a MAX phase via etching, and MXene delamination, Reproduced with permission from ref. [90] Copyright (2019), Royal Society of Chemistry. B) Expansion of MXene sediment upon delamination after several centrifuge cycles; the top-right inset shows the obtained MXene film after filtration, and the bottom-right inset displays leftovers of multilayer MXene and unetched MAX phase at the centrifuge tube. C) XRD results showing that the peak at $2\theta \sim 39^\circ$ of Ti_3AlC_2 MAX phase disappears after etching and its 002 peak also downshift from $2\theta \sim 9^\circ$ (yellow spectrum) to around $2\theta \sim 7^\circ$ (red spectrum), Reproduced with permission from ref. [85] Copyright (2017), American Chemical Society.

2.4.1.1 Large-scale Production

Ti_3C_2 MXene has usually been synthesized using a top-down approach. Although it looks simple at the first glance, the scale up of the approach needs great attention to heat transfer, mixing,

and safety issues. To synthesize MXene from a MAX phase in large quantities, a reactor with following properties is needed: 1) A screw feeder to feed a MAX phase automatically and gradually to the reaction medium to minimize the exposure of human staffs to dangerous HF acid as well as to assure the uniform addition of MAX phase; 2) A cooling jacket to remove heat from the reactor, preventing exothermic reaction runaway; 3) A gas outlet to release the generated gases; 4) Engineered mixing blades to improve homogeneity and prevent MAX phase settlement; 5) Internal gas feeding to feed a gas into the reaction medium if needed; and 6) An internal thermocouple [91]. Using a reactor with the aforementioned features, Shuck et al.[91] synthesized 50 g single-layer MXene in one batch and found that the properties of the obtained MXene are similar to the properties of the MXene obtained via 1 g synthesis procedure. Figures 3A and 3B show the reactor that they used and the product that they obtained from that reactor. In MXene synthesis, yield is defined as the ratio of the obtained single-layer MXene to the fed MAX phase. A 60 % yield is usually obtained when MXene synthesis starts with 1 g MAX phase. However, this value decreased to 52% when the synthesis started with 50 g MAX phase. Losing some of materials in discarded supernatants in each washing cycle, inability to delaminate all multilayer MXene, and multilayer MXene sedimentation are the main reasons for the decrease in the yield [91].

Comparing properties of a single-layer MXene synthesized in a small reactor with those of a MXene produced in a large reactor, it was found that there is no difference in terms of particle size, surface functional groups, optical properties, crystalline structure, atomic composition and conductivity. Figures 3C and 3D show the similarity of XRD and UV-Vis spectra of MXenes produced in a small and a large reactor. The scaleup does not require changing the temperature, reaction time or any other reactor operating conditions. Finally, this scale up approach to synthesize single-layer Ti_3C_2 seems to be applicable to other kinds of MXenes[91].

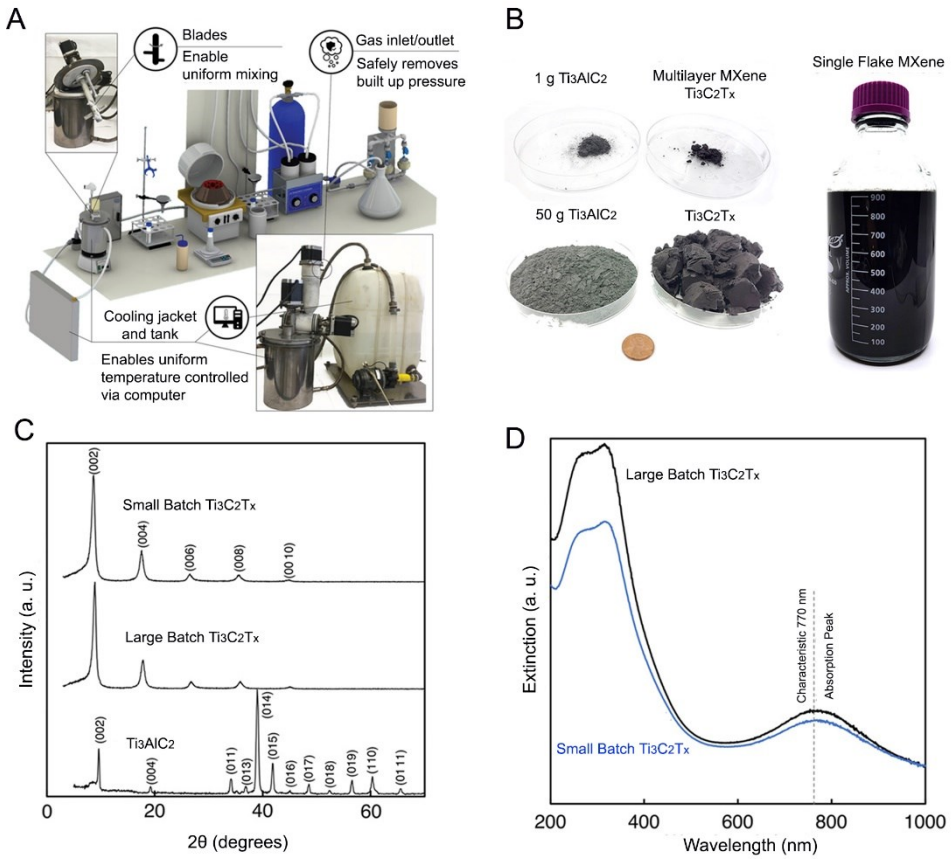

Figure 3. A) A pilot-scale setup including a reactor to synthesize a large quantity of MXene ~ 50 g. B) Images of showing 1 g and 50 g of the produced MXene as well as colloidal single-layer MXene. C) XRD results. D) UV-Vis spectra showing the similarity of spectra of the large-batch-produced MXene and the small-batch-produced MXene, Reproduced with permission from ref. [91] Copyright (2020), Wiley Online Library.

2.4.2 Bottom-up Synthesis

This approach is widely used for the synthesis of MXenes other than Ti_3C_2. Although the focus of this review is on Ti_3C_2, for completeness we briefly review bottom-up synthesis methods. In these methods, the synthesis starts from smaller building blocks, like atoms and molecules. CVD is a usual bottom-up approach for the synthesis of MXenes. For example, CVD has been used to synthesize defect-free φ-Mo_2C crystals with a lateral size of around 100 microns, which is much bigger compared with that of defect-prone MXenes synthesized with top-down methods (around 10 microns). So, for applications where a high lateral length and a perfect crystalline structure are required, CVD is recommended [92]. φ-Mo_2C was synthesized at a reaction temperature of 1085 ℃ while gaseous methane was fed to the reaction medium as a carbon source and a bilayer

substrate of Cu/Mo was used as the source of Mo. At such a high temperature, the Cu/Mo substrate melts and an alloy of Cu-Mo forms. The Mo species from the Cu/Mo interface diffuse through the molten Cu layer to reach the surface of Cu layer where decomposed methane gas exists as a source of carbon. When the reaction between Mo and carbon is complete, the system needs to be cooled down carefully to let the formation of perfect defect-free 2D layers [92]. Plasma-enhanced-pulsed-laser deposition can be also used in conventional CVD to improve the efficiency of the reaction between Molybdenum and carbon and prevent the former from oxidation[93].

Salt-templated synthesis is another bottom-up approach for the synthesis of 2D nanomaterials. Here, 2D metal oxides are used as precursors for the synthesis of 2D metal nitrides via the ammoniation reaction. For example, to synthesize MoN, firstly a MoO_3-coated NaCl powder is obtained via the reaction of Mo precursor at NaCl powder under argon environment at 280 ℃. The 2D MoO_3-coated NaCl is ammoniated in an NH_3 environment at 650 ℃. This ammoniation reaction converts MoO_3 to MoN, and NaCl helps MoO_3 keep its 2D structure during the conversion. The leftover NaCl in the final product can be washed out by deionized water [94]. Similar to the protocol described above for the synthesis of MoN, the synthesis of Mo_2C through the conversion of MoO_2 is possbile[95].

3 Ti_3C_2/Polymer Nanocomposite Fabrication

3.1 Solvent Selection and Solvent Exchange

Selection of a solvent to disperse MXene is the first step for solvent-mixing processes. The solvent should be able to dissolve the concomitant polymer to form a stable solution. In this section, important parameters and selection criteria are laid out to identify suitable processing conditions for fabricating MXene/polymer nanocomposites. Also, in this section, several MXene surface modification methods are reviewed. Fabrication of foams, hydrogels, and aerogels from MXene and MXene/polymer mixtures is discussed as well.

MXene synthesis in water is well established[1]. Aqueous colloids of single-layer Ti_3C_2 possess excellent stability and safety for processing, and are inexpensive to prepare[1]. However, MXenes in the presence of water and oxygen degrade over time. In addition, water intercalated between MXene flakes may decrease MXene's performance in electrochemical applications. A stable suspension of a MXene in an organic solvent is sometimes needed for mixing the MXene with a polymer. A stable suspension is a suspension in which MXene flakes do not agglomerate

over time (Figure 4A). Drying single-layer Ti_3C_2 MXene to remove water and then redispersion in an organic solvent have shown that the MXene is stable in ethanol, DMF, DMSO, NMP, and PC. However, it has poor stability in 1,2 dichlorobenzene, hexane, toluene and methanol[63]. Figure 4B shows the dispersibility of single-layer Ti_3C_2 in different organic solvents right after, 24 hours after, and 96 hours after the redispersion[63].

To analyze systematically the suitability of a solvent for MXene dispersion, the surface tension, viscosity, dielectric constant, and boiling points of various solvents should be considered. As a rule of thumb, a polar solvent with high boiling point, high surface tension and high dielectric constant is a decent choice for MXene dispersion. Thermodynamic properties like Hilderbrand and Hansen solubility parameters of the solvents allow for a better evaluation of a solvent[63]. A good solvent for MXene dispersion should ideally have high dispersion interactions and high polarity. However, establishing of hydrogen bonds is not important. As an evidence, H_2O, NMP, PC, DMF, and DMSO are good solvents for MXene dispersion, as they exhibit high polarity and dispersion interactions. An analysis of solvent properties with thermodynamic tools helps one to design a mixture of poor solvents in a way to convert it into a good solvent for MXene dispersion. For example, acetonitrile is a poor solvent for MXenes while it is highly polar. On the other hand, aromatic solvents are not polar but have high dispersion interactions. A 1:8 v/v mixture of DMF and chloroform has been reported to disperse Ti_3C_2 well[96]. Thus, a right composition of proper solvents is needed for good single-layer MXene dispersion[63].

It is also possible to modify the surface of a single-layer MXene to tailor its dispersibility in different solvents. Surface energies of MXenes are strongly dependent on their surface chemistry which consequently determines MXene wettability by different solvents[97]. For example, the presence of long hydrocarbon chains on single-layer MXene surface may negatively affect its dispersibility in DMF which is already known to be a good solvent for pristine single-layer MXene [97]. Moreover, it is observed that the dispersibility of pristine single-layer MXene in water decreases by grafting of 2-isocyanatoethyl methacrylate on its surface. At the same time, however, DMF disperses this kind of surface modified MXene better than water [98]. Surface chemistry and consequently the dispersion of MXene in a solvent may be affected by etchant composition. For example, MXene etched by HF may show a slightly different dispersibility in a solvent compared with a MXene etched by LiF/HCL mixture. The reason is difference in population of surface functional groups and the kind of species between MXene layers[63].

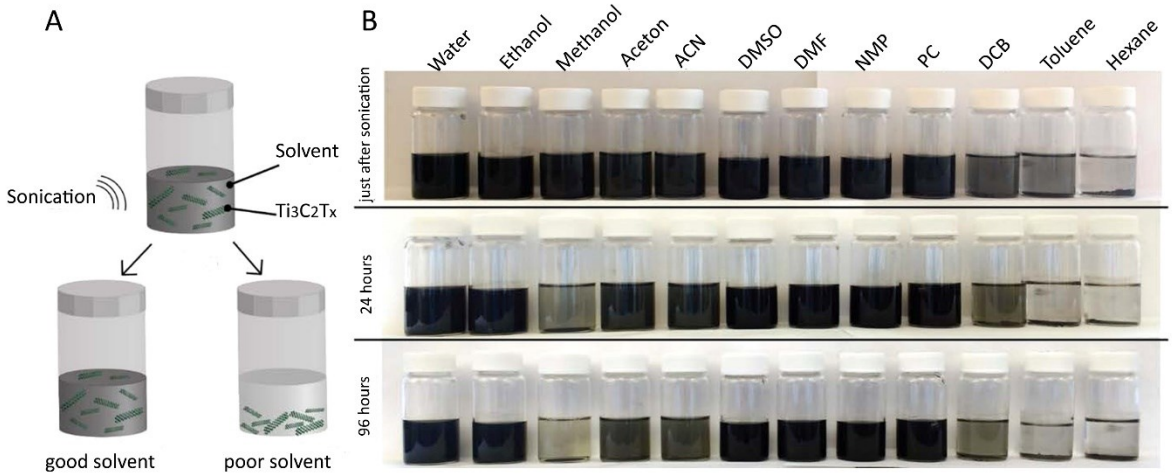

Figure 4. A) Images showing the stability of Ti_3C_2 flakes in a good and a poor solvent after sonication. B) the evolution of Ti_3C_2 colloid stability over time shows that only ethanol, water, DMSO, acetone, NMP, DMF, and PC are good solvents for Ti_3C_2 dispersion, Reproduced with permission from ref. [63] Copyright (2017), American Chemical Society.

3.2 MXene Surface Engineering

MXene inherently has hydroxyl, fluorine and oxygen groups on its surface. However, for many other applications, new surface functional groups are required. Hydrophobic Ti_3C_2 membranes were synthesized by reacting single-layer Ti_3C_2 with a silane coupling agent bearing fluorine groups. This allowed for selective salt filtering in water treatment (solar desalination)[17]. Silane coupling agents were also used to develop vertically-aligned Janus Ti_3C_2-based aerogels where one end is hydrophilic, and the other end is hydrophobic for seawater purification through solar desalination. The hydrophobic end of the aerogel inhibits salt accumulation on the surface, increasing the longevity of the polymer membrane for longer durations of functional usage[99]. Non-inherent surface functional groups may also be created by alteration in MXene synthesis steps. For example, applying sound waves during MAX phase etching creates peroxide groups on the surface of a MXene. This new functional group enables a MXene to work as a conventional initiator to initiate a free-radical polymerization. Acrylate monomers in the presence of peroxide-containing single-layer MXene are recently polymerized[100]. Similarly, the addition of alcohol to water during

678 the etching step may lead to the creation of alkoxyl group on MXene surface which is a non-
679 inherent functionality[101].

680 The presence of amine groups on MXene surface opens many new applications for
681 MXenes. Aminosilane coupling agents can be grafted on MXene surface (Figure 5A). It is shown
682 that the surface charge of pristine Ti_3C_2 changes from negative to positive in a wide pH range 2 to
683 ~10.5 due to the grafting of an aminosilane coupling agent and the protonation of its amine
684 groups[82]. Other silane coupling agents bearing methacrylate[102], perfluoroalkyl[17] as well as alkyl
685 groups[103] are also grafted on Ti_3C_2 surface. These silane coupling agents usually react with
686 hydroxyl groups on the surface of Ti_3C_2[82]. In one example, methacrylate bearing silane coupling
687 agents were grafted on the surface of Ti_3C_2 followed by grafting of sulfonated polyelectrolyte
688 brushes on Ti_3C_2 surface by polymerization of sodium-p-styrenesulfonate from the methacrylate
689 sites. These modified MXenes were then used as nanofillers to incorporate into sulfonated poly
690 (ether ether ketone) or chitosan to make proton conducting membranes[102].

691 Grafting of polymer brushes on MXene surfaces through surface initiated photografting
692 and polymerization can generate hybrid structures where the polymerization initiates with solution
693 mixing of the constituents and then the UV irradiation of the system. Although this review paper
694 focuses on Ti_3C_2 MXene, in following we discuss a paper published on the surface modification
695 of V_2C MXene as it introduces a novel method for surface modification. In Figure 5B, grafting of
696 poly(2-(dimethylamino)ethyl methacrylate) brushes on the surface of vanadium carbide (V_2C)
697 resulted in a hybrid stimuli-responsive material which shows sensitivity with change in
698 temperature and carbon dioxide concentration. Poly(2-(dimethylamino)ethyl methacrylate) has an
699 LCST around 40 ℃ and its grafting on Ti_3C_2 MXene surface improves MXene dispersibility in
700 water at T<40 ℃. In the presence of CO_2, its tertiary amine groups can get protonated and show
701 increased conductivity. Thus, these stimuli-responsive behaviors may open new applications for
702 MXene/polymer nanocomposites in new areas such as sensors and biological areas[104].

703 To give Ti_3C_2 the chance of participation in free-radical polymerization, Huang et al.[98]
704 modified the surface of single-layer Ti_3C_2 by 2-isocyanatoethyl methacrylate. They dispersed 0.1
705 g of Ti_3C_2 powder in DMF by bath sonication and added 3 gr of 2-isocyanatoethyl methacrylate
706 (weight ratio of 30). In surface modification reactions of nanoparticles, it is always recommended
707 to add the modifying agent in excess. The reaction was continued for 4 hours. It is believed that
708 the bonding happens due to the reaction between -N=C=O groups of the surface modifier and OH

groups of MXene. The modified Ti_3C_2 was obtained by centrifugation and then vacuum drying [98]. Here, it is necessary to remind that most of surface modification reactions of Ti_3C_2 occur through its OH groups.

The impregnation of Ti_3C_2 with PEG is another example of surface modification of MXenes. When a PEG grade with molecular weight of 10000 g/mol was used, the interlayer distance between Ti_3C_2 flakes increased from 15.4 to 19.7 Å. PEG is a water-soluble polymer. Thus, it can be added to aqueous dispersion of Ti_3C_2 easily. By freeze-drying of the Ti_3C_2/PEG at -60 ℃ for 96 hours, PEG-treated Ti_3C_2 had been obtained and then was added to TPU. The increase in interlayer distance and interaction improvement between oxygen/hydroxyl groups of Ti_3C_2 and polar groups of TPU cause enhancement in the dispersion of Ti_3C_2 in TPU during a melt blending process[105].

PANI has been polymerized on the surface of Ti_3C_2 to change Ti_3C_2 surface charge and to increase its interlayer distance. In acidic media, aniline changes into a radical-cationic monomer and undergoes polymerization. It is also possible to impregnate Ti_3C_2/PANI hybrid with CTAB which is a cationic surfactant. This process also changes the surface charge of pristine Ti_3C_2 from negative to positive. It is important here to highlight that even without impregnation with CTAB, Ti_3C_2/PANI shows positive surface charge up to pH~ 8.5. However, impregnation with CTAB causes multilayer Ti_3C_2/PANI to keep its positive surface charge in wider pH range of 3-12[106]. Thus, in addition to aminosilane coupling agents, one can consider PANI polymerization or cationic surfactant impregnation as methods to change the surface charge of Ti_3C_2 from negative to positive. In addition to CTAB, the impregnation of Ti_3C_2 with other cationic surfactants like OTAB, DTAB, and DDAB has also been practiced. As Figure 5C shows, these cationic surfactants interact with single-layer Ti_3C_2 through their positively-charged head[97].

Silver has plasmonic and antibacterial properties. Similarly, Ti_3C_2 has excellent antibacterial and antifouling properties. Several researchers have impregnated Ti_3C_2 with silver nanoparticles to take the advantage of possible synergistic effects. For example, single-layer Ti_3C_2 was impregnated with silver nanoparticles to develop ultrahigh-flux, fouling-resistant nanofiltration membranes for water purification and biomedical applications[107]. The process of incorporation of silver nanoparticles into Ti_3C_2 usually starts by the addition of aqueous solution of $AgNO_3$ to aqueous suspension of the MXene. The Ag^+ ions are absorbed on the surface functional groups of Ti_3C_2, OH for example, due to electrostatic attractions. Subsequently, the

740 cation receives an electron from Ti_3C_2 and undergoes a further reduction reaction to form Ag^0. The
741 latter works as a nucleation center for further growth of silver nanoparticles on single-layer MXene
742 surface. In this hybrid system, usually named AgNP@MXene, spherical silver nanoparticles are
743 anchored firmly to Ti_3C_2 surface, and their size is usually between 20 to 50 nm [108].
744
745
746
747
748
749

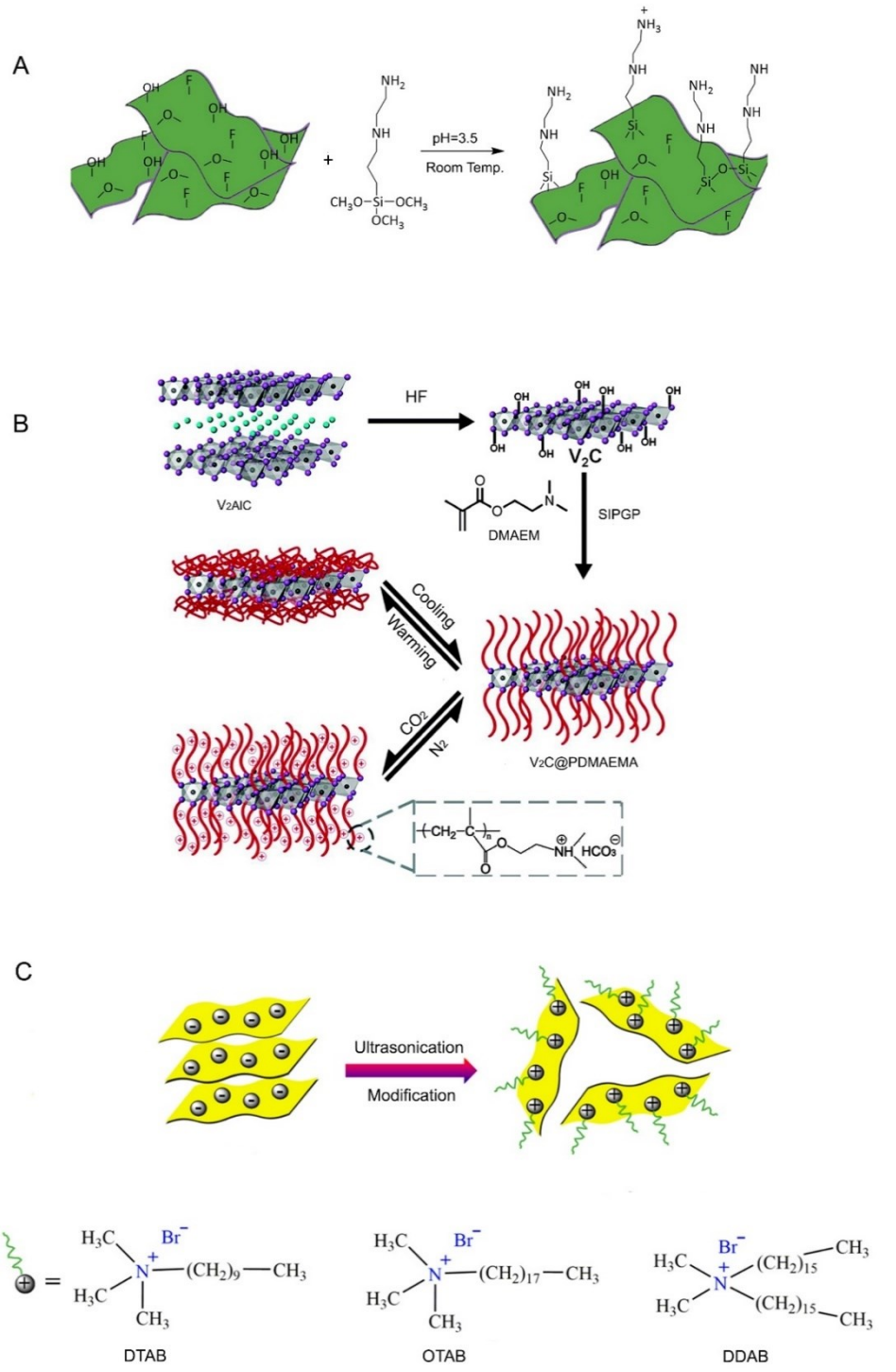

Figure 5. A) Grafting of an aminosilane coupling agent on the surface of a MXene, Reproduced with permission from ref. [82]Copyright (2020), Wiley Online Library. B) Grafting of a stimuli responsive polymer brush on the surface of a MXene by polymerization of dimethylaminoethyl methacrylate to produce a hybrid material sensitive to heat and CO_2, Reproduced with permission from ref.[104] Copyright (2015), Royal Society of Chemistry. C) Attachment of three different cationic surfactants to the surface of a MXene by electrostatic attraction, Reproduced with permission from ref. Copyright (2019), MDPI [97].

3.3 Hydrogels, Foams and Aerogels

This section describes several important MXene-based intermediate products such as foams, hydrogels, and aerogels made. It then reviews processing techniques that can be applied to these products to make devices for real-world applications.

Hydrogels are a three-dimensional network of hydrophilic polymer chains connected to each other by crosslinking agents[109-111]. Hydrogels are used usually as water absorbents. Nanocomposite hydrogels containing a MXene as the crosslinking agent can be synthesized by in-situ polymerization of a monomer like acrylamide in the presence of a colloidal MXene. As Figure 6A shows, conventional initiators like KPS can be used to synthesize hydrogels through a free-radical polymerization[112]. Zhang et al.[112] sonicated re-dispersed Ti_3C_2 powder for three days continuously in water. They then added acrylamide which is a water-soluble monomer to the colloidal Ti_3C_2 along with KPS to initiate the polymerization. Compared with conventional hydrogels made from organic crosslinkers like N,N-methylene bisacrylamide possessing an irregular collapsed pore structure, their Ti_3C_2-based hydrogels had honeycomb regular fine structure. In addition to hydrophilic acrylamide groups of the polymer, hydroxyl and fluorine groups on the surface of Ti_3C_2 form hydrogen bonds with water molecules resulting in a significant water uptake by such Ti_3C_2-based hydrogels[112].

It is even possible to synthesize a MXene-based hydrogel via free-radical polymerization without using any conventional initiator. Tao et al.[100] introduced a method called sonication-assisted MILD etching method in which delamination simultaneously happens with etching. MXene produced by this technique inherently has peroxide groups on its surface. Thus, it is possible to initiate a free-radical polymerization without a need to add any conventional initiator. It is believed that cavitation bubbles, produced by sound waves, generate H_2O_2 in the etching reaction medium which then interacts with OH groups on the surface of MXene to form peroxide groups. However, experiment results have shown that these peroxide groups on the surface of Ti_3C_2 stay active around one week at room temperature and then lose their activity to initiate polymerization. Single-layer Ti_3C_2 MXene with peroxide surface functional groups are still water dispersible and the addition of monomers like isopropylacrylamide to them gives the chance of running a free-radical polymerization (Figure 6A). In addition to isopropylacrylamide, Ti_3C_2-based hydrogels made from the polymerization of other monomers including acrylamide, N,N

dimethylacrylamide, methyl methacrylate and hydroxyethyl methacrylate have been synthesized by peroxide-decorated Ti_3C_2[100].

It is also possible to use two polymers simultaneously to synthesize a MXene-based hydrogel. For example, Liao et al.[69] mixed an aqueous solution of PVA with acrylamide monomer, methylene-bis-acrylamide crosslinker, AIBI initiator, single-layer Ti_3C_2 aqueous suspension and then in-situ polymerized the mixture at 60 ℃ to form a hydrogel (Figure 6B, steps 1-3). They also added borax (sodium tetraborate decahydrate) to the polymerization system to give the ability of dynamic crosslinking between the hydroxyl groups of PVA and tetrahydroxyl borate ions. The dynamic bond formation endows the hydrogel with the chance of self-healing. A part of water was also exchanged with EG to give it anti-freezing feature [69] (Figure 6B, step 4).

In a research by Wu et al.[113], three polymers were used simultaneously to synthesize a hydrogel. Dopamine grafted sodium alginate and phenylboronic acid grafted sodium alginate were mixed with water/glycerol mixture and then acrylamide was polymerized in-situ to make the third polymer of the hydrogel network. The presence of three polymers as the hydrogel network creates a self-healing structure which will be discussed in detail in following sections. Glycerol was added to the hydrogel to increase its moisture retention. Glycerol establishes hydrogen bonds with water, helping hydrogel to keep its moisture for a long time. Consequently, the retention of moisture endows the hydrogel enough flexibility to be bended and twisted without any mechanical damage over a long period of time [113]. Keeping a high amount of water in a hydrogel structure is advantageous. Ti_3C_2/cellulose hydrogels made via crosslinking of cellulose with epichlorohydrin were able to keep 98 wt.% water in their structure and also showed stable drug release and heat-generation upon UV-irradiation[114]. This huge amount of water is stored inside the pores of the Ti_3C_2/cellulose hydrogels. It is also possible to adjust the size of the pores by light irradiation.

Foams and aerogels are other MXene-based products that can be used for various applications. The conversion of a MXene film to a MXene foam is possible by using hydrazine as a foaming agent. Hydrazine reacts with hydroxyl groups on the surface of MXene resulting in the generation of many gaseous products upon the occurrence of a series of reactions. The pressure generated by these gases overcomes the Van der Waals forces between MXene layers which pushes them apart from each other. As a result, a porous cellular MXene structure is formed. This process changes a MXene from a hydrophilic material to a hydrophobic one but does not alter the MXene's electrical conductivity even in the foam state[115].

MXene-based foams with higher mechanical properties can be fabricated by incorporating a polymer into MXene structure. Compared with pure MXene foams which were discussed in the previous paragraph, the MXene/polymer foams are durable and keep their electrical and mechanical properties after several hundreds of compression cycles[116]. To develop such foams, in what follows we describe a method based on freeze-drying technique, which is widely used by researchers for foam fabrication. The first step is the preparation of an aqueous solution of a water-soluble polymer like sodium alginate and then the addition of MXene suspension to the solution (Figure 6C-1). We call this polymer as the primary polymer. The role of the primary water-soluble polymer, e.g., sodium alginate, in this process is improving gelation ability of MXene sheets to keep the porous structure of the system and to improve its stability after foam formation. The next step is (non-)directional freezing by immersing the system in liquid nitrogen (Figure 6C-2). It is important to know that when just one side of a container containing colloidal MXene is in contact with a cold source like liquid nitrogen, the orientation of MXene flakes to form an unidirectional system occurs upon freezing [117]. Next step is freeze-drying which causes the formation of a porous material through the sublimation of the ice between MXene flakes (Figure 6C-3). To incorporate a secondary reinforcing polymer into the foam structure, the material is immersed in a pre-polymer. Curing of the pre-polymer improves mechanical properties of the foam (Figure 6C-4). Usually an elastic polymer like PDMS is used as the secondary reinforcing polymer to coat interior parts of the foam[116]. Such aerogels are able to withstand a load 1000 times higher than their original weights (Figure 6C-5)[116]. It is also important to note that the amount of the primary water-soluble polymer affects the size of vertically formed channels.

PVA is a decent polymer for fabricating MXene/polymer foams. Because of the strong hydrogen bonds between surface functional groups of single-layer Ti_3C_2 and hydroxyl groups of PVA, the foam is able to withstand a load ~5000 times higher than its own weight[118]. Polyimide is also another decent choice for foam fabrication[119]. In a study by Liu et al., colloidal single-layer Ti_3C_2 was mixed with polyamic acid, and the mixture was then undergone a freeze-drying technique. Strong interactions between this polymer and surface functional groups of single-layer Ti_3C_2 caused the formation of 3D robust aerogel structure[119]. Thermal annealing of the aerogel at 300 ℃ in an argon atmosphere converted polyamic acid to polyimide[119].

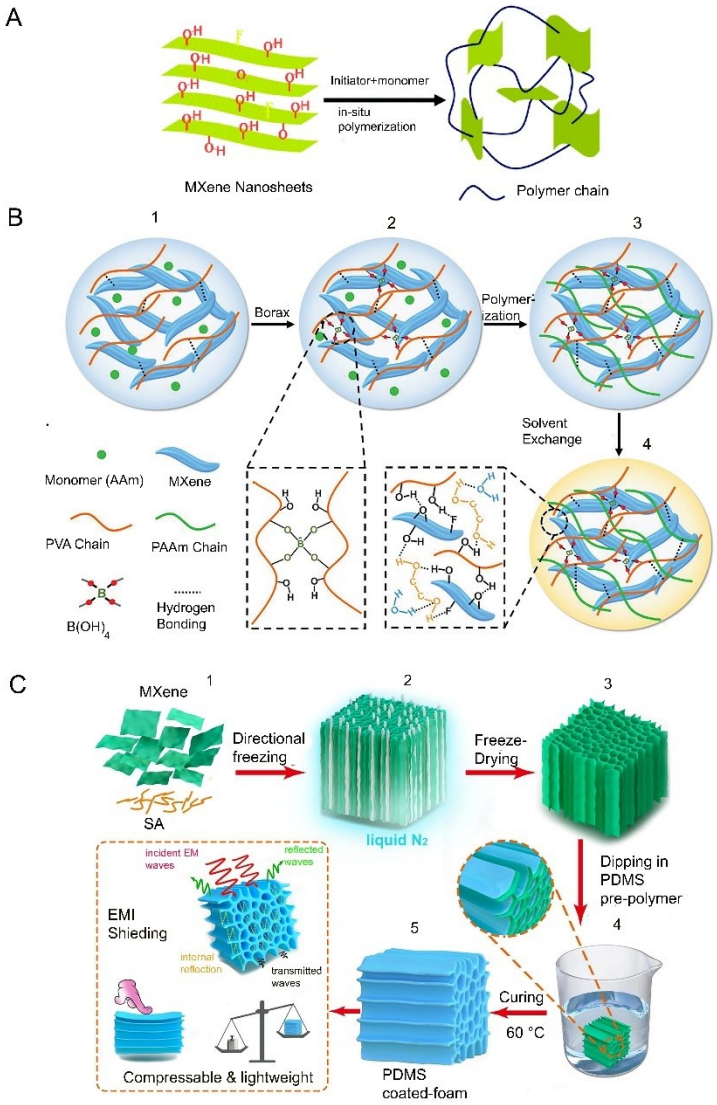

Figure 6. A) In-situ synthesis of a MXene-based hydrogel by free-radical polymerization where the MXene plays the role of crosslinking agent, Reproduced with permission from ref.[120] Copyright (2020), Royal Society of Chemistry B) Synthesis of a MXene-based hydrogel with two polymers as the hydrogel matrix (3) and ethylene glycol (4) as liquid phase with the ability of hydrogen bond formation and dynamic covalent bonding for self-healing application, Reproduced with permission from ref. [69] Copyright (2019), Wiley Online Library C) Synthesis of a foam with oriented MXene flakes (2) by freeze-drying technique (3) coated with PDMS (4) for EMI shielding (5), Reproduced with permission from ref. [116]Copyright (2020), Elsevier.

4 Ti_3C_2/Polymer Nanocomposite Processing

4.1 Rheology of MXene Containing Systems

Rheological properties of MXene are required to be known to select an appropriate processing method for shaping MXene-based products. Here, various coating, thin film and

nanocomposite processing methods are described in detail. To keep the paper short and focused, however, we do not discuss the coatings and thin film processing techniques that are not used widely in academia. Interested readers are referred to Ref. [121-123].

Good dispersion of MXenes in a polymer solution is the first step to obtain homogenous MXene distribution in a thin polymer film after solvent removal. Rheology can be used to evaluate the distribution of a MXene in a polymer solution based on the quality of interactions in the solution. An increase in storage modulus (G') indicates the possibility of the formation of a 3D elastic network between a polymer and Ti_3C_2. Mirkhani et al.[124] assessed the dispersion of Ti_3C_2 in a PVA solution and determined that there are strong interactions between Ti_3C_2 and PVA[124].

Having a good understanding of rheological properties of MXenes is necessary to select a suitable processing method for a specific target. Some of these processing methods are solution casting, vacuum filtration, spray coating, spin casting, dip-coating, latex blending, electrostatic assembly, wet spinning, electrospinning, ink-jet printing, and extrusion printing. It is shown that rheological properties of single-layer Ti_3C_2 in water is very different from rheological properties of their multilayer counterparts[125]. For example, multilayer Ti_3C_2 aqueous suspensions with the concentration of 70 wt.% still show flowability while a single-layer Ti_3C_2 aqueous suspension shows elasticity at much lower concentrations. Generally, rheological properties of Ti_3C_2 colloids depend on their surface charge, particle size, surface chemistry and the number of layers in a MXene sheet stack[125].

Processability charts for single-layer and multilayer MXenes (Figure 7) help to select a suitable processing method based on an application. Colloids with dominant loss moduli ($G'/G" < 1$) are suitable for a process with a high shear rate such as spray or spin coating. However, colloids with dominant elastic moduli ($G'/G" > 1$), which are able to keep their given shape, are suitable for a process such as extrusion that requires a high viscosity. These processing charts work like a map. By knowing the type of the MXene suspension (single-layer or multilayer), and the shear rate that the suspension will experience, we can locate a point inside these maps and determine whether the located point is in the region of our intended processing method or not. Usually, single-layer MXene colloids are used for high shear-rate processes while multilayer MXene colloids for low shear-rate processes[125].

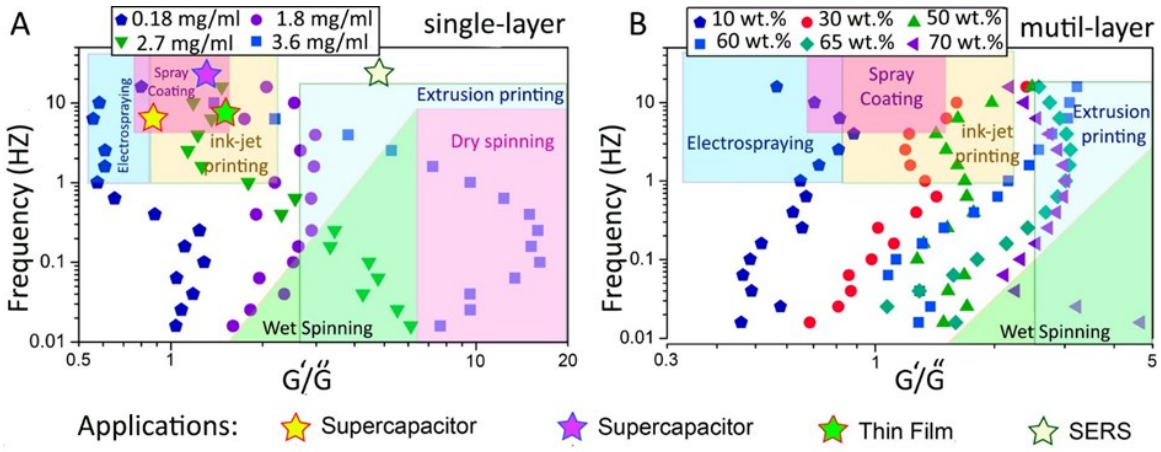

Figure 7. Processability chart (frequency versus the storage-modulus-to-loss-moduli ratio) determines the suitability of electrospraying, spray coating, ink-jet printing, wet spinning, dry spinning, and extrusion printing for an aqueous MXene suspension depending on the applied share rate (A) single-layer Ti_3C_2 and (B) multilayer Ti_3C_2 , Reproduced with permission from ref. [125] Copyright (2018), American Chemical Society.

4.2 Coating Techniques

Solution casting is a simple method to make pure MXene and MXene/polymer nanocomposite films. Pristine or surface functionalized MXene is dispersed in a solvent in which the polymer is also soluble. Sonication and/or magnetic stirring are usually required to improve the homogeneity of the mixture. By casting of the mixture and then the evaporation of the solvent, a thin solid film will be obtained (Figure 8A). Casting can also be carried out by some automatic instruments to have higher quality thin films, compared with manual casting[126]. For water-soluble polymers, usually water is used to dissolve the polymer and also disperse MXene. For organic polymers, usually DMF is used as it is a good solvent for both polymer dissolution and MXene dispersion. For example, MXene flakes with surface grafted sulfonated polyelectrolyte brushes were dispersed in DMF where sulfonated poly(ether ether ketone) was also dissolved in DMF as polymer matrix. The mixture was then cast on a glass substrate and annealed at 60 ℃ for 12 hours to develop a proton conducting membrane[102]. In another study, acrylic terpolymers of styrene, butyl acrylate and hydroxyethyl acrylate were dissolved in DMF [127]. Pristine Ti_3C_2 or PPy-intercalated Ti_3C_2 were also dispersed in DMF, and the mixture was undergone stirring, sonication and then casting onto a Teflon disc to develop nanocomposite films with high dielectric constant. After casting, it is recommended to dry the product in an oxygen-free environment like glove box

and then carry out a thermal annealing process to assure the removal of solvent residues. To ensure safety, the thermal annealing is better to be carried out in a vacuum oven to avoid oxygen.

Solution casting can be utilized to stimulate an in-situ reaction during the nanocomposite formation process. For example, after the addition of single-layer Ti_3C_2 to epoxy resin Epon 862 in acetone, it was cured in-situ with diethyl methyl benzene diamine[48]. The mixture was stirred at 70 ℃ for 1 hour, then transferred to a mold for casting, and finally cured at 120 ℃ for 5 hours[48]. Multilayer casting is also a good technique to produce alternative multilayered films (Figure 8B). As the first step, a polymer solution, like PVA in water, with a predetermined concentration is cast on a substrate and then left to dry. This is followed by depositing colloidal suspension of Ti_3C_2. This cycle can be repeated many times to develop a multi-layer film with desired numbers of layers [128].

Vacuum filtration is another widely used technique for coating/thin-film fabrication. Starting material in this technique is usually a suspension of a MXene or a MXene/polymer mixture. Filtration setup consists of a filter paper with a pore size smaller than MXene flake size and a Buchner flask connected to a vacuum pump to accelerate solvent suction. The final product is a dried or paste-like thin film[129, 130]. Water-soluble polymers are often selected for this technique. When there are interactions between polymer and MXene (e.g., via hydrogen bonding or electrostatic attraction), defect-free, mechanically-stable thin composite film can be fabricated. Pristine MXene or MXene/polymer thin films with adjustable thicknesses can be obtained by changing the concentrations of the materials introduced to the vacuum filtration setup. Due to the presence of a vacuum force in this technique, the flakes can be oriented in the force direction enabling the development of hierarchically structured films[124].

Vacuum filtration is suitable for the fabrication of MXene-based nanocomposite films from electrically-neutral polymers such as PVA or electrically-charged polymers like PADC. To prepare a solution for vacuum filtration, it is sometimes necessary to warm up the MXene/polymer mixture to obtain a homogenous system. This may worry one about MXene degradation specially in aqueous systems. For example, PVA dissolves in water at high temperatures and the addition of aqueous colloid MXene to warmed PVA solution may degrade the MXene. However, no MXene degradation is reported even by stirring a single-layer MXene/polymer aqueous mixture at 80 ℃ for 12 hours [131]. A single-layer MXene/cellulose nanocomposite is another system that was

fabricated by vacuum filtration technique thorough dispersing/dissolving both components in deionized water[132].

Alternative vacuum filtration is another technique for the fabrication of multilayered thin films where each layer is made from pristine MXene or pure polymer. Figure 8C shows a multilayer film containing 6 layers of CNF and 5 layers of MXene. During this process, MXene suspensions and CNF solutions are filtered alternatively and usually the top and bottom layers of the multilayered structure are made from polymers. It is important to know that when a single-layer composite film of MXene/CNF with similar composition to that of the multilayered film was made by mixing of the CNF and MXene and running the vacuum filtration for one cycle, the properties of single-layer structure were not comparable with multilayer counterpart. The multilayer one with exact chemical composition showed higher electrical conductivity, mechanical properties and EMI shielding capability[112]. It is also interesting to know that the electrical conductivity and EMI shielding capability are dependent on the number of MXene and polymer layers in the multilayer film.

The pore size of the filter and the intensity of the vacuum are important factors determining the required time for vacuum filtration process[121]. In addition, enough attention should be paid to peeling off the MXene/polymer thin film from the filter to avoid any damage. As vacuum force causes orientation of MXene flakes, the samples prepared by vacuum filtration may show some changes in their XRD pattern compared with a similar sample prepared by other methods like solution casting. As a result, one can conclude that under similar chemical composition, a processing method of MXene/polymer mixture for the fabrication of a thin film may affect its X-ray diffraction pattern by changing the intensity and broadness of the peaks[133].

Spray coating is an easy-to-use technique to make a MXene-based coating over a large surface area (Figure 8D)[73, 134]. Thin, transparent, conductive, pure MXene or MXene-based nanocomposite films can be developed by this method. An advantage of this method is its compatibility for different kinds of substrate, the creation of a coating without surface damages and its flexibility for using with different kinds of MXene suspensions containing different intercalants[73]. Spray coating was used to coat the surface of PU foams by a flame-retardant mixture containing single-layer Ti_3C_2[98]. The mixture was dispersed in DMF and then applied on the surface of PU by spray coating[98]. The thickness of the coatings can be controlled by the concentration of the sprayed material as well as the spraying duration[121].

Spin coating is a widely used technique for the creation of thin films from a solution or suspension[135, 136]. A tiny amount of a liquid containing the depositing material is placed on a substrate, and the rotation of the substrate then starts (Figure 8E). Most of the material is usually thrown away from the substrate, and what is left forms a thin, defect-free homogenous smooth film. The thickness of the film can be adjusted by controlling the rotation speed, amount and the concentration of the depositing material in the liquid. In addition to usual substrates, thin MXene-based films can be deposited on a transparent substrate by this technique to develop conductive and transparent systems[121].

The substrate that is used in a spin coating process may affect the properties of the deposited film. Thus, it is necessary to minimize the contact of the depositing material with the substrate. Wu et al.[137] developed thin hybrid films of multilayer Ti_3C_2 and PDT by adding the components to DMF and carrying out a spin coating process on Ti_3C_2-FTO substrate. After the process, the system was dried up at 80 ℃ under vaccum for 8 hours, and the thin hybrid MXene/PDT film was carefully peeled off from the Ti_3C_2-FTO substrate. The FTO substrate itself was coated with Ti_3C_2 to minimize the direct contact of PDT/Ti_3C_2/DMF paste to FTO, preventing from the possible effects of the FTO on the structural and mechanical properties of the obtained film. Other researchers also have used this technique to deposit MQD/PVP on ITO electrode[138].

Similar to spin or solution casting, dip coating is a robust and controlled technique for developing homogenous MXene/polymer hybrids (Figure 8F)[139]. Complex polymer materials such as electrospun polymer fibers or thermoplastic polymers such as PU can be coated with a MXene to develop a uniform film thickness on their surface. The thickness of the deposited film is dependent on the viscosity of the dipping solution and the dipping/withdrawal velocities of the substrate[121]. Moreover, in typical dip coating processes, the thickness of the coatings can be controlled by regulating the number of dipping cycles and the rate of solvent evaporation during thermal annealing. PET surfaces were coated with PPy-functionalized Ti_3C_2 by dip coating process to fabricate conductive textile for EMI shielding applications[140]. Similarly, a PU sponge was coated with single-layer Ti_3C_2 to develop free standing MXene-polymer foams for flame-retardancy applications[141].

Layer-by-layer dip-coating was used to fabricate MXene/polyelectrolyte multilayers. In case of using pristine Ti_3C_2 that has a negative surface charge, the coating process starts with immersing the substrate in the polycation solution for a specific amount of time. Next, it is removed

from the solution, rinsed for several minutes, and then immersed in colloidal MXene suspension. This process is repeated several times to reach a desired thickness. Two points should be highlighted here. First, the thickness of each layer in the final multilayer film can be adjusted by changing the immersion duration. In other words, it is not necessary to have an equal immersion time for both positively and negatively charged components. Second, layer-by-layer dip-coating has advantages over ordinary dip-coating. For example, layer-by-layer dip coating is suitable for coating with charged components[142], as mixing of the charged components may cause the precipitation of the components before the formation of a coating, which decreases the smoothness and homogeneity of the final coating. For example, layer-by-layer dip-coating has been used for the deposition of single-layer Ti_3C_2 that has negative charge and chitosan that has positive charge on the surface and internal pores of PUF (Figure 8G)[143]. Also, dip-coating was used to coat small-size and large-size single-layer MXene on cellulose yarns[144].

Latex blending is a common method of fabricating polymer blends. It involves mixing of two lattices and then removing the liquid phase. A latex can be also mixed with colloidal MXene to make a nanocomposite. Polymer lattices produced by emulsion, suspension, and dispersion polymerizations can be used in this process[145, 146]. Lua et al.[147] used this technique to make a nanocomposite of single-layer Ti_3C_2 and NR. In the pH range of 2-12, both Ti_3C_2 and NR nanoparticles have negative surface charge and the electrostatic repulsion between them assures their homogenous dispersion in water. Vacuum filtration of the mixture led to a flexible and conductive MXene/NR nanocomposite film. It was shown that Ti_3C_2 flakes locate between NR particles and make a conductive network of flakes across the cross section of the film. It is also possible to use this method to crosslink a rubber by adding crosslinkers such as dicumyl peroxide followed by thermal compression. For example, the obtained single-layer MXene/NR nanocomposite was crosslinked at 170 ℃ under pressure 10 MPa for 20 min[147].

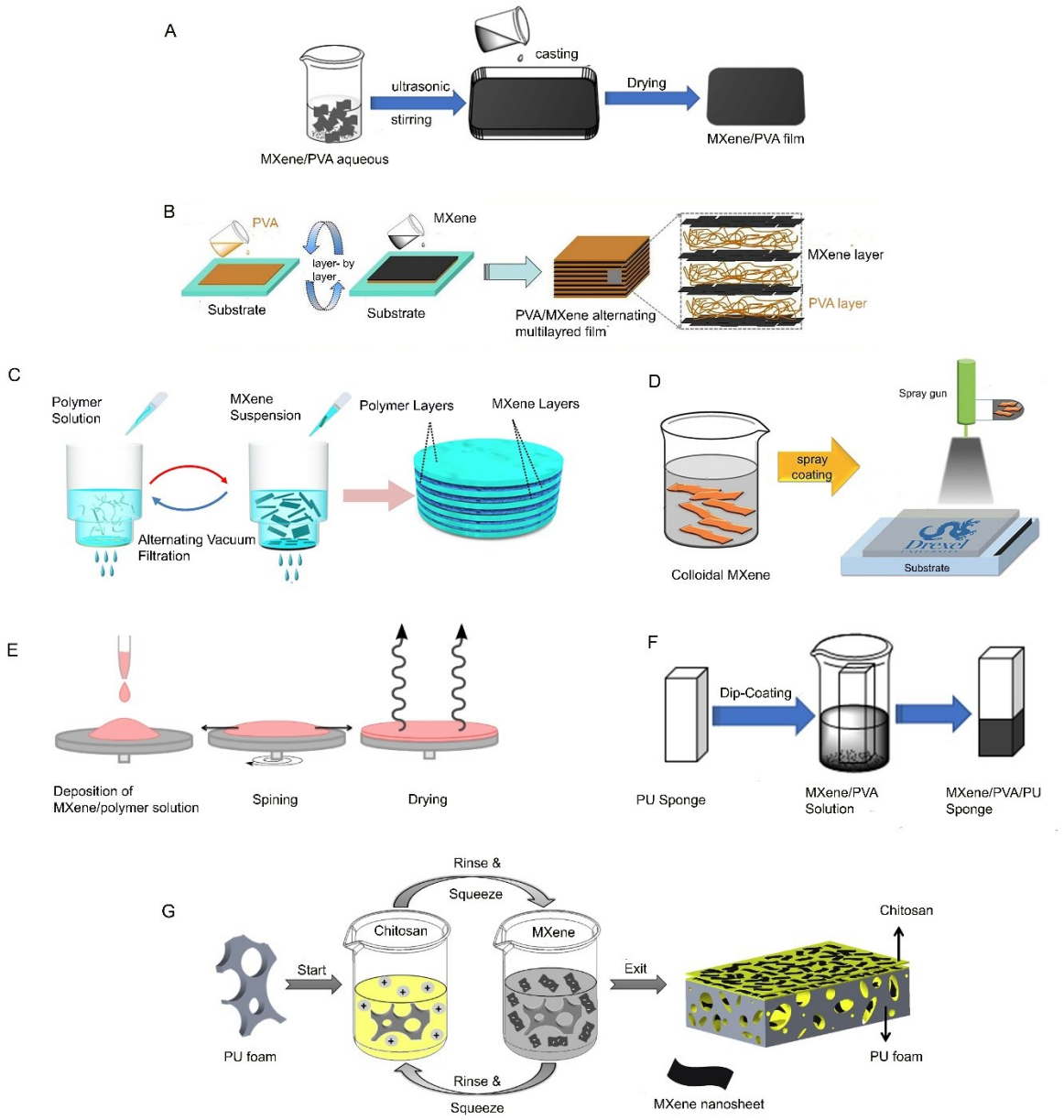

Figure 8. A) Solution casting method for the fabrication of MXene/polyvinyl alcohol thin films, Reproduced with permission from ref.[141] Copyright (2019), Elsevier. B) Multilayer casting of a polymer solution and MXene suspension, Reproduced with permission from ref.[128] Copyright (2020), Elsevier. C) Alternative vacuum filtration to produce multilayer MXene/polymer thin films, Reproduced with permission from ref. [112]Copyright (2020), American Chemical Society. D) spray coating process to make a thin film from a MXene colloid, Reproduced with permission from ref. [73]Copyright (2016), Wiley Online Library. E) Spin coating process to make a thin film from a MXene colloid or MXene/polymer mixture consisting of three steps of deposition, spinning and solvent drying. F) Dip-coating of a foam in a MXene colloid bath, Reproduced with permission from ref.[141] Copyright (2019), Elsevier. G) Layer-by-layer dip-coating process, Reproduced with permission from ref. [143]Copyright (2020), Elsevier.

MXenes inherently have negative surface charge due to the presence of hydroxyl and oxygen groups on their surface. Thus, it can participate at electrostatic assembly coating. MXenes stick to any species with positive surface charge due to electrostatic attraction. The positively charged species can be a single polycation chain (Figure 9A), a positively charged polymer particle (Figure 9B), or any other (in)organic nanoparticle with positive surface charge. As steps 3 and 4 in Figure 9A show, the coating process can be repeated several times to reach a desired thickness. Usually, layer-by-layer assembly technique works well for the fabrication of nanocomposites from components that establish electrostatic attraction with each other. The nanocomposites made from the oppositely charged species are defect-free and have high structural and mechanical stabilities. Here, we bring some examples to highlight the versatility of this technique. A tiny amount of Ti_3C_2, 0.26 vol.%, was added to a positively charged polystyrene latex to make conductive polymeric nanocomposite thin films (Figure 9B). When Ti_3C_2 content was increased to 1.9 vol.%, the conductivity increased to 1081 $S.m^{-1}$. To reach such high conductivity with a conventional compression molding method, a larger amount of single-layer Ti_3C_2 is required[148]. Another example is self-assembly between MXene flakes driven by electrostatic attraction. By grafting aminosilane coupling agents on the surface of single-layer Ti_3C_2, positively charged flakes were synthesized and retained their positive charge in a wide pH range up to ~10.5. Upon mixing with pristine single-layer Ti_3C_2 that inherently has negative surface charge, a multilayer film was formed due to the contact of these oppositely-charged species[82]. Pristine single-layer Ti_3C_2 can also participate in self-assembly or layer-by-layer assembly processes with other positively charged species such as modified carbon nanotubes[139]. One advantage of layer-by-layer assembly is its repeatability. The process can be repeated many times to form several layers of depositing material to reach a desirable thickness[139]. It is worth to mention that the concept of electrostatic assembly can be implemented via different techniques such as layer-by-layer dip, spin, and spray coatings, which are discussed in detail in Ref.[121].

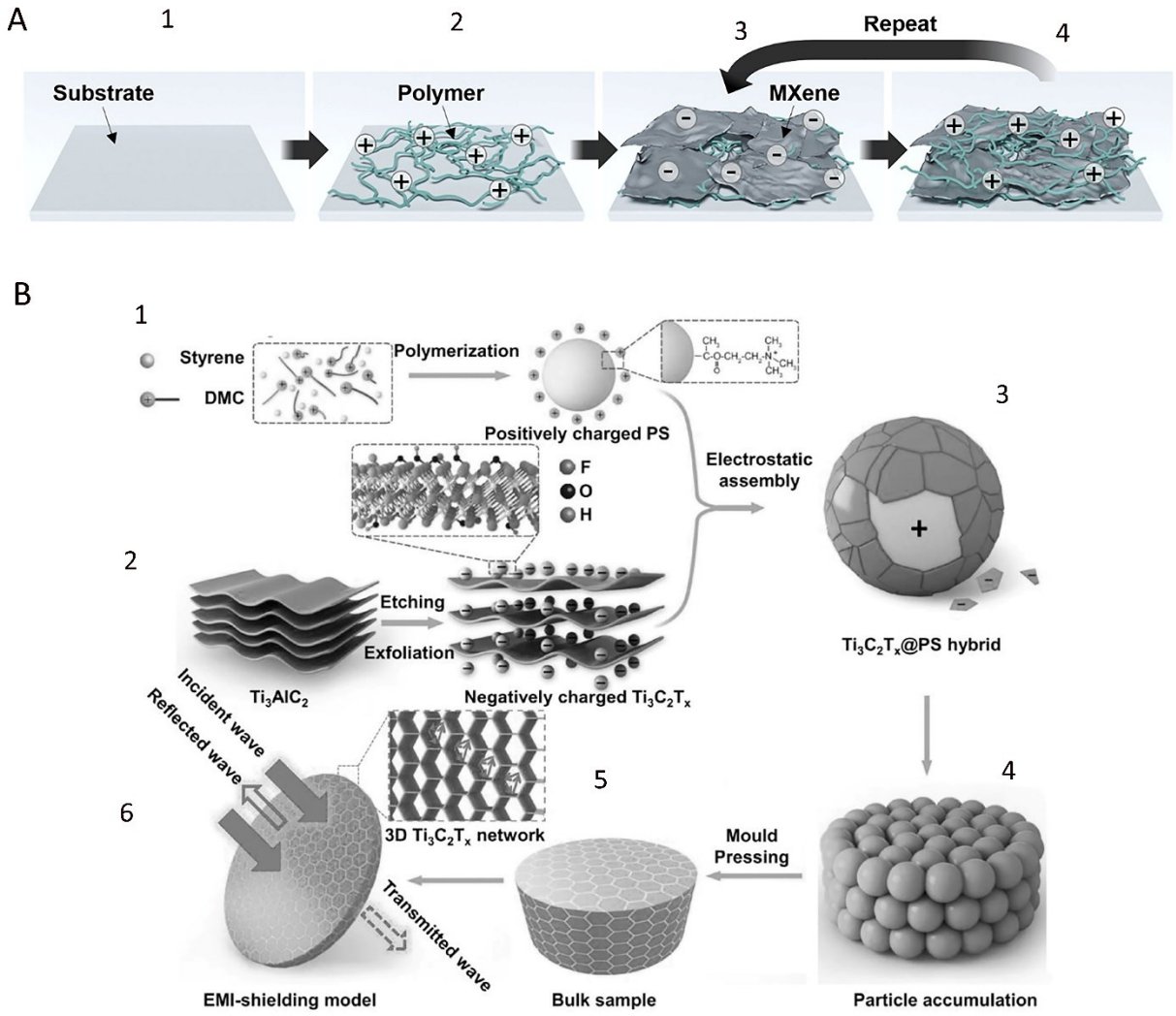

Figure 9. A) layer-by-layer assembly driven by electrostatic attraction between Ti_3C_2 with negative surface charge and a polymer chain with positive surface charge, Reproduced with permission from ref. [142]Copyright (2019), American Chemical Society. B) Self-assembly between positively-charged polystyrene nanoparticles produced by emulsion polymerization (1) and Ti_3C_2 (2) leading to a Ti_3C_2/polymer nanocomposite (3) through latex blending and filtration (4) and then molding (5) to get a thin nanocomposite film (6) for EMI shielding, Reproduced with permission from ref.[148] Copyright (2017), Wiley Online Library.

4.3 Fiber Spinning and Melt Processing

Wet spinning is a fiber processing method in which a polymer solution is passed through a spinneret and then enters into a coagulation bath containing polymer non-solvent (Figure 10A)[149]. Upon solvent/non-solvent exchange, polymer fibers are formed. To prepare a MXene/polymer

mixture for wet spinning, the solvent of polymer and dispersing medium of the MXene should be similar. If they are not similar, the solvent exchange technique allows for using a similar solvent for polymer dissolution and Ti_3C_2 dispersion. Using the solvent exchange technique, Syedin et al. [62] fabricated Ti_3C_2/PCL, Ti_3C_2/PAN and Ti_3C_2/PVDF fibers by wet spinning. Solvent was exchanged from water to DMF allowing Ti_3C_2 to be mixed homogeneously with PCL, PAN and PVDF solutions. SEM images of the obtained fibers show that Ti_3C_2 disperses in the polymers very finely and creates an electrically conductive fiber with very smooth surface morphologies. As mentioned before, solvent exchange without using sonication retains the larger Ti_3C_2 flakes and delaminates them further. This caused Ti_3C_2/PCL nanocomposite with 23 wt.% Ti_3C_2, produced by wet spinning technique, shows conductivity 1.84 mS/cm, which is ideal for applications requiring active conductive pathways[62].

Electrospinning is a widely used technique for the fabrication of nanofibers from polymer solutions or polymer melts by using electrical force (Figure 10B). The electrospinning setup consists of an injection pump, syringe, needle, high-voltage supply, and a collector. An electrical field is generated between tip of the needle and the collector by applying high voltage. Upon pumping of the polymer solution, charged threads are formed and are drawn toward the collector by electrical forces. In contrast to wet spinning, electrospinning does not require coagulation bath to solidify the ejected polymer thread from needle. Polymer solutions containing dispersed MXene flakes can also undergo electrospinning to produce composite nanofibers[150]. Conductive nanofibers from Ti_3C_2/PAA in DMF/water mixture, Ti_3C_2/PEO in ethanol/water mixture and Ti_3C_2/PVA in ethanol/water mixture were synthesized by electrospinning[151]. Different voltages and tip-to-collector distances are required to successfully run electrospinning process. Viscosity is another factor which needs to be adjusted as it significantly affects the diameter of the produced nanofibers. In MXene/polymer systems, viscosity is dependent on the concentration of the polymer as well as MXene/polymer interactions. Hydrogen bonding is one of these interactions. Hydrogen-bond-forming polymers like PVA and PEO interact with hydroxyl and fluorine groups of MXene and affect the viscosity of the system significantly. Positive effects of single-layer MXene on nanofiber properties, like conductivity, can be observed at concentrations as low as 1 wt.% with respect to polymer[151].

MXene coated nanofibers produced by electrospinning can be used for the fabrication of wearable electronics and sensors. To develop such devices, MXene can be dispersed in an aqueous solution containing a water-soluble polymer such as PEO and then coated on a substrate like PET by electrospinning. The coated yarns can be used for the manufacturing of wearable electronic and sensors [152]. These wearable devices have enough mechanical strength to keep their electroactivity even after thousands of bending cycles. An advantage of MXene/polymer electrospinning process is the self-orientation of 2D MXene nanosheets in the flow direction (Figure 10B). This phenomenon increases the chance of inter-connection of MXene flakes in a nanofiber and thus electrically conductive nanofibers can be obtained at lower MXene concentrations compared with a process in which self-orientation does not happen[153]

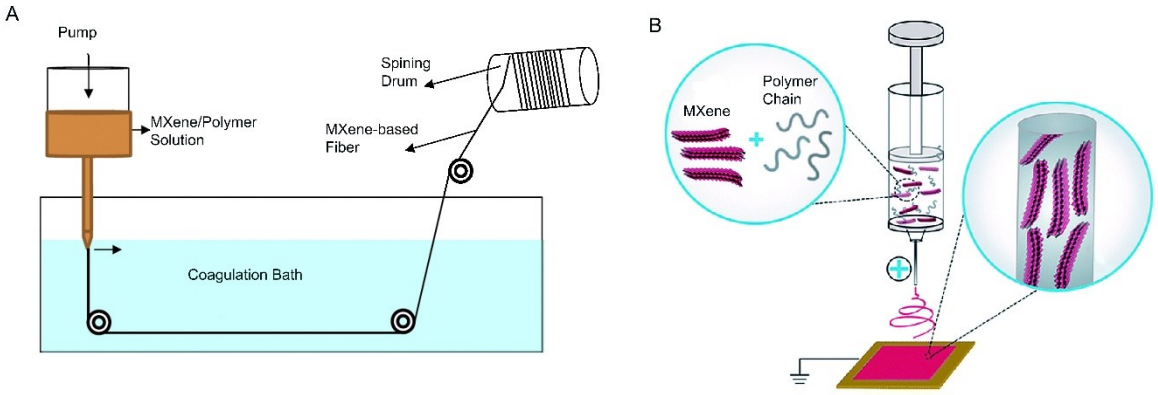

Figure 10. A) Wet spinning setup for the production of MXene-based nanocomposite fibers, Reproduced with permission from ref. [149]Copyright (2015), Elsevier. B) Electrospinning causing the orientation of MXene sheets along the axis of the nanocomposite nanofibers, Reproduced with permission from ref.[150] Copyright (2019), Royal Society of Chemistry.

Compression molding is another method of nanocomposite manufacturing. In this method, the applied pressure reduces contact resistance between MXene nanosheets in a nanocomposite. It was used to enhance the conductivity of films made from a single-layer Ti_3C_2/polystyrene composite[148]. In this study, the mixture was compression molded for 30 min at 130 ℃ under pressure 500 MPa, and no Ti_3C_2 degradation was reported[148]. In another study[154], multilayer Ti_3C_2/UHMWPE was compression molded. A Ti_3C_2 powder was mixed with a UHMWPE powder by a high-speed mixer, and the mixture was then warmed up at a rate of 10 ℃/min to 220 ℃ and kept at that temperature for 30 min under a pressure of 10 MPa. Again, no thermal degradation of

multilayer Ti_3C_2 was reported under this processing condition[154]. Compression molding of multilayer Ti_3C_2/PVDF at 190 ℃ for 20 min at a pressure of 5 MPa has also been practiced[155]. These studies showed that Ti_3C_2 does not degrade in high temperature processes. An advantage of compression molding is that the thickness of the MXene/polymer films can be easily adjusted by controlling the hot-pressing parameters like pressure and temperature[105].

Extrusion and melt blending are other techniques of nanocomposite manufacturing. Extruders can be used for polymer compounding, adding an additive to a polymer, and dispersing nanoparticles within a polymer. Using this technique, Cao et al.[156] added Ti_3C_2 into LLDPE where no degradation of Ti_3C_2 is reported under this extrusion process[156]. Using a melt blending technique, Sheng et al.[105] blended PEG-treated-Ti_3C_2 with TPU in a Brabender Plasticorder mixer working at 180 ℃ for 6 min with a screw speed 60 rpm. They then compression molded these samples at 180 ℃ for 10 min at the pressure of 10 MPa. They did not report a need for an inert gas stream to prevent Ti_3C_2 degradation. These studies indicate that Ti_3C_2 keeps its outstanding physical, chemical and mechanical properties even after being processed at those high temperatures and pressures[105].

5 Applications Based on MXene Properties

In this section, various applications of MXene-based devices are discussed. These applications include textile engineering, fire retardancy, sensors, self-healing coatings, and electromagnetic interference shields. For each of these applications, a suitable processing method is described. We categorize applications of MXene/polymer devices based on each MXene property that is of interest.

5.1 Heat Generation Capability

5.1.1 Joule Heating and Wearable Heaters

Wearable heaters can appear in the form of a cloth, bandage, or knee brace made from thin films or fabrics that produce heat upon applying an external stimulus like sunlight or voltage. Before the discovery of MXenes, other materials like graphene, CNT, silver nanowires and copper wires had been used for Joule heating applications[157-159]. However, the discovery of MXenes revolutionized these applications. For the sake of human safety, it is important to develop Joule

heating clothes that generate enough heat by applying low voltages. Fortunately, MXene-based fabrics are able to generate huge amount of heat and provide temperatures as high as 150 ℃ just by applying a voltage as low as 6 V. An ordinary cotton fabric can be converted to a Joule heating cloth by spray-drying of a Ti_3C_2 colloid on its surface. Zhang et al.[158] used a spray gun and a hairdryer to repeat a spray-drying cycle for several times to produce a single-layer Ti_3C_2-based Joule heating fabric (Figure 11A). The process is robust and allows for mass production of Joule heating fabrics.

In MXene-based Joule heating fabrics, the amount of generated heat increases with voltage and with the amount of incorporated MXene. Figure 11B-1 shows that the temperature of a cotton fabric containing 6 wt.% Ti_3C_2 goes from room temperature to 150 ℃ in less than one minute upon applying a voltage of 6 V. The temperature stays at 150 ℃ as long as the voltage is applied. When these Ti_3C_2-containing cotton fabrics are worn by a human, it is possible to locally warm a part of the body which is in contact with the fabric (Figure 11B-2). The amount of incorporated MXene to induce Joule heating property is usually not high to impair the breathability of the fibers.

Thin transparent films of PU containing AgNP@MXene can generate heat under sunlight [108]. Figure 11C shows a 100-micron thick film that attaches to human's skin very easily. The film contains only 0.08 wt.% of the AgNP@Ti_3C_2 [108]. The ability of the film to convert sunlight to heat was monitored in an experiment in which the ambient temperature was -12 ℃ and the human's skin temperature was initially 18.3 ℃. The figure shows that the irradiation of sunlight for 1 min increased the temperature of the bare skin to 18.8 ℃ and the temperature of the part covered by the PU nanocomposite film to 24.3 ℃. This experiment shows the effectiveness of AgNP@Ti_3C_2/PU nanocomposites as a skin-mountable, sunlight-driven wearable heater[108].

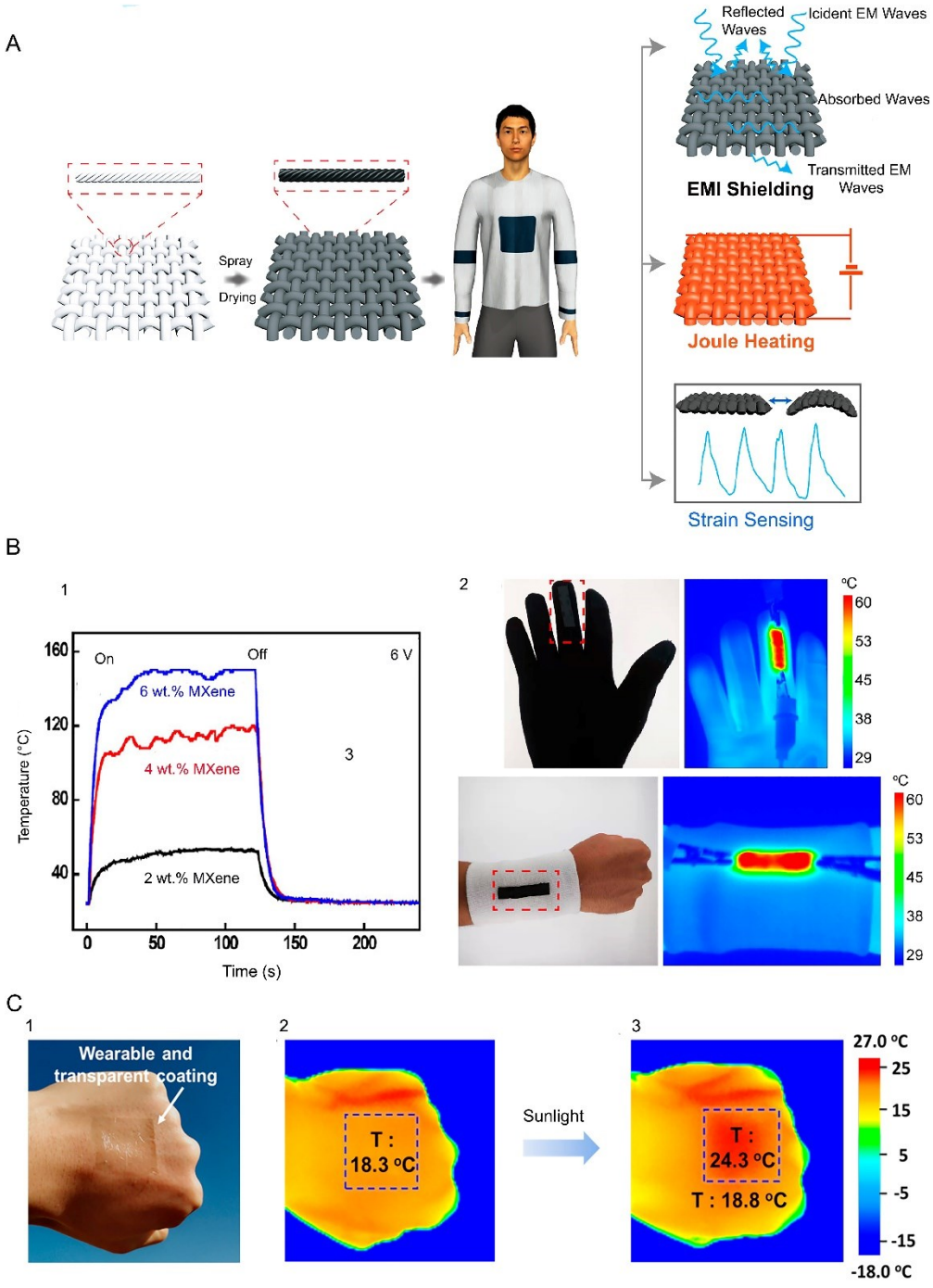

Figure 11. A) Coating of a cotton fabric with colloidal Ti_3C_2 and its applications as an EMI shield, a Joule heater and a motion sensor. B) Joule heating ability of Ti_3C_2-coated cotton fiber which reaches to 150 ℃ after 1 min under applied voltage 6 V (1) and local heating of a body part when the fabric worn by a person (2), Reproduced with permission from ref.[158] Copyright (2020), American Chemical Society. C) transparent sunlight-driven Ti_3C_2-based wearable

heater mounted on a human's hand, Reproduced with permission from ref.[108] Copyright (2019), American Chemical Society.

5.1.2 Self-healing Coatings

Nature has inspired engineers to develop self-healing coatings that are able to repair their physical damages and recover their original functionality without any intervention or with minimum intervention[160]. There are mainly two underlying mechanisms for self-healing: the formation of dynamic covalent bonds and the establishment of non-covalent interactions. Imine bonds, coordination bonds, bonds formed in the Diels-Alder reaction, Boronate ester bonds, and disulfide bonds are some examples of dynamic covalent bonds. Electrostatic interactions, hydrophobic interactions, host-guest interactions, and hydrogen bonds are examples of non-covalent interactions that can be used for the formation of self-healing coatings (Figure 12A)[161]. To have a real self-healing polymer coating, remote activation and suitable mechanical properties are required.

Any functional filler with the capability of converting light, electrical field, or (electro)magnetic field into heat is favorable for the self-healing application. The incorporation of a MXene into a polymeric coating not only increases the mechanical properties of the coating, but also enhances its light-to-heat conversion efficiency, which is of interest in self-healing coatings. In addition, MXenes have hydrogen-bond-forming groups on their surface that can be exploited to develop self-healing polymer coatings. A necessary condition to have a self-healing coating is the reversibility of polymer network. A crosslinked polymer network should dissociate to let polymer chains move to fill the damaged part of the coating under an external stimulus like heat or light. Upon the removal of the stimulus, the crosslinked polymer network should then be re-formed. By the addition of Ti_3C_2 to PVA, self-healing hydrogels were developed by hydrogen bond formation between surface groups of the Ti_3C_2 and hydroxyl groups of the polymer [162]. Single-layer MXene/epoxy self-healing coatings are also prepared using the Diels-Alder reaction [163]. Based on this reaction, a crosslinked network of an epoxy resin dissociates at high temperatures around 150 ℃ and forms again when the coating cools down (Figure 12B). As this figure shows, an epoxy oligomer bearing dangling furan rings is formed by reaction between DGEBA and FA. In the presence of Ti_3C_2, this oligomer reacts with BMI at 60 ℃ for 12 hours to form a crosslinked

network via a reaction between furan rings and maleimide of BMI. The same reaction is reversed at 150 ℃.

Light-induced self-healing coatings are much more valuable than thermally-induced self-healing coatings, as they allow for repairing damaged parts of the coatings remotely. In such a coating, solar radiation can be used to stimulate the coating and repair the damaged area. As Ti_3C_2 is an excellent photothermal filler for both near infrared and solar light, a 3-minute 3.28 $W.cm^{-2}$ solar irradiation has been found to increase temperatures of epoxy coatings with 0.57, 1.42, 2.8 and 5.44 wt.% Ti_3C_2 from room temperature to 33.1, 43.4, 68.4, and 125.9 ℃, respectively. Figure 12C shows the trend of temperature increase of the epoxy coating containing different amounts of Ti_3C_2 versus sunlight irradiation intensity. Thanks to remote-triggered self-healing capability, a crack in a Ti_3C_2/epoxy coating containing 2.8 wt.% Ti_3C_2 can be fixed after 10 min by the irradiation of a 4 W. cm^{-2}-intensity solar light[163].

As mentioned before, MXene-based hydrogels with a double network of PVA and PAAm show self-healing properties due to the presence of borax, $Na_2B_4O_7.10\ H_2O$. In the presence of borax, dynamic crosslinking bonds between hydroxyl groups of PVA and tetrahydroxyl borate ions are formed. In addition, some interactions between PVA, multilayer MXene and solvent-exchanged EG endow the hydrogel with self-healing property. Similarly, in hydrogels made from a tertiary polymer network of dopamine grafted sodium alginate, phenylboronic acid grafted sodium alginate and PAAm, the presence of B-O-C leads to the formation of dynamic covalent ester bonds which endow the hydrogel with self-healing abilities[113]. Ti_3C_2-based hydrogels are conductive where their conductivity correlates with their self-healing abilities. Any rupture or damage in the hydrogels deteriorates the continuity of electron-conducting passages and consequently reduces the conductivity of the hydrogel. On the other hand, reforming the passages by taking the advantage of the self-healing properties facilitates electron transport, and increases the conductivity of the hydrogel. As Figure 12D shows, un-damaged hydrogel is conductive and transfers electrical current in a circuit to light up an LED lamp. However, the light turns off when the hydrogel is cut. The lamp turns on again as the Ti_3C_2-based hydrogel wire heals. This example shows the high capability of the hydrogel for the recovery of the damaged parts and the retrieval of its electrical properties[69].

Thermoplastic polymers can be used for developing of a self-healing coating as well. The chains of this family of polymers have enough mobility to move and fill a crack or ruptured area

at a temperature higher than their melting point. Thus, adding effective light-to-heat converting nanoparticles to a thermoplastic material and taking the advantage of visible or infrared light result in the fabrication of self-healing thermoplastic coatings. For example, AgNP@single-layer-MXene was added to PU matrix with melting temperature ~ 95 ℃. The presence of 0.16 wt.% of the nanoparticle in PU coating with the thickness of 100 micron, caused temperature increase to 106 ℃ and 145 ℃ after 1 and 5 min, respectively, under the irradiation of Vis-IR light with 600 mW. cm^{-2} intensity. This excellent photothermal conversion property of AgNP@MXene originates from the synergistic effects and cannot be obtained by using a single-layer MXene or silver nanoparticles alone[108]. The presence of silver in AgNP@MXene helps this hybrid nanoparticle to absorb more light in the wavelength range 400 to 650 nm. Driven by its plasmonic effect, the silver part of the AgNP@MXene, similar to its MXene part, converts light to heat and then transfers the generated heat to MXene sheets which are located in their close vicinity. Moreover, due to high aspect ratio and thermal conductivity of MXene sheets, the generated heat is distributed homogeneously in the whole of the coating. By this mechanism, it is shown that healing efficiency of transparent PU coatings containing just 0.16 wt.% AgNP@MXene is 98%[108].

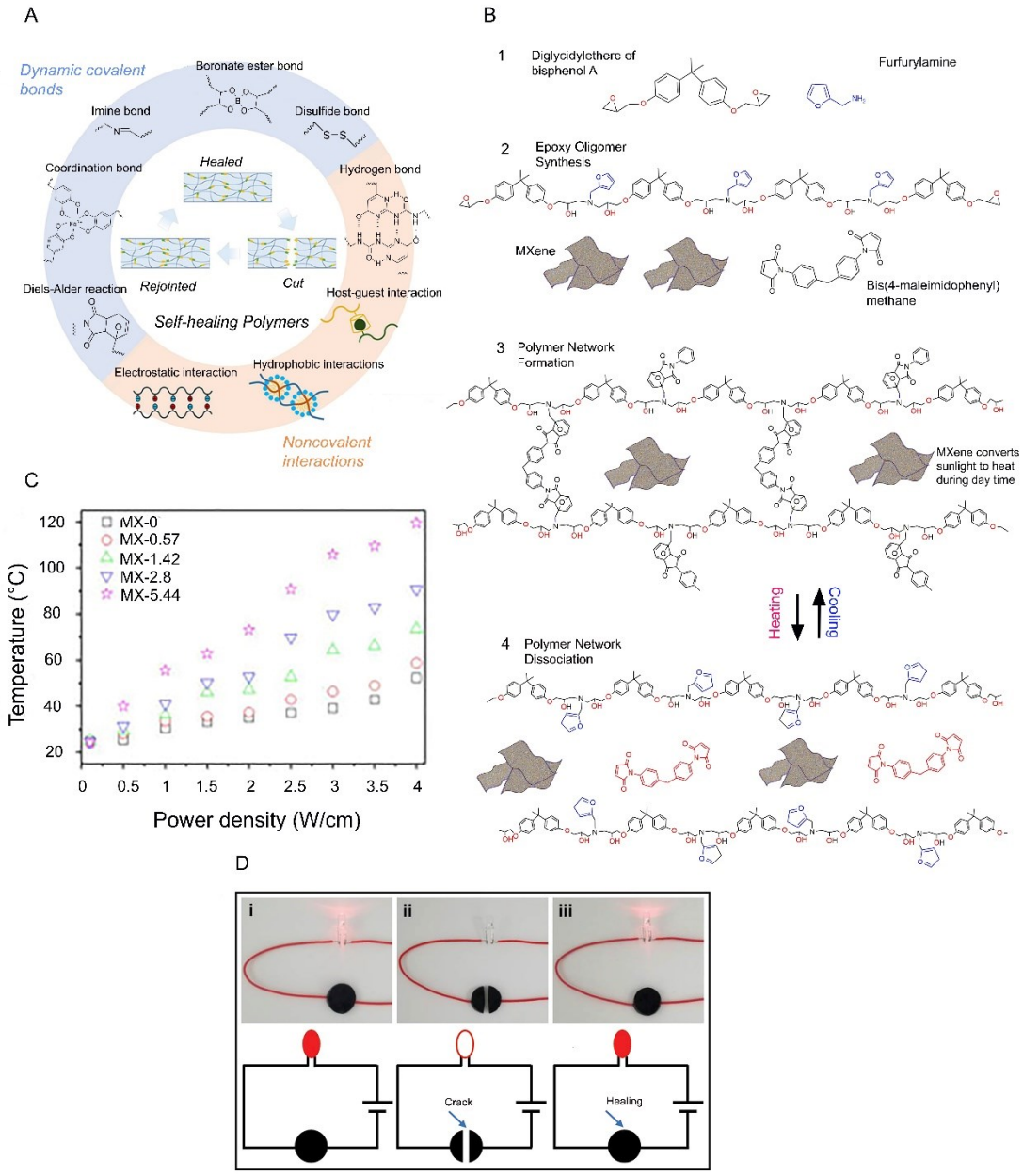

Figure 12. A) Various dynamic covalent bonds and noncovalent interactions for developing self-healing coatings, Reproduced with permission from ref.[161] Copyright (2019), Elsevier. B) Monomer used for epoxy oligomer synthesis (1), the oligomer mixing with Ti_3C_2 (2), crosslinking to form a polymer network (3), dissociation of polymer network upon temperature increase to develop an Ti_3C_2/epoxy self-healing coating (4). C) Temperature increase in an epoxy coating containing different amount of Ti_3C_2, Reproduced with permission from ref.[163] Copyright (2018), MDPI. D) Ability of a hydrogel for passing of electrical current (i), its inability when it is damaged (ii), and retrieving its conductivity to pass electrical current after self-healing (iii), Reproduced with permission from ref.[69] Copyright (2019), Wiley Online Library.

5.2 Thermal Conductivity and Heat Stability

5.2.1 Thermally Conductive Nanocomposites

MXene has excellent thermal conductivity along with exceptional electrical conductance. MXene addition to polymers which are usually thermally insulators can convert them to conductive counterpart. Compared with graphene-based nanocomposites that showed typical thermal conductivities of 0.14 to 0.41 W/mK for a 2 wt% loading[164, 165], MXene-based polymer hybrids have exhibited a slightly better thermal properties of 0.5 W/mK with less filler loadings,[166,167]. Thermal conductivity requires strong interactions between the polymer and the additives to facilitate the kinetics of heat transfer. MXenes' high thermal conductivity significantly overcomes the thermal resistivity of polymeric matrix leading to a uniform and high thermal conductivity, when the concentration of MXene is high enough to form a network.

To develop an efficient thermally conductive system, it is important to make a connection between MXene flakes inside the nanocomposite to form a MXene network. The concentration at which network formation happens is called percolation concentration. To have a percolation at a low concentration, it is recommended to embed a 3D network of oriented MXene flakes inside a polymer matrix, rather than just randomly dispersing MXene flakes, Figure 13A. As it was mentioned before, the synthesis of a unidirectional, 3D MXene structure is possible by freeze-drying. It is shown that such 3D oriented structure provides excellent heat transfer pathways in a polymer matrix (Figure 13B). The incorporation of just 0.7 wt.% of single-layer Ti_3C_2 into PDMS, a thermally insulator polymer, improved the thermal conductivity of the polymer by 220% and its electrical conductivity by 14 orders of magnitude[117]. Yan et al.[168] deposited silver nanoparticles on the surface of single-layer Ti_3C_2 and then connected Ti_3C_2/Ag nanoparticles to each other by using silver nanowires through a hot pressing technique. The silver nanoparticles on Ti_3C_2 surface acted as welding points for the attachment of the silver nanowires. Yan et al.[168] reported that the thermal conductivity of an epoxy nanocomposite containing just 15 wt.% of the Ti_3C_2/Ag nanoparticles is 100% higher than that of pure Ti_3C_2[168]. Liu and Li[169] reported that adding 12.71 wt.% PVA into Ti_3C_2 decreased the thermal conductivity of Ti_3C_2 from 55.2 to 47.3 W/m.K, which is still higher than many materials such as stainless steel, Fe, SiO_2, Al_2O_3. This indicates that the Ti_3C_2/PVA nanocomposite can ideally replace many materials that are used in thermal conduction applications[169].

Having high thermal conductivity is advantageous when a nanocomposite is designed to work as EMI shielding material[170]. In fact, high thermal conductivity helps to dissipate EM energy as heat quickly. For example, Ti_3C_2/PVDF nanocomposites are used as EMI shielding materials. The thermal conductivity of the nanocomposite with 22.55 vol.% Ti_3C_2 is 0.766 W/m.K, which is four times higher than that of pure PVDF. In these nanocomposites, the heat generated upon the absorption of EM wave dissipates quickly due to the existence of phonon transfer pathways. By quick heat dissipation here we mean that their cooling thermogram shows an exponential decay with time[155].

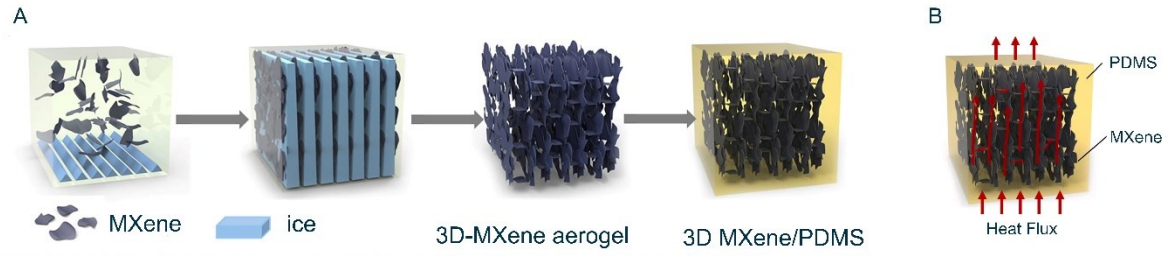

Figure 13. A) The formation of a 3D MXene network by freeze-drying technique and then embedding it in a PDMS matrix. B) Heat transfer pathways generated in a PDMS matrix by a MXene network, Reproduced with permission from ref.[117] Copyright (2020), Elsevier.

5.2.2 Anti-dripping, Flame-retardancy and Smoke Supprsive Nanocomposites

In order for polymer nanocomposites to have more real-life applications, their thermal properties should be improved[171-173]. When plastics burn, the combustion products can form a liquid droplet which possibly separates from the bulk of the burning material. This unfavorable phenomenon is called dripping which is dangerous as it can spread fire and accelerate fire growth[174]. Anti-dripping additives are usually added to virgin polymers to improve their resistance during a fire incident. MXenes can work as an excellent anti-dripping additive. The addition of single-layer Ti_3C_2 to PVA thin films and PU sponges improved anti-dripping properties of both polymers[141].

The thermal behavior of MXenes and how they increase thermal resistance of polymer nanocomposites can be explained as follows. Upon heating of Ti_3C_2, firstly entrapped water molecules between MXene flakes evaporate. This usually happens up to 130 ℃. In the next step,

when temperature increases up to 350 ℃, surface functional groups of Ti_3C_2 including O, F and OH are removed according to:

$$Ti_3C_2T_x \rightarrow Ti_3C_2 + T_x$$

In the next step when temperature goes up to 550 ℃, the oxidation of Ti_3C_2 to TiO_2 happens:

$$Ti_3C_2 + 3O_2 \rightarrow 3TiO_2 + 2C$$

Figure 14A schematically shows the conversion of Ti_3C_2 via combustion in air. Thus, when a polymer nanocomposite containing Ti_3C_2 burns in air, Ti_3C_2 oxidizes into TiO_2 which forms a protective layer on the surface of the nanocomposite endowing excellent anti-dripping properties. Figure 14B also schematically shows the formation of this protective layer.

PU is used in many laboratories, industrial areas, and residential places. However, its flammability and rapid flame spread have been always a concern. Ti_3C_2 has been used to develop self-extinguishing PU foams. Ti_3C_2 as a part of intumescent flame-retardant mixture was coated on PU foams by spray coating. The presence of Ti_3C_2 synergistically helps to the formation of a barrier layer during a fire incident. This layer which is called intumescent char layer works as an insulator and sticks to the surface of PU. Ti_3C_2 flakes work as a compact protective layer during combustion and suppress oxygen, fuel and heat transfer between PU foam and the fire zone by creating a tortuous barrier layer. A burning PU foam coated by Ti_3C_2 self-extinguished after 10 seconds and did not reignite. However, the same PU foam without a Ti_3C_2 coating burned out completely after 20 seconds[98].

When using a MXene as a flame-retardant agent, it is important to incorporate an optimal amount of MXene. An excess amount of MXene in an intumescent flame-retardant mixture decreases MXene's efficacy for flame retardancy, smoke suppression, and self-extinguishment. It increases thermal conductivity of the protecting layer, which is unfavorable here, and outweighs the favorable barrier effect of the MXene. In addition, it decreases the interfacial adhesion of the char layer and consequently lessens its fire protection efficiency. Excellent fire protection properties are usually obtained only by adding 1 wt.% single-layer MXene, while the addition of more than 2 wt.% is not recommended[98]. Regarding the smoke suppression ability of single-layer Ti_3C_2, it is believed that during the combustion, the Ti_3C_2 converts into anatase TiO_2 in-situ where the latter reduces the amount of CO_2 and CO emissions during burning[98]. In a similar research[143], to improve the thermal stability (flame-retardancy and smoke suppression) of PUF, a single-layer Ti_3C_2/chitosan coating was applied by a layer-by-layer dip coating process. It was found that 8

bilayers of Ti_3C_2/chitosan endow the best flame retardancy and smoke suppression as the total smoke and heat release decreased by 66.5% and 71.1% respectively, compared with neat PUF. Similar to previous reports, the presence of Ti_3C_2/chitosan improved char layer formation during the combustion, which works as a protective layer and prevents from the release of combustion volatile products to the outer environment[143]. The addition of PEG-treated Ti_3C_2 to TPU also increased onset degradation temperature, maximum degradation temperature as well as char formation amount [105]. Technically, onset degradation temperature is a temperature at which 5 wt.% weight loss is observed. Single-layer Ti_3C_2/PI aerogel also showed anti-flammability properties[119]. Pan et al.[175] showed that the addition of Ti_3C_2 into PVA retards thermal decomposition of the nanocomposite and significantly reduces the release of hydrocarbons and carbonyl products formed by the combustion of the PAV matrix[175]. Si et al.[97] used a grade of single-layer Ti_3C_2 modified with a cationic surfactant to enhance flame-retardancy and smoke suppression of polystyrene. They reported improvements in the latter properties due to enhanced dispersion of the modified Ti_3C_2 in the polystyrene matrix, thanks to the presence of the cationic surfactants.

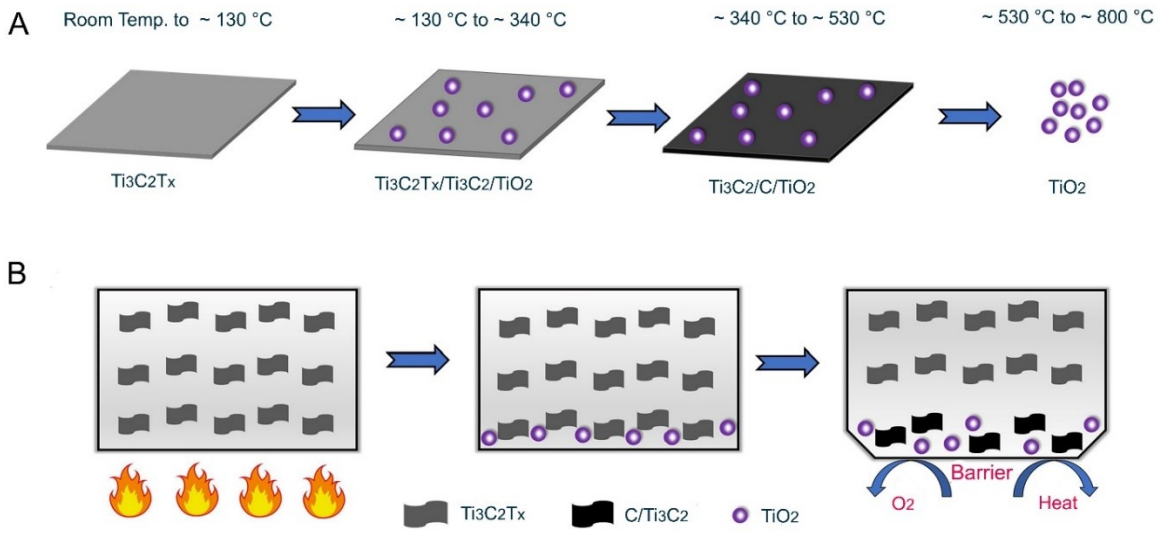

Figure 14. A) Conversion of Ti_3C_2 to TiO_2 via combustion in air. B) Formation of a fire protective layer, made mainly from TiO_2, in a Ti_3C_2/polymer nanocomposite which undergoes combustion in air, Reproduced with permission from ref.[141] Copyright (2019), Elsevier.

5.3 Electrical Conductivity

5.3.1 Conductive Films

Polymers in general are electrical insulators. However, they can turn into conductive nanocomposites by the addition of conductive nanomaterials like MXene. When conductive nanoparticles are added to polymers, there is a concentration at which filler percolation happens. This causes an insulating polymer turns into a conductive material with an isotropic electronic conductivity. A conductive polymer nanocomposite can be fabricated with lower MXene contents if MXene lateral size increases. Ti_3C_2 in acrylic polymers has shown a percolation threshold as low as 6-7 vol.%[127]. Conductive, flexible, transparent, and self-standing nanocomposite films are obtained by adding 1.7 vol.% of single-layer Ti_3C_2 to the copolyimide-6,10, resulting in improved conductivities and flexibility[126].

Water-soluble polymers are a decent option for the fabrication of the MXene-based conductive nanocomposite thin films. For example, water-soluble PAAm-based nanocomposites exhibited a conductivity of 3.3×10^{-2} S/m by incorporating 6 wt.% Ti_3C_2[176]. Reaching a desirable conductivity with a smaller amount of MXene is feasible by replacing multilayer MXene with single-layer one. The intercalation of Ti_3C_2 by intercalants like DMSO facilitates the production of single-layer MXene. The addition of intercalated MXene to a polymer solution and then processing of such a system leads to a conductive polymer film with isotropic properties[176]. Surface chemistry of Ti_3C_2 is an important aspect, which affects the conductivity of Ti_3C_2/ polymer nanocomposites. The removal of surface functional groups from the surface of MXene eliminates electron transfer resistance sites, which ultimately increases the conductivity of a Ti_3C_2/polymer nanocomposite. Conductive Ti_3C_2/epoxy nanocomposites have been developed for EMI shielding application. The epoxy resin containing 15 wt.% annealed Ti_3C_2 shows 176% and 37% higher electrical conductivity and EMI shielding, respectively, compared with an epoxy resin containing 15 wt.% pristine single-layer Ti_3C_2 [48]. As discussed before, annealed Ti_3C_2 does not have OH or F groups. Some other examples of hybrid systems to fabricate conductive nanocomposite films are Ti_3C_2/PI[119], Ti_3C_2/NR[147] and Ti_3C_2/C hybrid foam/epoxy [177]. In general, the addition of MXenes to polymer matrices can be similar to other nanomaterials. However, recent studies on Ti_3C_2 MXene exhibited the highest electrical conductivity of 15,000 to 20,000 S/cm [66, 178] obtained up to now from any solution processed 2D material. This high conductivity

outweighs the advantages of MXenes over other nanomaterials, including reduced graphene oxide, for conductive nanocomposite fabrication.

5.3.2 Sensors

5.3.2.1 Motion Sensors

Sensitive tools for the cognition of molecular species, and tiny movements as well as effective algorithms are required to monitor a process and safely operate it [179, 180]. The development of hybrids materials containing low-defect fillers for sensing application is widely investigated to fulfill the latter purposes. Defect-free MXene can be synthesized via a top-down synthesis approach with mild etching procedures. A relative advantage of MXenes over other materials such as graphene[24] is its easy and cost-effective synthesis with minimal structural defects. MXene-based nanocomposites are excellent motion detectors with capability to detect both intensity and direction of a motion. Their working principle is based on change in resistivity upon compression and tensile deformations. Under tensile deformation, the distance between MXene flakes in a MXene-based sensor increases which results in less contact between MXene flakes, harder electrical charge transport and consequently lower electrical conductivity. On the other hand, under compression deformation, the distance between MXene flakes decreases which means higher chance of charge transport and thus higher electrical conductivity. Usually MXene-based hydrogels are used as a sensor. They are sensitive enough to show lower or higher electrical conductivity, depending on the direction of a moving object on their surface. For example, when a cylinder moves on the surface of a MXene-based PVA hydrogel, it shows increase in electrical conductivity if the cylinder moves in *x*-direction while shows decrease in electrical conductivity if the cylinder moves in *y*-direction. The reason is that movement in *x*-direction creates compression deformation and movement in *y*-direction creates tensile deformation. In addition, the extent of change in the electrical conductivity varies upon change in the speed of the moving cylinder. These observations confirm that PVA hydrogel sensors containing single-layer MXene are both speed and direction detectors. These hydrogels easily attach to various parts of human's body without any adhesive. They were attached to fingers, hands, and forehead of a human and successfully detected different movements of each of these parts (Figure 15A). For example, when a finger bends, resistivity increases by 20% (Figure 15A-1). Another interesting application of these hydrogels is signature detection (Figure 15B). Each person has his own unique style of signing

and writing. This means that the amount of the pressure that a person puts on a pen or his speed of signing vary from another one. This means each person creates a distinct pattern of change in electrical conductivity if he signs on a piece of such hydrogels sensors[162]. Figure 15B also shows that writing the word "ok" with different styles leaves a different pattern of change in resistivity.

MXene-based hydrogel sensors made from a tertiary polymer network of dopamine grafted sodium alginate, phenylboronic acid grafted sodium alginate and PAAm were synthesized. Again, the deformation of the sensor changes its electrical conductivity. An important parameter in designing MXene-based sensors is the amount of the added MXene. As mentioned before, deformation changes the distance between MXene flakes in a polymer network. If flakes get close to each other upon deformation, conductivity increases and vice versa. If more-than-required MXene is loaded to a polymer network, the flakes are always in contact with each other regardless of the deformation extent. Thus, the system usually shows high conductivity and consequently is not sensitive enough to work as a good sensor. By adjusting the amount of single-layer Ti_3C_2, Wu et al. developed a wearable, self-adhesive, healable epidermal sensor which is able to detect very tiny movements in chest upon breathing[113].

MXene-based hydrogels made from a double network of PVA and PAAm can act as a motion-detection sensor. As before, relative electrical resistivity changes upon sensor deformation due to change in distance between MXene flakes and consequently change in the ease of electron transfer. In fact, the sensing response is defined as $R/R_0\,(\%) = ((R-R_0)/R_0) \times 100(\%)$. In this equation, R_0 is orginal resitance of the sensor before deformation and R is the resistance of the sensor after the deformation. Sensors developed from single-layer Ti_3C_2/PVA/PAAm are such sensitive that can detect the motion of a throat during swallowing or motion of a finger upon bending[69]. Three more examples are: Ti_3C_2/chitosan nanocomposite biosensors to detect organophosphate based pollutant in water and foods[181], single-layer Ti_3C_2/PI aerogel sensors for motion detection[119], and single-layer Ti_3C_2/ cellulose fibers as pressure sensors.[144]

5.3.2.2 Humidity Sensors

MXene/polymers are used as humidity sensors and their underlying mechanism is similar to motion sensors. As Figure 16A shows, these sensors are sensitive enough to detect humidity change by human breathing. Upon change in humidity, water molecules can be adsorbed or desorbed reversibly into a MXene-based sensor which changes the interlayer distance between

single-layer Ti_3C_2 flakes. Consequently, this affects the electron tunneling resistance. Figure 16B shows a multilayer structure of Ti_3C_2/PDAC made by layer-by-layer dip coating technique used for humidity sensing. When humidity is low, the interlayer distance decreases and thereby resistivity (conductivity) decreases (increases). In the same figure, equivalent electrical circuit corresponding to dry and humid states are shown as well. R_{t1} and R_{t2} resistances are added to the circuits when a sensor experiences a humid environment. Another assumption is that water (polar molecules) adsorbed by Ti_3C_2, at a high humidity environment, interacts with surface functional groups of Ti_3C_2 and decreases the conductivity. However, experimental results show that change in interlayer distance upon water adsorption is the dominant mechanism in decreasing the conductivity rather than water interaction with single-layer Ti_3C_2 surface functional groups [142]. One of the outstanding features of Ti_3C_2-based humidity sensors is their fast response and recovery times. They are quick enough to distinguish inhalation/exhalation rates of a person during running from walking[142]. The results of the sensors are accurate enough as they show that both frequency and domain of the resistivity signal are low when the person is walking. However, they increase when that person starts to run and again decrease when the person walks again[142].

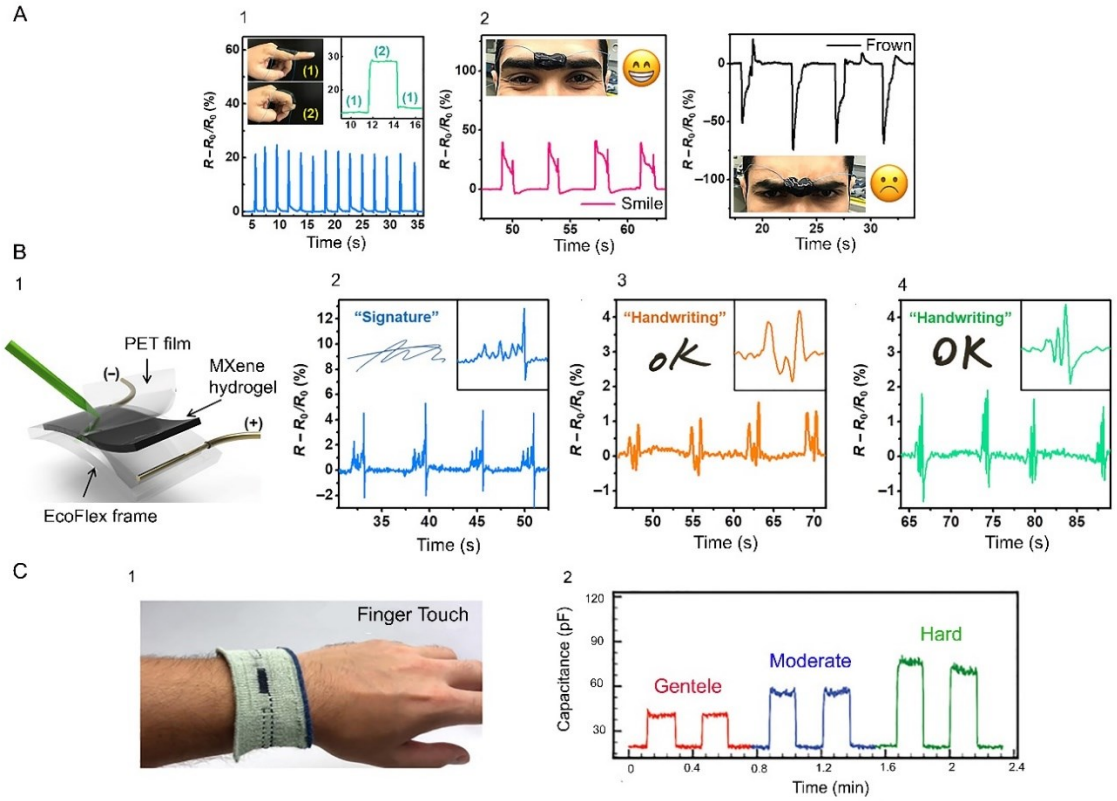

Figure 15. A) PVA/Ti_3C_2 sensor is able to detect bending of a finger (1), and forehead movement (2). B) PVA/Ti_3C_2 hydrogel assembly (1) used as surface sensor which is able to generate a specific resistivity pattern upon signing on the surface (2) and also generate different resistivity patterns upon changing the writing style of the word "OK", Reproduced with permission from ref.[162] Copyright (2018), Science. C) pressure sensors made from Ti_3C_2-containing fabric worn by a person (1) and its capacitance sensitivity to a finger touch (2), Reproduced with permission from ref.[144] Copyright (2019), Wiley Online Library.

5.3.2.3 Bio-electrochemical Sensors

MXene-based biosensors are used for measuring the concentrations of urea, uric acid, and creatinine in the blood of a patient continuously and online during a hemodialysis treatment. This online monitoring system determines the required dialysis time to reach an acceptable level of the species in a patient's blood. Liu et. al.[182] developed a bio-electrochemical sensor which consists of four different layers for blood analysis. The top layer receives the blood and sends it to the second layer, which works as a dialysis member and lets just some species in the blood (Da <1000) to reach the third layer. The third layer contains some microchannels and a detection chamber that collects the species that had the chance to pass through the second layer. The sensing electrode which contains single-layer Ti_3C_2 is the fourth layer, which is able to analyze the blood sample

accumulated in the detection chamber. In the work of Liu et. al.[182], urea, uric acid and creatinine were three species of interest that were simultaneously detected by a Ti_3C_2 biosensor through three different detection mechanisms.

Uric acid is an electroactive material which allows it to be detected by Ti_3C_2-based biosensor. Through hydrogen bonding with the surface functional groups of Ti_3C_2, the uric acid is absorbed on the surface. This causes change in the electrical flow rate (I) of Ti_3C_2-based biosensor depending on the concentration of the absorbed uric acid. To detect creatinine, it is first brought into contact with copper cations, the complex is adsorbed on the negatively-charged surface of Ti_3C_2, and creatinine is then detected using square wave voltammetry. Urea detection is also possible through immobilizing urease on MXene and using glutaraldehyde to catalyze urea, generating specific signals for urea analysis. Detailed mechanisms of the detection can be found elsewhere[182]; however, the important point here is that Ti_3C_2-based biosensors can simultaneously detect several components in a blood sample through different mechanisms.

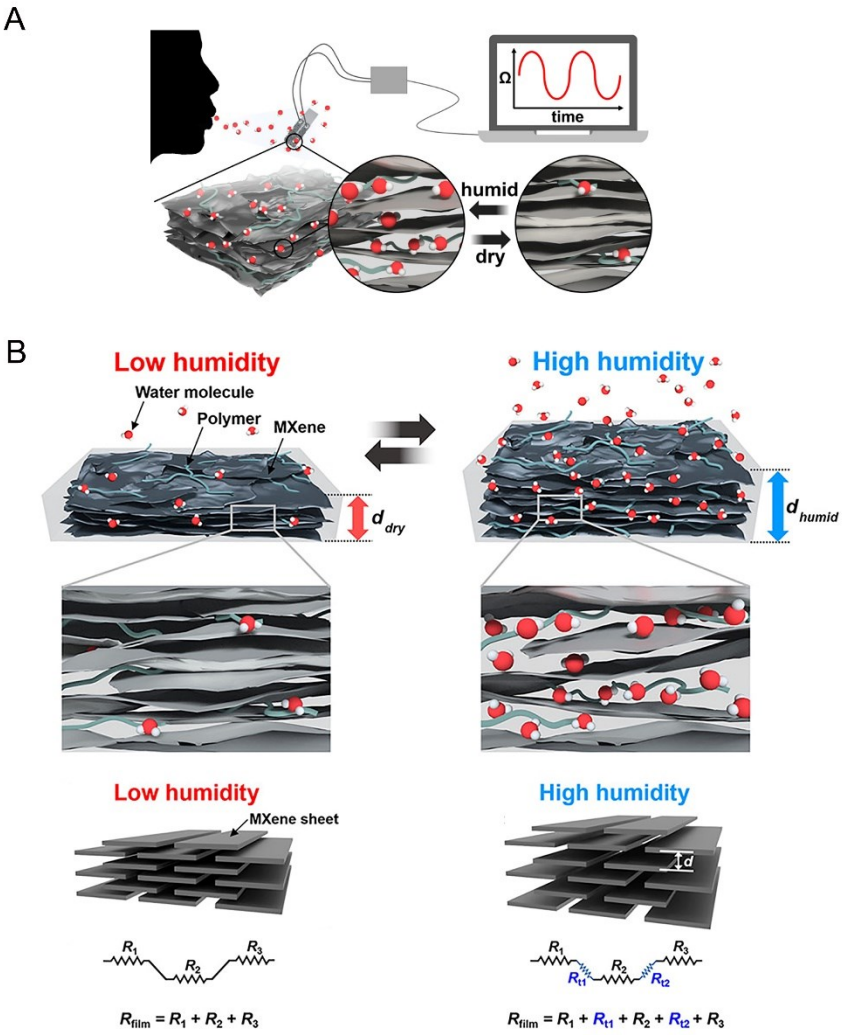

Figure 16. A) Ti_3C_2/polymer sensors are sensitive enough to detect change in humidity by human breathing. B) Change in interlayer distance of a Ti_3C_2/polymer humidity sensor upon water absorption/desorption and the corresponding electrical circuit in both dry and humid states, Reproduced with permission from ref.[142] Copyright (2019), American Chemical Society.

5.4 2D Layered Structure

5.4.1 Polymer Reinforcement

Similar to many other 2D nanomaterials, MXenes can improve mechanical properties of polymers[183]. The morphology of MXene/polymer nanocomposites is usually recognized as "brick-and-mortar". This morphology is favorable for increasing mechanical properties of hybrid structures. In a "brick-and-mortar" morphology, a single-layer MXene works as the brick and

polymer plays the role of the mortar, which facilitates stress transfer to MXene flakes. In fact, the polymer works as an intermedia glue to improve mechanical properties of the nanocomposite[133]. However, Zhou et al.[112] showed that sometimes multilayer structure of a MXene/polymer system is more effective than "brick-and-mortar" structure for improving mechanical properties of nanocomposites. For example, they showed that in comparison with a single-layer Ti_3C_2/CNF film with "brick-and-mortar" morphology, the multilayer Ti_3C_2/CNF film with the same composition shows 1.2, 1.9, and 2.4 higher tensile strength, fracture strain and toughness, respectively. They believe that this difference originates from the different mechanism of crack propagation in these two systems under pressure and is discussed in details in reference[112].

Simulation results on Ti_3C_2/epoxy system have shown that the presence of Ti_3C_2 improves elastic properties of the nanocomposites. Acrylate resins which are a family of polymers with low glass transition temperature and high flexibility are also mixed with Ti_3C_2[184-186]. Experimental results have shown that the addition of Ti_3C_2 flakes to acrylate resins increases their glass transition temperature and elastic modulus due to limiting polymer chains movements [127]. If Ti_3C_2 flakes orient in a specific direction in a nanocomposite, the enhancement of mechanical properties in the alignment direction will be more pronounced. Moreover, the extent of improvement in mechanical properties correlates with Ti_3C_2 aspect ratio. Usually, higher aspect ratio endows higher stiffness to a MXene/polymer system[187]. Surface functional groups of MXenes also play an important role in improving mechanical properties of MXene-based nanocomposites, as they are the sites which form interactions with polymers. For example, due to strong hydrogen bonding between surface functional groups of Ti_3C_2 and PVA, their nanocomposite showed improved tensile strength and elongation at break, compared with pristine PVA, just with the addition of 2 wt.% Ti_3C_2[175]. A similar improvement in mechanical properties was reported when single-layer Ti_3C_2 was mixed with NR[147]. On the other hand, annealed Ti_3C_2 which has less surface functional groups is not effective enough in improving mechanical properties of polymers compared with pristine single-layer Ti_3C_2, which has hydroxyl, fluorine and oxygen groups[48].

The addition of Ti_3C_2 to polymers can increase their crystallinity, as it works like a nucleation agent. Ti_3C_2 may increase both crystallinity and crystallization temperature of a polymer[155]. Higher crystallinity subsequently improves thermal and some of mechanical properties. Also, creep resistance of a polymer can be improved just by the addition of a tiny amount (~ 2 wt.%) of a MXene, if a perfect interface between the polymer and the MXene is

formed. To have a perfect interface, usually surface modified MXenes are used as filler. For example, a surface modified multilayer Ti_3C_2 was added to UHMWPE, and a perfect interface between the polymer and multilayer Ti_3C_2 was formed which facilitated stress transfer[154]. The presence of multilayer Ti_3C_2 also decreases the friction coefficient of the polymer, improves abrasion resistance as well as hardness of UHMWPE[154]. The addition of Ti_3C_2 to LLDPE also showed that Ti_3C_2 works as a nucleation agent in this polymer and increases the polymer crystallization rate in 2 wt.% loading. However, crystallization rate decreased upon 4 wt.% Ti_3C_2 loading due to chain movement restrictions. For crystallization, polymer chains need to nucleate and then move to complete crystal structure. High mobility is not favorable because it prevents from nucleation. Low mobility is not also favorable as it does not let polymer chains move and reorganize themselves as a crystal. This is the reason that maximum crystallization rate in polymers happens in a temperature between glass transition temperature and melting temperature. Glass transition temperature is the region with high chance of nucleation and low rate of chain movement. Melting temperature is a region with high chance of chain movement and low rate of nucleation. Thus, maximum crystallization rate occurs in a region where an acceptable combination of nucleating rate and chain movement exists. The addition of 4 wt.% multilayer Ti_3C_2 to LLDPE decreases the movement of chains such significantly that reduces the crystallization rate [156].

MXenes can affect the crystallization rate of water-soluble polymers as well. Ti_3C_2/PEO nanocomposites with 0, 0.1%, 0.5%, 1%, 2% and 5 wt.% Ti_3C_2 were prepared by Huang et al.[188] using the latex blending method. Maximum crystallization rate and minimum half-crystallization time were observed for the nanocomposite containing 0.5 wt.% Ti_3C_2 as nucleation agent causing optimum nucleation and chain movement rates at this Ti_3C_2 weight percentage. In addition to the improvement in crystallization properties, the presence of Ti_3C_2 enhanced the ionic conductivity of PEO nanocomposites. This is important as PEO is widely used as a solid electrolyte in energy storage devices [188]. PVA as a water-soluble polymer, along with a Ti_3C_2, can undergo a solution blending process to make a nanocomposite. Due to the presence of many hydroxyl groups in PVA structure, there is a high chance of hydrogen bond formation between the polymer and Ti_3C_2. These favorable interactions make a perfect interface between the nanocomposite's component and develop a mechanically durable nanocomposite. In fact, stress is easily transferred to Ti_3C_2 flakes when the PVA/Ti_3C_2 nanocomposite undergoes an external load. These favorable

interactions also improve the stiffness and the strength of the nanocomposite films [130]. The same favorable interactions exist when a polycation is selected as the water-soluble polymer matrix to be mixed with a MXene.

As mentioned above, surface modified MXenes are added to polymers in the sake of improving interfacial interactions and developing a perfect interface. For example, the addition of 0.5 wt.% PEG-treated Ti_3C_2 to TPU increased tensile strength and elongation at break simultaneously. Covering of Ti_3C_2 sheets with PEG chains caused their favorable interactions with TPU and consequently Ti_3C_2 exfoliation in TPU matrix. The interactions were effective enough to increase tensile strength without deteriorating the toughness of the nanocomposite. In fact, the PEG chains establish hydrogen bonds with TPU causing the creation of a perfect interface between Ti_3C_2 and TPU. At the same time, the stiffness of Ti_3C_2/TPU nanocomposite as well as glass transition temperature of TPU were increased which are attributed to chain movement restrictions [105]. These evidences show that MXene has positive dual effects on toughening and strengthening of a polymer nanocomposite.

Regarding hydrogels, MXenes improve their mechanical properties by optimizing their pore structure. For example, single-layer Ti_3C_2-based polyacrylamide hydrogel showed enhanced mechanical properties due to honey-comb pore structure induced by the presence of Ti_3C_2. This structure facilitates the release of mechanical stresses significantly due to its uniform fine structure[112]. Ti_3C_2-based hydrogels have shown elongation up to 1000% and bending deformation up to 180 degrees. After deformation or compression, such hydrogels can recover to their initial geometry very quickly. These outstanding mechanical properties are obtained just by the addition of 0.0145% to 0.0436 Wt.% Ti_3C_2 with respect to polyacrylamide [112]. Compared with regular hydrogels made from organic crosslinkers, Ti_3C_2-based hydrogels show higher deformation tolerability and quicker recovery. These properties are derived due to the lower crosslinking density of Ti_3C_2-based hydrogels compared with that of the hydrogels made from organic crosslinkers. Moreover, Ti_3C_2-based hydrogels have higher chain molecular weight between crosslinking points which endows them higher flexibility and extensibility[112].

Ti_3C_2 with surface-grafted sulfonated polyelectrolyte brushes was added to sulfonated poly(ether ether ketone) to make a proton conducting membrane. The surface-grafted Ti_3C_2 increased Young modulus, tensile strength, and thermal stability of the proton conductive membrane, but decreased its elongation at break [102]. The addition of Ti_3C_2 to PVA hydrogels

increased its elastic modulus, toughness, and stretchability significantly. For example, a piece of 2.5 cm hydrogel was stretched to 86 cm which means stretchability of 3400%. Under similar conditions, the same hydrogel without MXene showed maximum stretchability of 2200% [162].

5.4.2 Corrosion Resistive Coatings

Metal substrates are vulnerable against corrosion when they are in contact with water or aqueous electrolytes such as salt solutions. Organic coatings on a metallic substrate can decrease corrosion rate by preventing the diffusion of corrosive media into metal/coating interface. Yan et al.[189] mixed few-layer Ti_3C_2 with epoxy resin and then applied the obtained mixture on the top of a steel sheet to analyze the anti-corrosive properties of the coating. The best anti-corrosion results were obtained with the addition of 1 wt.% Ti_3C_2. This is the concentration at which the pores of the epoxy coating are covered by Ti_3C_2 flakes. The organic coatings applied on a metal substrate usually contain some micron-size pores which are channels for the diffusion of corrosive materials to the metallic substrate. Thus, the presence of 2D MXene flakes can cover these pores and increase the anti-corrosive properties of a coating. It is shown that the presence of Ti_3C_2 in the epoxy coating limits the diffusion of corrosive species like O_2, $Cl^-$and H_2O toward the metallic surface[189].

The presence of Ti_3C_2 in an epoxy coating also decreases its water absorption over time. For example, the immersion of pure epoxy coating in a 3.5% NaCl solution for 96 hours caused the absorption of 0.96 wt.% water, however, under the same condition, the epoxy coating containing 1 wt.% Ti_3C_2 just showed water absorption of 0.23 wt.%. Spray salt test results also showed improved anti-corrosion properties of epoxy coating by the addition of Ti_3C_2. It confirmed that the presence of an epoxy coating containing 1 wt.% Ti_3C_2 on the metal surface significantly suppresses the metal corrosion after a 15 days period [189].

5.4.3 Electromagnetic Interference Shielding

To lower the extent of damages caused by radiation pollutions, materials with electromagnetic interference shielding ability are needed[190]. Shielding is important to assure safe operation of sensitive electronic devices as well as the safety of humans. Electrically conductive polymer nanocomposites are favorable to be used for EMI shielding applications due to their light weight and enough electrical conductivity to work as a shield.

Currently, effective EMI shielding materials have a thickness higher than 1 mm[133]. Figure 17A shows the correlation between thickness and EMI shielding efficacy of some common materials and compares the performance of MXene with other ones as well. Although increase in thickness improves shielding efficiency, increase in material consumption and weight gain disqualify this strategy for improving EMI shielding efficiency. Given that, lightweight, low density, ultrathin and efficient materials are always favorable for EMI shielding, these properties are attainable through MXene-based polymeric nanocomposites. Excellent EMI shielding of MXenes originates from their high conductivity, layered structure, and their unique surface chemistry especially their fluorine functional groups.

EMI shielding usually happens by reflection or absorption of an electromagnetic wave. When a wave hits a MXene flake in a MXene/polymer nanocomposite shield, a part of the wave is reflected due to the presence of the free electrons on the surface of MXene. The non-reflected portion of the wave passes through the layers of MXene and losses a part of its energy upon traveling through each flake of MXene. As Figure 17B shows, each MXene layer acts as a barrier of the wave and dissipates some of its energy. In addition to absorbing the energy of the wave, the MXene flakes inside the shield can work as a reflection surface where repetitive internal reflection of some traveling waves inside the shield further intensifies the energy dissipation. At last, the dissipated energy of the waves will increase the temperature of the EMI shield[129]. Thus, shielding is the result of absorption and reflection of the waves in a material.

Thin Ti_3C_2-based films mainly have good EM wave absorption capability[129]. It is advantageous to develop absorption-dominant EMI shielding materials as they minimize the twice the electromagnetic pollution compared with the reflection-dominant counterparts[118]. When an EM wave reaches an EMI shielding material, it can enter the material or reflect from its surface. The chance of entrance is higher for absorption-dominant ones compared with reflective-dominant counterparts. Usually high number of free electrons on a material surface increases the chance of wave reflection[133]. If the EM wave enters a MXene-based polymer nanocomposite foam material, it has a high chance to undergo several internal reflections to dissipate its energy as heat. The porous structure of the foam and the layered structure of MXene hasten the energy dissipation of the EM wave. However, the same MXene-based polymer nanocomposite with the same chemical composition in the form of a thin film does not have the ability to dissipate the EM wave quickly. Thus, to have an absorption-dominant EMI shielding material, foams are recommended[118].

Morphology of a MXene-based nanocomposite also affects its EMI shielding mechanism. In a thin MXene-based nanocomposite film with "brick-and-mortar" morphology, there are a lot of interfaces between MXene flakes for wave scattering and repetitive reflections. Thus, the hybrid nanocomposite behaves as an absorption-dominant EMI shielding material [133]. However, multi-layer morphology can result in the development of reflective-dominant EMI shielding materials. Zhou et al.[112] made single-layer Ti_3C_2/CNF polymer nanocomposites with alternative vacuum filtration technique and found that the EMI shielding capability of the nanocomposite depends on the number of Ti_3C_2 and CNF layers. Maximum shielding was obtained when 4 layers of Ti_3C_2 and 5 layers of CNF. More than 90% of the incident EM waves were reflected right after reaching the system due to the conductivity of the nanocomposite and the high impedance mismatch. In fact, when the impedance mismatch in the interface of the air and the nanocomposite increases, the chance of reflection of the EM waves from the interface increases. Zhou et al.[112] showed that multilayer Ti_3C_2/polymer systems, compared with single-layer mixed Ti_3C_2/polymer systems, are more effective in developing reflection-dominant EMI shielding materials due to increased impedance mismatch [112].

In EMI shielding materials, the energy of a wave is dissipated as heat. Thus, for stable operation, it is necessary to transfer the generated heat. As an electron and heat conductive material, Ti_3C_2 conducts both electrons and phonons efficiently. Thus, a defect-free network of Ti_3C_2 in a thin nanocomposite film creates an expressway for phonon transport and increases in-plane thermal conduction of the nanocomposite. The dissipation of EM waves as heat can significantly increase the temperature of a shield and create the risk of burning. Thus, in addition to thermal conductivity, an efficient EMI shielding material should possess high thermal stability and anti-dripping properties. Fortunately, Ti_3C_2 endows a Ti_3C_2/polymer nanocomposite with excellent flame-retardancy and anti-dripping properties, as discussed before [128]. Thermally stable polymer nanocomposite with a degradation temperature over 100 ℃ are fabricated for EMI shielding application by mixing single-layer MXene as thermally-stable nanoparticle with PANI, which is a conductive polymer[191].

Pure Ti_3C_2 foams with a hydrophobic surface are introduced as excellent EMI shielding material for working under wet condition[115]. Nanocomposites of single-layer Ti_3C_2 and water soluble polymers are also used as EMI shields [129]. An increase in the MXene content of these nanocomposites caused improvement in their EMI shielding efficiency. Some other conductive

Ti_3C_2/polymer nanocomposites used for EMI shielding are single-layer Ti_3C_2/polystyrene thin films[148], single-layer Ti_3C_2/PDMS foams[116], single-layer Ti_3C_2/epoxy[192], PET fibers coated by single-layer PPy-functionalized Ti_3C_2[140], PVB/$Ba_3Co_2Fe_{24}O_{41}$/Ti_3C_2[193], single-layer Ti_3C_2/cellulose nanofiber[132], Ti_3C_2/PEDOT:POSS[194], polyaniline/Ti_3C_2[195], etc[196]. Graphene-based polyurethane composites were also developed as EMI shielding materials. However, the presence of less-conductive pathways (compared with MXene-conductive pathways) resulted in a decreased ability in EMI shielding of graphene-based material.[197]

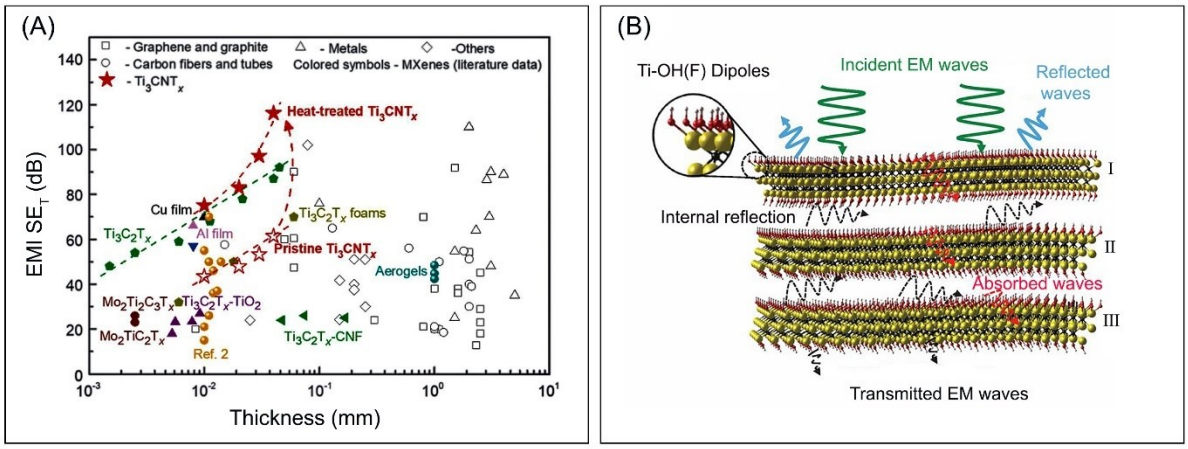

Figure 17. A) Correlation between thickness and EMI shielding efficiency as well as comparison between the ability of Ti_3C_2 with other materials for this application, Reproduced with permission from ref.[198] Copyright (2020), Science. B) Mechanism of internal reflection of an electromagnetic wave between three Ti_3C_2 flakes to dissipate its energy, Reproduced with permission from ref.[129] Copyright (2016), Science.

5.4.4 Gas Separation and Air Filtration

Two-dimensional materials have evolved as building blocks for developing high performance membranes towards selective ion permeation, gas separation, water treatment, bio-fouling resistant, and nanofluidics[199-203]. Their sub-atomic level thickness, stacking behavior coupled with high structural and morphological integrity, endow them minimal transportation resistance and high permeation flux which are ideal for selective sieving of intercalating species[204, 205].

MXenes due to their layered morphology with a single-layer thickness of ~1 nm possesses a highly active surface containing termination groups such as -O,-F,-OH and sometimes -COOH,[1, 206] enabling strong and favorable interactions, dispersion, and stability within the incorporating matrix. Due to its lamellar structure, the created channels in the hybrid matrix provide selective transport of ions and particles by generating micro-pathways **(**Figure 18A)[207]. In addition, high solubility in aqueous media along with precisely tailorable interlayer spacing of MXene sheets can enable the confinement of a specific molecule while allowing other species to permeate easily through the porous inter-planar channels.

MXenes' stacking behavior, tunable interlayer spacing and surface properties as discussed earlier have created great opportunities to explore MXene-based composites for membrane applications[208]. Low membrane resistance is favorable for selective separation. In addition, MXenes' active surface can be chemically functionalized to adjust selective interaction between species based on the nature of the permeating species. For example, membranes with reversible carrier activity are envisioned which are capable of interacting selectively to one gas component while allowing free permeation to other components in the mixture[209].

Pristine Ti_3C_2 films have exhibited diffusion control mechanisms [27] causing molecular sieving effects that are ideal for separation membranes. Single-layer Ti_3C_2 MXene films exhibit a H_2 permeability greater than 2,000 Barrer exceeding the Robeson upper bound[210]. In membrane gas separation, there is always a trade-off between selectivity and permeability. The performance (selectivity and permeability) of a membrane in separating a gas pair is evaluated relative to the most-recent Robeson bound for the gas pair[211, 212]. A membranes, the separation performance of which is above the Robeson bound is better than one with a performance below the bound[212].

A freestanding Ti_3C_2 MXene lamellar membrane was developed to harvest osmotic power generated by the salinity gradient. These ion-selective membranes exhibited an osmotic energy conversion efficiency of 40% at room temperature[203]. Ti_3C_2 MXene-based flexible polymer hybrids (mixed matrix membranes) were developed for CO_2 capture using PEBAX-1657 with high CO_2/N_2 permeability above 2008 CO_2/N_2 upper bound, Figure 18B&C [213]. Liu et al developed stable, robust Ti_3C_2-based poly(ether-block-amide) (PEBA) hybrid membrane for CO_2 absorption with a Ti_3C_2 loading as low as 0.15% and got permeation rates as high as ~22 GPU. In another study, single-layer Ti_3C_2 decorated PAN fibers were developed for selective trapping of

atmospheric particulates enabling a one-step air purification in-tandem to anti-bacterial functionality[48]. The membranes exhibited extended performance life coupled with stable structure morphology, Figure 18D. In another study, borate and polyethylenimine (PEI) molecules interlocked between Ti_3C_2 MXene sheets exhibited H_2/CO_2 selective transport and separation[214]. MXene's additional functionality as an active bacteriostatic agent can further be harnessed to integrate and develop multi-role purification and anti-biofouling functionalities for membranes in industry scale air/water treatment facilities.

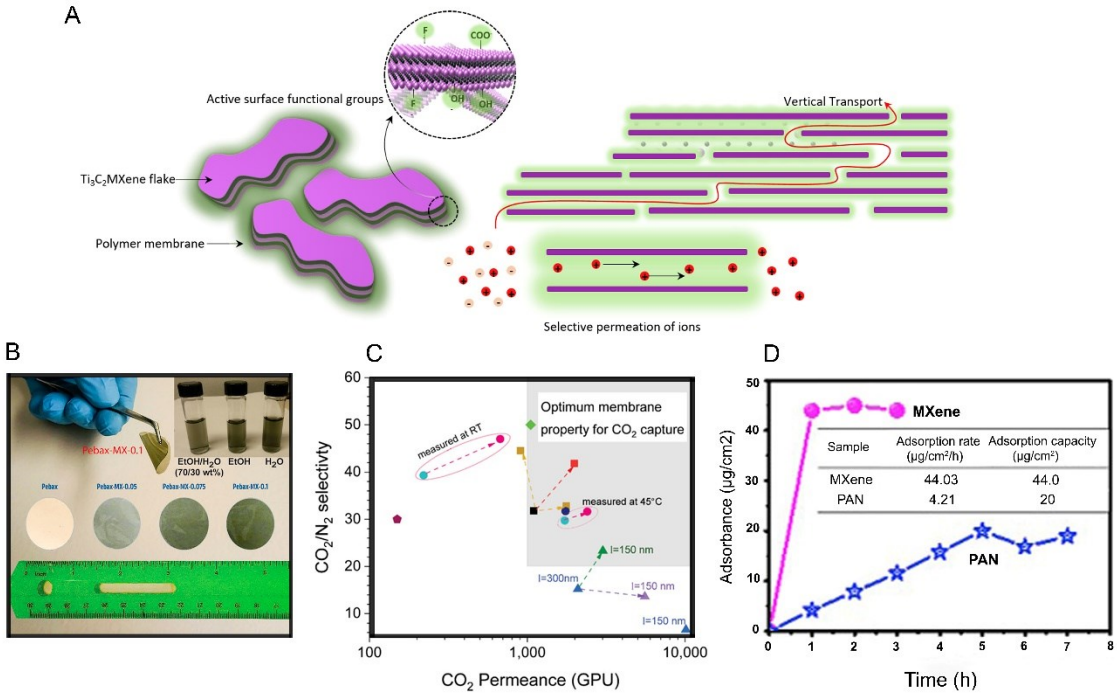

Figure 18. A) Schematic diagram of selective permeation of species through MXene-polymer membranes. B) Flexible Ti_3C_2-PEBAX membranes exhibiting high functional stability, Reproduced with permission from ref.[213] Copyright (2020), American Chemical Society. C) High CO_2 permeance of the membranes. D) Absorbance rates of Ti_3C_2-PAN membranes with extended performance and durability, Reproduced with permission from ref.[48] Copyright (2019), Elsevier.

5.4.5 Wastewater Treatment

Polymer membranes containing nanoparticles are used widely in wastewater treatment and desalination applications[215, 216]. High surface hydrophilicity is favorable in such membranes as it

prevents from the fouling and increases the membrane service life. Han et. al. developed a MXene/polysulfone membrane to separate dyes and inorganic salts from water. They also reported that dye and salt rejection rates of the membrane improve by increasing the single-layer Ti_3C_2 content [217]. Tradeoff between membrane flux and solute rejection has been an ever-existing challenge in alcohol-purifying membranes based on graphene and other filler materials such as metal organic frameworks[218, 219]. Ti_3C_2 can address this tradeoff. The addition of Ti_3C_2 to polyethyleneimine is practiced to develop membranes for purifying alcohol-based mixtures. The presence of Ti_3C_2 facilitates the transport of alcohol through the membrane thanks to its surface hydroxyl groups and, at the same time, blocks the transport of solutes with molecular weight cut off 200 Da. [220].

The development of MXene/polymer hybrid materials for membrane applications is relatively new which provides a large scope for future development. In a recent study, flexible and structurally stable single-layer Ti_3C_2-cellulose photothermal membranes exhibited near 100% efficiency in inhibiting bacterial growth and showed efficient solar-driven water evaporation[221]. The inherently strong interactions between a Ti_3C_2 and cellulose fibers enable a synergistic coupling of flexibility without the loss of the membrane's functional integrity which envisions an easily scalable and sustainable fabrication process for long-term wastewater treatment technologies.

To remove nitro compound pollutants from wastewater, nanofiber of PVA/PAA/Fe_3O_4/Ti_3C_2@AgNP are produced by electrospinning process. Ti_3C_2@AgNP here means Ti_3C_2 nanosheets containing silver nanoparticles on their surface. This nanocomposite nanofiber is capable to catalytically reduce 4-nitrophenol and 2-nitroaniline which are two well-known nitro compound pollutants. The presence of Fe_3O_4 endows single-layer Ti_3C_2 with magnetic properties and recyclability [131].

5.4.6 Textile Engineering

Wearable electronics, energy storage devices, and sensors are some applications of MXenes in textile engineering. MXenes let the production of multifunctional fibers which are conductive, water repellent and possess exceptional EMI shielding. In addition, such fibers and mats can have excellent Joule heating performance to create heat by applying an electrical voltage to them. These multifunctional textiles, for example, can be used to produce cloth for a pregnant

woman who concerns to protect her fetus from detrimental microwaves radiations. Wearable heaters for self-heating garments, thermotherapy and sensor fabrics are some areas that these multifunctional textiles can be used [140, 158].

PET is a polymer which is used widely for fiber manufacturing and its combination with MXenes can lead to the development of multifunctional textiles. To improve interactions between PET and Ti_3C_2, Wang et al. polymerized pyrrole between Ti_3C_2 layers to prepare a stable conductive single-layer Ti_3C_2 ink[140]. PPy creates additional polar groups on Ti_3C_2 surface and improves the adhesion of Ti_3C_2 to PET. Next, PET fibers were coated by this ink through repetitive dip coating process. Finally, to change hydrophilic fibers into hydrophobic counterparts, a silicon coating was applied on the Ti_3C_2-containing PET fibers again by dip coating process. Compared with hydrophilic fibers, hydrophobic ones can keep their performance in humid environments for a long time and protect their sensitive components, like MXenes, from oxidation and degradation [140]. Hydrophobic fibers not only work for a long time, but also are durable against repetitive washing with detergents. In addition, they keep their breathability even though a hydrophobic coating, like silicon, is applied on their surface. Regarding the combination of a MXene and PET in textile engineering, single-layer Ti_3C_2/PEO nanofibers coated on a PET yarn were developed for supercapacitor applications. Such yarn supercapacitors with excellent flexibility, strength and high-power density can be used in wearable energy storage devices[152].

Having low mechanical properties is one of the challenges in producing MXene-based nanofibers. To overcome this problem, it is possible to add another filler to MXene/polymer mixture for reinforcing of the system. For example, mechanical properties of Ti_3C_2-based PVA nanofibers produced by electrospinning were improved by the addition of CNC. In fact, when two fillers are used in a polymer matrix simultaneously, tailoring of electrical, mechanical and thermal properties is much easier compared with the time that just one filler is used. As both CNC and MXene are fillers with high aspect ratio, both have the chance of self-orientation along the fiber axis. Thus, their simultaneous presence not only improves mechanical properties of the nanofiber significantly, but also enhances its thermal stability without impairing flexibility. These excellent set of properties introduce multilayer Ti_3C_2/CNC/PVA nanofibers for flexible and wearable energy storage devices [153].

Flexibility of Ti_3C_2-containing fibers is very important as they are supposed to be knitted by industrial knitting machines. Fibers undergo higher tension and bending stresses when are

knitted by industrial machines, compared with hand knitting. Figure 19 shows three usual patterns of fiber knitting where each one needs a different level of fiber flexibility. For example, Single jersey knitting pattern needs the highest fiber flexibility while half gauge pattern needs the lowest one. It is possible to adjust the flexibility of MXene-containing fibers by changing the size of the incorporated MXene flake. Usually, fibers coated with bigger MXene flakes show higher conductivity/lower flexibility and vice versa. As a result, when both conductivity and flexibility matter, a fiber can be coated with a mixture of small and large MXene flakes to possess both flexibility and conductivity in an acceptable level. In addition, great attention should be paid to knitting method. Less-flexible fibers cannot be knitted through Single jersey pattern which needs the bending of fibers with short bending radius; however, they can usually withstand bending and tension stresses exerted by other knitting patterns like half-gauge and interlock, Figure 19 [144].

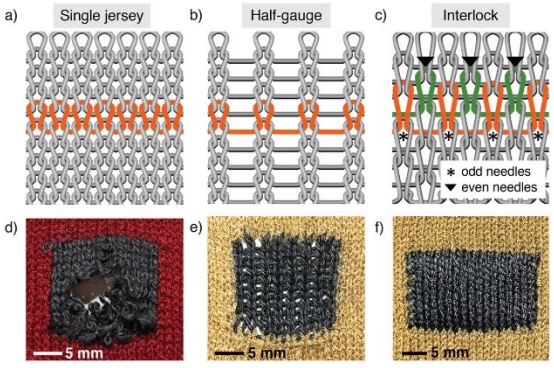

Figure 19. Different knitting patterns: single jersey (a, d), half-gauge (b, e), and interlock (c, f), Reproduced with permission from ref.[144] Copyright (2019), Wiley Online Library.

5.5 Electrochemical Activity

5.5.1 Supercapacitors

The advent of MXenes has further advanced the battery and supercapacitors technologies. A combination of a MXene and a conductive polymer, like MXene/PPy one, is usually used for supercapacitor applications. The advantage of MXene/conductive polymer nanocomposites is addressing of the tradeoff between transport properties and charge storage capability of a supercapacitor [222]. In-situ electrochemical polymerization technique can be used to synthesize a nanocomposite thin film of MXene/conjugated conductive polymer. The electrochemical

polymerization in the presence of a MXene can be carried out for polymerization of different organic monomers and the produced nanocomposites can be used in mobile power supplies, micro-portable electronic and electromechanical systems [223].

PPy homopolymer has intrinsic flexibility as well as high electrochemical activity, however, suffers from low capacitance and limited charging/discharging cycling stability. Intercalation of PPy chains between MXene flakes overcomes these problems [224]. To efficiently intercalate MXene, pyrrole is polymerized between MXene layers by the electrochemical polymerization mechanism:

Like the polymerization of pyrrole, the polymerization of PANI occurs between Ti_3C_2 MXene layers. The in-situ polymerization of PANI allows the development of bendable, and foldable electrodes for the fabrication of all-solid-state supercapacitor[225].

MXenes have been used widely as anodes in supercapacitors, while their usage as a cathode has been limited due to the risk of oxidation in this electrode. To overcome this problem and develop a high-performance supercapacitor, an asymmetric structure with MXene as negative electrode and MXene/PANI nanocomposite as the positive electrode of the supercapacitor was introduced [226]. This novel positive electrode showed a volumetric capacitance of 1,632 $F\,CM^{-3}$ and a rate capability of 827 $F\,CM^{-3}$ at 5,000 $mV\,s^{-1}$ which are among the highest ever-reported values. The asymmetric supercapacitor made from this MXene/PANI positive electrode and pure MXene negative electrode showed a high energy density of 50 Wh L^{-1} and a power density of 127 KW L^{-1} [226].

Recently a nice review paper on MXene-based supercapacitors was published by Hu et. al. [227]. The review discusses different topics including charge storage mechanisms in aqueous and non- aqueous media, and the effects of surface chemistry of MXene and the structure of the MXene- containing electrodes on the performance of the supercapacitor. Other topics like MXene-containing symmetric supercapacitors, asymmetric supercapacitors, microsupercapacitors, and transparent supercapacitors are also discussed. Covered in this review paper are also MXene/polymer composites used for supercapacitor fabrication. Other examples of Ti_3C_2/polymer nanocomposites used for energy storage are Ti_3C_2/polysulfide[228], Ti_3C_2/poly(3,4-

ethylenedioxythiphene), Ti_3C_2/PDT[137], Ti_3C_2/PANI/CCG[106], and Ti_3C_2/PVA as on-chip micro-supercapacitors[229]. Another recent review on MXene-based nanocomposites for rechargeable batteries and supercapacitors is Ref.[230], which is worth reading, as it extensively discusses MXene/carbon nanocomposites, MXene/metal oxide/sulfide nanocomposites, MXene/metal nanocomposites.

5.5.2 High Dielectric Materials

High dielectric materials are used in semiconducting industry to replace silicon dioxide. In this context, an ideal material is the one which stores a lot of electrical charges with minimum loss. To successfully develop a material with high dielectric constant, high dielectric permittivity and low dielectric loss are required. The former demonstrates the ability of a material to store electrical charge and the latter represents how dissipated a material is with respect to an external electric field.

Single-layer Ti_3C_2/PVA nanocomposite has shown extremely high dielectric constant, because Ti_3C_2 is a conductive nanoparticle and disperses well in PVA matrix. The good dispersion of Ti_3C_2 causes the formation of a network of nanocapacitors. High conductivity of Ti_3C_2 also causes a significant electrical conductivity disparity between the MXene and PVA, which increases interfacial polarization. If MXene sheets align perfectly in a way to face each other completely, a larger surface and consequently a larger network of nanocapacitors can be formed, compared with random orientation. This provides the chance of storing a huge amount of electrical charge. Every manufacturing technique which increases the alignment of MXene flakes to face each other completely, creates a nanocomposite with higher dielectric constant. This is the reason that under similar composition, single-layer Ti_3C_2/PVA nanocomposites made from vacuum filtration show higher dielectric constant compared with the ones made from solution casting [124]. It is very important to mention that the formation of a network of nanocapacitors by MXene flakes is favorable here. However, the formation of a conductive network by MXene flakes in the polymer matrix must be avoided extremely as it causes the leakage of electrical charge. The presence of an insulator polymer between MXene flakes prevents from charge leakage. To avoid charge leakage, it is also important to keep the loading content of MXene lower than its percolation threshold. A "brick-and-mortar" morphology, containing no inter-connected network of MXene flakes is favorable here. Ti_3C_2/PVA nanocomposite films with 10 wt.% single-layer Ti_3C_2 obtained by

solution casting and vacuum filtration have been reported to have dielectric constants of 371 and 3166, respectively[124]. These dielectric constant values highlight the importance of MXene orientation in a polymer matrix. As another example, the addition of Ti_3C_2 to PVDF has been reported to increase dielectric permittivity significantly[231].

5.5.3 Artificial Muscles and Actuators

Electroactive polymers are used as actuators and artificial muscles. In these systems, stored electrical energy is converted into mechanical deformation. To work as an actuator, a material should have acceptable bending strength, quick response time, long service life in air as well as low driving voltage. Each actuator consists of three parts including an electrolyte and two electrodes. An ionic polymer membrane can be used as the electrolyte which is sandwiched between two conductive electrodes [232].

MXenes have enough electrical conductivity to be used as an electrode. However, its low stretchability limits its application in actuators. To overcome this problem, polymers like PP are mixed with a MXene. The polymer ionically bonds to MXene surface and causes its intercalation. This hybrid structure has fast charge transport as well as ion intercalation/de-intercalation ability with improved stretchability, rendering this so-called ionically-crosslinked Ti_3C_2/PP nanocomposite an excellent material for electrode fabrication of actuators. The polymer is able to establish hydrogen bonds with oxygen and hydroxyl groups on the surface of the Ti_3C_2, and to work as a pillar to prevent from the restacking of Ti_3C_2 flakes. It can also facilitate reversible transportation of electrons and ions between the electrolyte and the electrodes[232].

Actuators made with Nafion as the electrolyte and a mixtures of Ti_3C_2:PP (1:2 wt.) as an electrode were fabricated[232] . They showed 1.37% bending strain when they were subjected to 1 V. To develop durable actuators, adhesion between the electrolyte and the electrodes is important. A pristine MXene film as electrode does not make a good adhesion with the electrolyte. However, its hybrid nanocomposite with PP showed significant adhesion to the electrolyte which lets the actuator to keep its functionality even after 18000 bending cycles[232]. Figure 20A shows that the actuator made from a pristine MXene cannot tolerate manual bending while the actuator made from Ti_3C_2/PP electrode undergoes bending without mechanical degradation.

Different nanoparticles like GO[233] and carbon nanotube[234] can be also used for actuator manufacturing. However, Ti_3C_2 is superior to other nanoparticles for actuator development due to

its high capacitance. It is important to know that the magnitude of the bending deformation and the response time of ionic actuators are directly proportional to the capacitance of electrodes. MXene-based actuators show high energy transduction which is defined as the ratio of received electrical energy to generated mechanical energy. To show a few applications, artificial flowers made from Ti_3C_2-based actuators are displayed in Figure 20B. Similar to the blooming of a real flower, applying of an electrical current can open the artificial flower. It is also interesting to know that under voltage 2 (V), this actuator generates a force which is 28 times higher than its weight [232]. Figure 20C shows the driving force of the bending. Higher ion migration and faster charge transfer cause larger bending strain in the actuator. Under an applied voltage, the Ti_3C_2-based electrode intercalates with a higher number of cations on the cathode size of the actuator. This increases the Ti_3C_2 interlayer distance, causes swelling of the electrode, and bends the actuator[232].

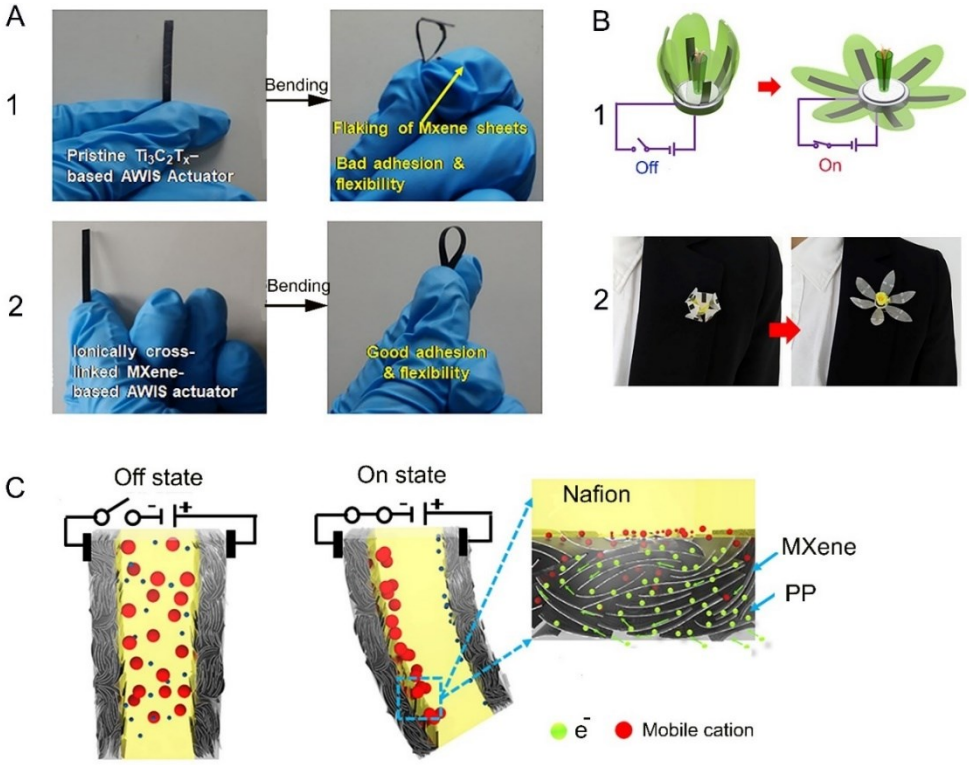

Figure 20. A) Pristine Ti_3C_2 as electrode does not have enough adhesion to electrolyte to make a mechanically stable actuator against bending (1). However, its nanocomposite with PP improves its adhesion and makes it possible to fabricate an actuator with bending ability (2). B) Ti_3C_2-based artificial flower blooms like a real flower upon connection of electrical current (1) and can be mounted on a coat for decoration (2). C) Ion migration is the driving force for the bending of an actuator, Reproduced with permission from ref.[232] Copyright (2019), Science.

5.6 Biocompatibility

Like graphene, MXenes are bio-compatible nanomaterials. Consequently, their applications in biomedical areas are expanding, thanks to their large surface area, cytocompatibility, good adhesion for cell proliferation, tunable surface chemistry, and high absorbance in near-infrared region[235]. MXene/polymer nanocomposites are widely used in nanomedicine due to their synergistic antibacterial properties, excellent light-to-heat conversion, selectivity, and stimuli-responsiveness toward malignant cells. Recently, two review papers discussing the applications of MXene/polymer nanocomposites in medicine science were published[235, 236]. Below we briefly review some applications of MXene/polymer nanocomposites in biomedicine area.

MXene/polymer nanocomposites are used as antimicrobial agents. It is reported that 2D nanoparticles improve cell membrane permeability, damage membrane cell by their sharp edges, and destroy the DNA of bacteria[237]. Compared with other 2D nanosheets, Ti_3C_2 has outstanding antibacterial properties even better than GO due to its high electrical conductivity, which causes better interaction with the cell membrane. Ti_3C_2 oxidation causes the formation of TiO_2 which is also a well-known antibacterial agent [38]. MXene's ~100% light-to-heat conversion efficiency as well as its high thermal stability compared with organic materials enable MXene/polymer nanocomposites to be used as a photothermal agent for cancer treatment. Recent studies have explored mono-elemental 2D materials based on borophene, silicene, germanene, stanene, phosphorene, arsenene, antimonene, bismuthene, selenene, gallenene, and tellurene, which are chemically tractable materials for cancer nanomedicine[238]. MXene-based polymer nanocomposites in-tandem with other mono-elemental materials such as germanene have potentials towards clinical translation in near future[239-241]. In a research by Xing et. al.[114], a Ti_3C_2/cellulose hydrogel was used as an anticancer treatment. The hydrogel attacked the tumor cells by two different mechanisms of photothermal and chemotherapy activities. As a chemotherapy approach, an anticancer drug was loaded to the hydrogel where its in-vivo controlled release was also possible. As a photothermal approach, irradiation of near infrared light let Ti_3C_2 to generate heat locally in the vicinity of tumor cells and fortunately malignant cells are vulnerable against the generated heat. Given that, the photothermal efficacy of the Ti_3C_2/cellulose hydrogel is dependent on light irradiation duration, laser power, and the amount of the Ti_3C_2 in the hydrogel. In addition, the light irradiation helped the chemotherapy approach by faster drug release

under near infrared light irradiation. In fact, the pores of the hydrogel storing the drug in themselves expand under light irradiation and release more drug over time[114].

Drug delivery is another area in which MXene/polymer nanocomposites have been used. As Ti_3C_2 has negative surface charge, drugs with positive surface charge can attach to it. A polymer with negative surface charge is usually coated on drug-loaded MXene flakes to protect it during circulation in bloodstream. The drug-loaded MXene has been reported to be pH and temperature responsive. Fortunately, tumor cells have a lower pH compared with healthy cells. Thus, pH responsive materials like MXene/polymer nanocomposites can distinguish healthy cells from malignant counterparts to deliver the drug to the target cells. Ti_3C_2-based polyacrylamide hydrogels are found as excellent drug career as a high amount of drug can be loaded to them. The hydrogels also show high drug release rate compared with the conventional polyacrylamide hydrogels with no Ti_3C_2. Uniform porous structure as well as high water-uptake of Ti_3C_2-based hydrogels are the main reasons for such excellent drug career properties. In addition, conductive MXene-based polyisopropyl acrylamide hydrogels show a LCST around 34 ℃ which is a great property for drug delivery. The latter is used as photothermal agent for drug delivery and cancer treatment[100].

In addition to drug delivery, MXene-based nanocomposites have found applications in bioimaging and bone regeneration[236]. Following are some other examples showing MXene/polymer nanocomposite applications in the areas of health and medicine science. MXene/PVDF membranes as antibacterial surfaces[242], MXene/Polyoxometalates for tumor cell eradication [243], MXene/Polycaprolactone with hydrophilicity, protein absorption and cell viability for bone tissue engineering, cancer therapy and wound dressing[96].

5.7 Other Properties

5.7.1 Mechanical Dampers

Having excellent reversible compressibility is a necessary condition for a material to work as a damper. Ti_3C_2/PI aerogels have shown excellent reversible compressibility even under large strains up to 80%. After such large deformations, MXene/PI aerogel returns to its original shape, while keeping its robust structure. The aerogel shows energy loss upon deformation which is required for a good damper. For example, under a strain deformation of 80%, an energy loss coefficient of 80% was observed. High reversible compressibility and excellent damping

capability nominate Ti_3C_2/PI aerogel as an appropriate material for shock absorption. When a piece of this damper is attached on back side of a glass slide, the protected glass can withstand against a mechanical strike exerted by a pendulum. However, the removal of the damper causes the fracture of the un-protected glass upon the same strike. In addition, the intensity and extent of the pendulum's return after strike are significantly lower in the presence of the damper. This shows excellent ability of the damper in energy dissipation[119]. It is also worth mentioning that the aerogel is very deformable and superlight that can stand on top of the dandelion. It has exceptional fatigue resistance as showed just 7% volume deformation after 1000 loading-unloading cycles at a fixed strain 50%. In addition to good reversible compressibility, the aerogel showed acceptable reversible stretchability below 20% strain. Thus, it can be concluded that reversible compressibility of a material can be different from its reversible stretchability[119].

5.7.2 Data Storage and Flash Memories

MXene quantum-dots are tiny MXene flakes with a size of about 3 nm. Ti_3C_2 quantum-dots can be produced by carrying out the following steps[138]: disperse a multilayer Ti_3C_2 powder in water; add a very small amount of ammonia (1-2 drop per 0.3 gr MXene in 20 ml water) to the mixture; and let the mixture undergoes a hydrothermal process at 100 ℃ for 6 hours. The Ti_3C_2 quantum dots obtained with this method are less than 10 nm in lateral size and show higher hydrophilicity as well as a higher edge effect compared with the pristine Ti_3C_2. Quantum dot Ti_3C_2, which contains the same F, O and OH surface groups, disperses in solvents like ethanol[138].

Similar to MXenes, MXene quantum dots (MQDs) disperse easily in aqueous solutions containing water-soluble polymers. For example, Quantum dot Ti_3C_2 can be dispersed in a PVP matrix finely. It is possible to adjust the conductivity of this MQD/PVP by changing the amount of MQDs in the system. In fact, this system can show insulator, irreversible resistive switching, reversible resistive switching and conductor behavior with increased amount of MQD in the system. These materials with irreversible resistive switching property show write-once-read-many times effect and materials with reversible resistive switching property benefit from Flash Memory effect. These features suggest MQD-based polymeric nanocomposites as secure data storage materials[138].

6 Risk Assessment of MXene/Polymer Nanocomposites

In every technology, process safety is of prime importance. Despite advances in process safety and the introduction of increasing tighter safety regulations, more than 50 serious incidents happened in the U.S. over the past ten years[244]. Product safety is also of great importance, as the users of a product and the environment should not be harmed by the product. Risk assessment allows for identifying and evaluating process and product safety risks.

Although MXene/polymer nanocomposite devices provide a lot of benefits, their production and usage cannot be risk-free to human health, equipment, or the environment. Risks associated with each step of MXene synthesis and MXene/polymer nanocomposite fabrication can be summarized as follows. The first step is the synthesis of a MAX phase. Aluminum, titanium, titanium carbide or graphite that are used in the MAX phase synthesis are combustible powders. Thus, there is a risk of dust explosion. The risk of the dust explosion increases, as the particle size of the raw materials decreases[245]. After sintering of the powders to prepare the MAX phase, a milling step is required to convert the bulk material to a powder. Here again dust inhalation and dust ignition risks exist. To overcome these risk factors, powders should be handled in a gentle way to prevent their release into the environment, and any static charge generation should be avoided. It is also advantageous to work in an inert environment like argon to avoid oxygen, which is an essential element for explosion and fire[245].

MXene synthesis itself starts by the direct addition of HF to MAX phase or in-situ generation of the acid by a mixture like LiF/HCL. HF is very corrosive and dangerous to human health. If it comes into contact with a human's tissue, it can degrade it and even dissolve the bone. In addition, HF used for the synthesis of MXene can create a great risk for metal-based and glass-based instruments. HF can dissolve and damage any glassy or metallic part of an instrument that comes into contact with HF during MXene synthesis. Heat, hydrogen gas, and water vapor which are generated during etching a MAX phase are other sources of possible incidents. Hydrogen is highly flammable and its generation rate should be determined especially if the etching process is going to be scaled up. A MAX phase should be added to an etchant solution at a very slow rate, as the reaction is very exothermic [etching of one gram of Ti_3AlC_2 releases 9.12 kJ heat]. For example, when 500 gr of the MAX phase is suddenly added to an etchant solution, the reaction medium temperature can increase up to 270 ℃ [245].

Moreover, a large amount of acidic wastewater is produced during MXene synthesis. These are the waters that are used for washing of the etched MAX phase to increase the pH of the medium to neutral one around 6~7. As an estimation, for each gram of MXene production, near 1 litter of water is needed for washing out the acid. As a result, a large amount of water is consumed for MXene synthesis and consequently a great amount of acidic wastewater is generated which needs appropriate treatment and disposal procedures.

For the fabrication of some MXene/polymer systems, solvent exchange is required. Thus, water should be replaced with an organic solvent, as many polymers are not water soluble. This process involves the evaporation of water and then redispersion of solid MXene in an organic solvent by sonication. Sound waves generated during the sonication process can be dangerous to humans[246]. The added organic solvent to dissolve the polymer is then removed during the MXene/polymer nanocomposite fabrication process. This removal can be through evaporation, interacting with a non-solvent, etc. Regardless of the solvent removal method, a release of an organic solvent to the environment happens. This is detrimental to the environment.

MXene/polymer nanocomposite devices can cause some risks to humans and the environment as well. Wearable MXene/polymer heaters that are worn by a person may cause burning. These devices generate heat by applying a voltage or receiving sunlight. Exceeding safe voltage may be very dangerous to the person by the generation of a lot of heat. Wastewater membranes that include a MXene on their structure may release the MXene over time. The effect of the leached MXene on marine animals is not understood and needs to be studied. Another possible risk in MXene/polymer nanocomposite devices exist when they are used as electromagnetic interference shields. In this application, the device dissipates the energy of a wave by converting it to heat. Although MXenes have good thermal conductivity and heat stability, a significant accumulation of heat may lead to burning of the device. These are just some examples of the possible risks associated with MXene/polymer nanocomposite devices and should be addressed before introducing these devices to the market.

As MXenes have some properties similar to GO, a risk analysis of GO can give some hints on possible risks of MXene and MXene/polymer nanocomposite devices. Fadeel et al.[247] recently have published a paper on environmental and health risks of graphene-based materials. With respect to health risks, they discussed interaction of immune system of a human with graphene-based materials, the effects on reproductivity and pregnant women, biodegradation of graphene-

based materials, and dermal effects of graphene-based materials, as well as their effects on central nervous system. Pulmonary effects, cardiovascular effects, and gastrointestinal effects are some other health-related risk factors discussed by Fadeel et al.[247] With respect to environmental risks, the effect of graphene-based materials on bacteria, photoautotrophs, seed plants, invertebrates, vertebrates, and ecotoxicology are discussed. Occupational exposure to graphene-based materials is also discussed by them. All of these risk assessments may be required for MXene-based materials and should be carried out by researchers in this field.

7 Challenges and Future Outlook

This review discussed the development, synthesis, and applications of Ti_3C_2 MXene-based polymer composites. Ti_3C_2 MXene has diverse yet tailorable surface chemistries, tunable flake size, and high electrical and thermal conductivities. Coupled with its unique surface morphology, high aspect ratio, and solvent stability across a range of solvents, it has huge potential to be incorporated into polymer hybrids and heterostructures for various applications. Furthermore, the ability to modify the surface chemistry during the initial stages of synthesis process enables its synergistic coupling with polymers via conventional facile synthesis routes such as wet/melt processing, and coating. In addition, grafting or impregnation with functionalized nanoparticles have great potential for applications ranging from targeted drug delivery, energy storage, wearable heaters, self-healing coatings to developing nano-pesticide systems due to their high load carrying capacities (high volume ratios). However, developing robust MXene/polymer nanocomposites requires a better understanding on the impact of the filler material with the polymer chain conformation, mobility, and the degree of chain ordering. Functionalization routes based on covalent and non-covalent interactions may lead to the emergence of hybrids, which are sustainable and scalable for transition to industrial applications. Methods to diminish aggregation and clumping inherent to polymers matrix phases, to achieve uniform distribution of the filler is a challenge yet to be addressed. It is anticipated that a uniform distribution of MXenes in the matrix will facilitate isotropic material behavior with improved lifetimes and become the next generation of functional nanocomposite material along with other two-dimensional material hybrids. Development of responsive polymer matrixes with MXene filler have great potential for implementation in smart technologies such as intelligent membrane separation systems, adaptive

sensors, and multi-modal electronic switches. However, some properties of MXenes such as the control of interlayer spacing, surface terminations, and selective chemical activity require further investigation.

Acknowledgment

Hossein Riazi was partially supported by the U.S. National Science Foundation under Grant No. CBET–1804285. Any opinions, findings, and conclusions or recommendations expressed in this material are those of the authors and do not necessarily reflect the views of the National Science Foundation. H. Riazi and M. Soroush are thankful to Axalta Coating Systems for its financial support. The authors would like to thank Mrs. Golnoush Taghizadeh for her help with figures included in this article.

References

1. Handoko, A. D.; Fredrickson, K. D.; Anasori, B.; Convey, K. W.; Johnson, L. R.; Gogotsi, Y.; Vojvodic, A.; Seh, Z. W., Tuning the basal plane functionalization of two-dimensional metal carbides (MXenes) to control hydrogen evolution activity. *ACS Applied Energy Materials* **2017,** *1* (1), 173-180.
2. Jun, B.-M.; Kim, S.; Heo, J.; Park, C. M.; Her, N.; Jang, M.; Huang, Y.; Han, J.; Yoon, Y., Review of MXenes as new nanomaterials for energy storage/delivery and selected environmental applications. *Nano Research* **2019,** *12* (3), 471-487.
3. Gogotsi, Y.; Anasori, B., The rise of MXenes. ACS Publications: 2019.
4. Lim, K. R. G.; Handoko, A. D.; Nemani, S. K.; Wyatt, B.; Jiang, H.-Y.; Tang, J.; Anasori, B.; Seh, Z. W., Rational Design of Two-Dimensional Transition Metal Carbide/Nitride (MXene) Hybrids and Nanocomposites for Catalytic Energy Storage and Conversion. *ACS nano* **2020,** *14* (9), 10834-10864.
5. Naguib, M.; Kurtoglu, M.; Presser, V.; Lu, J.; Niu, J.; Heon, M.; Hultman, L.; Gogotsi, Y.; Barsoum, M. W., Two-dimensional nanocrystals produced by exfoliation of Ti3AlC2. *Advanced materials* **2011,** *23* (37), 4248-4253.
6. Anasori, B.; Lukatskaya, M. R.; Gogotsi, Y., 2D metal carbides and nitrides (MXenes) for energy storage. *Nature Reviews Materials* **2017,** *2* (2), 1-17.
7. Naguib, M.; Mochalin, V. N.; Barsoum, M. W.; Gogotsi, Y., 25th anniversary article: MXenes: a new family of two-dimensional materials. *Advanced materials* **2014,** *26* (7), 992-1005.
8. Anasori, B.; Xie, Y.; Beidaghi, M.; Lu, J.; Hosler, B.; Hultman, L.; Kent, P.; Gogotsi, Y.; Barsoum, M., Two-dimensional, ordered, double transition metals carbides (MXenes). ACS Nano 9 (10): 9507-9516. 2015.
9. Mashtalir, O.; Naguib, M.; Mochalin, V. N.; Dall'Agnese, Y.; Heon, M.; Barsoum, M. W.; Gogotsi, Y., Intercalation and delamination of layered carbides and carbonitrides. *Nature communications* **2013,** *4* (1), 1-7.
10. Mashtalir, O.; Lukatskaya, M. R.; Zhao, M. Q.; Barsoum, M. W.; Gogotsi, Y., Amine-assisted delamination of Nb2C MXene for Li-ion energy storage devices. *Advanced Materials* **2015,** *27* (23), 3501-3506.
11. Zhang, C. J.; Pinilla, S.; McEvoy, N.; Cullen, C. P.; Anasori, B.; Long, E.; Park, S.-H.; Seral-Ascaso, A. s.; Shmeliov, A.; Krishnan, D., Oxidation stability of colloidal two-dimensional titanium carbides (MXenes). *Chemistry of Materials* **2017,** *29* (11), 4848-4856.
12. Ravikumar, K.; Udayakumar, J., Preparation and characterisation of green clay-polymer nanocomposite for heavy metals removal. *Chemistry and Ecology* **2020,** *36* (3), 270-291.
13. Xia, X.; Weng, G. J.; Zhang, J.; Li, Y., The effect of temperature and graphene concentration on the electrical conductivity and dielectric permittivity of graphene–polymer nanocomposites. *Acta Mechanica* **2020**, 1-16.
14. Chen, J.; Li, Y.; Wang, Y.; Dong, J.; Xu, X.; Yuan, Q.; Niu, Y.; Wang, Q.; Wang, H., Significantly improved breakdown strength and energy density of tri-layered polymer nanocomposites with optimized graphene oxide. *Composites Science and Technology* **2020,** *186*, 107912.
15. Kuilla, T.; Bhadra, S.; Yao, D.; Kim, N. H.; Bose, S.; Lee, J. H., Recent advances in graphene based polymer composites. *Progress in polymer science* **2010,** *35* (11), 1350-1375.
16. Mukhopadhyay, P.; Gupta, R. K., Trends and frontiers in graphene-based polymer nanocomposites. *Plastics engineering* **2011,** *67* (1), 32-42.
17. Zhao, J.; Yang, Y.; Yang, C.; Tian, Y.; Han, Y.; Liu, J.; Yin, X.; Que, W., A hydrophobic surface enabled salt-blocking 2D Ti 3 C 2 MXene membrane for efficient and stable solar desalination. *Journal of Materials Chemistry A* **2018,** *6* (33), 16196-16204.
18. Lawal, A. T., Recent progress in graphene based polymer nanocomposites. *Cogent Chemistry* **2020,** *6* (1), 1833476.

19. Potts, J.; Dreyer, D.; Bielawski, C.; Ruoff, R., Graphene-Based Polymer Nanocomposites. *Polymer* **2011,** *52*, 5–25.
20. Bera, M.; Maji, P., Graphene-based polymer nanocomposites: materials for future revolution. *MOJ Poly Sci* **2017,** *1* (3), 00013.
21. Silva, M.; Alves, N. M.; Paiva, M. C., Graphene-polymer nanocomposites for biomedical applications. *Polymers for Advanced Technologies* **2018,** *29* (2), 687-700.
22. Barroso-Bujans, F.; Cerveny, S.; Verdejo, R.; del Val, J. J.; Alberdi, J. M.; Alegría, A.; Colmenero, J., Permanent adsorption of organic solvents in graphite oxide and its effect on the thermal exfoliation. *Carbon* **2010,** *48* (4), 1079-1087.
23. Guan, L.-Z.; Zhao, L.; Wan, Y.-J.; Tang, L.-C., Three-dimensional graphene-based polymer nanocomposites: preparation, properties and applications. *Nanoscale* **2018,** *10* (31), 14788-14811.
24. Krishnan, S.; Tadiboyina, R.; Chavali, M.; Nikolova, M.; Wu, R.-J.; Bian, D.; Jeng, Y.-R.; Rao, P.; Palanisamy, P.; Reddy, S., Graphene-Based Polymer Nanocomposites for Sensor Applications. 2019.
25. Zhang, L. L.; Zhao, X., Carbon-based materials as supercapacitor electrodes. *Chemical Society Reviews* **2009,** *38* (9), 2520-2531.
26. Holmes, J.; O'Connell, J.; Duffy, R.; Long, B., Surface Functionalization Strategies for Monolayer Doping. **2018**.
27. Achari, A.; S, S.; Eswaramoorthy, M., High performance MoS2 membranes: effects of thermally driven phase transition on CO2 separation efficiency. *Energy & Environmental Science* **2016,** *9* (4), 1224-1228.
28. Tu, S.; Jiang, Q.; Zhang, J.; He, X.; Hedhili, M. N.; Zhang, X.; Alshareef, H. N., Enhancement of Dielectric Permittivity of Ti3C2Tx MXene/Polymer Composites by Controlling Flake Size and Surface Termination. *ACS Applied Materials & Interfaces* **2019,** *11* (30), 27358-27362.
29. Mohan, V. B.; Brown, R.; Jayaraman, K.; Bhattacharyya, D., Characterisation of reduced graphene oxide: Effects of reduction variables on electrical conductivity. *Materials Science and Engineering: B* **2015,** *193*, 49-60.
30. Almajid, A.; Sorochynska, L.; Friedrich, K.; Wetzel, B., Effects of graphene and CNT on mechanical, thermal, electrical and corrosion properties of vinylester based nanocomposites. *Plastics, Rubber and Composites* **2015,** *44* (2), 50-62.
31. Mohan, V. B.; Lau, K.-t.; Hui, D.; Bhattacharyya, D., Graphene-based materials and their composites: A review on production, applications and product limitations. *Composites Part B: Engineering* **2018,** *142*, 200-220.
32. Lipatov, A.; Lu, H.; Alhabeb, M.; Anasori, B.; Gruverman, A.; Gogotsi, Y.; Sinitskii, A., Elastic properties of 2D Ti3C2Tx MXene monolayers and bilayers. *Science advances* **2018,** *4* (6), eaat0491.
33. Yorulmaz, U.; Özden, A.; Perkgöz, N. K.; Ay, F.; Sevik, C., Vibrational and mechanical properties of single layer MXene structures: a first-principles investigation. *Nanotechnology* **2016,** *27* (33), 335702.
34. Chen, J.; Huang, Q.; Huang, H.; Mao, L.; Liu, M.; Zhang, X.; Wei, Y., Recent progress and advances in the environmental applications of MXene related materials. *Nanoscale* **2020,** *12* (6), 3574-3592.
35. Gao, L.; Li, C.; Huang, W.; Mei, S.; Lin, H.; Ou, Q.; Zhang, Y.; Guo, J.; Zhang, F.; Xu, S., MXene/polymer membranes: synthesis, properties, and emerging applications. *Chemistry of Materials* **2020,** *32* (5), 1703-1747.
36. Wu, L.; Jiang, X.; Zhao, J.; Liang, W.; Li, Z.; Huang, W.; Lin, Z.; Wang, Y.; Zhang, F.; Lu, S., MXene-based nonlinear optical information converter for all-optical modulator and switcher. *Laser & Photonics Reviews* **2018,** *12* (12), 1800215.
37. Feng, X.-Y.; Ding, B.-Y.; Liang, W.-Y.; Zhang, F.; Ning, T.-Y.; Liu, J.; Zhang, H., MXene Ti3C2T x absorber for a 1.06 μm passively Q-switched ceramic laser. *Laser Physics Letters* **2018,** *15* (8), 085805.

38. Jimmy, J.; Kandasubramanian, B., MXene Functionalized Polymer Composites: Synthesis and Applications. *European Polymer Journal* **2019**, 109367.
39. Simon, P., Two-dimensional MXene with controlled interlayer spacing for electrochemical energy storage. *ACS nano* **2017,** *11* (3), 2393-2396.
40. Fredrickson, K. D.; Anasori, B.; Seh, Z. W.; Gogotsi, Y.; Vojvodic, A., Effects of applied potential and water intercalation on the surface chemistry of Ti2C and Mo2C MXenes. *The Journal of Physical Chemistry C* **2016,** *120* (50), 28432-28440.
41. Karlsson, L. H.; Birch, J.; Halim, J.; Barsoum, M. W.; Persson, P. O., Atomically resolved structural and chemical investigation of single MXene sheets. *Nano letters* **2015,** *15* (8), 4955-4960.
42. Hu, M.; Hu, T.; Li, Z.; Yang, Y.; Cheng, R.; Yang, J.; Cui, C.; Wang, X., Surface functional groups and interlayer water determine the electrochemical capacitance of Ti3C2 T x MXene. *ACS nano* **2018,** *12* (4), 3578-3586.
43. Sang, X.; Xie, Y.; Lin, M.-W.; Alhabeb, M.; Van Aken, K. L.; Gogotsi, Y.; Kent, P. R.; Xiao, K.; Unocic, R. R., Atomic Defects in Monolayer Titanium Carbide (Ti3C2T x) MXene. *ACS nano* **2016,** *10* (10), 9193-9200.
44. Lu, Z.; Wei, Y.; Deng, J.; Ding, L.; Li, Z.-K.; Wang, H., Self-Crosslinked MXene (Ti3C2T x) Membranes with Good Antiswelling Property for Monovalent Metal Ion Exclusion. *ACS nano* **2019,** *13* (9), 10535-10544.
45. Hope, M. A.; Forse, A. C.; Griffith, K. J.; Lukatskaya, M. R.; Ghidiu, M.; Gogotsi, Y.; Grey, C. P., NMR reveals the surface functionalisation of Ti 3 C 2 MXene. *Physical Chemistry Chemical Physics* **2016,** *18* (7), 5099-5102.
46. Caffrey, N. M., Effect of mixed surface terminations on the structural and electrochemical properties of two-dimensional Ti 3 C 2 T 2 and V 2 CT 2 MXenes multilayers. *Nanoscale* **2018,** *10* (28), 13520-13530.
47. Fan, Z.; Wang, Y.; Xie, Z.; Wang, D.; Yuan, Y.; Kang, H.; Su, B.; Cheng, Z.; Liu, Y., Modified MXene/holey graphene films for advanced supercapacitor electrodes with superior energy storage. *Advanced Science* **2018,** *5* (10), 1800750.
48. Gao, X.; Li, Z.-K.; Xue, J.; Qian, Y.; Zhang, L.-Z.; Caro, J.; Wang, H., Titanium carbide Ti3C2Tx (MXene) enhanced PAN nanofiber membrane for air purification. *Journal of Membrane Science* **2019,** *586*, 162-169.
49. Hu, T.; Hu, M.; Gao, B.; Li, W.; Wang, X., Screening surface structure of MXenes by high-throughput computation and vibrational spectroscopic confirmation. *The Journal of Physical Chemistry C* **2018,** *122* (32), 18501-18509.
50. Zha, X.-H.; Luo, K.; Li, Q.; Huang, Q.; He, J.; Wen, X.; Du, S., Role of the surface effect on the structural, electronic and mechanical properties of the carbide MXenes. *EPL (Europhysics Letters)* **2015,** *111* (2), 26007.
51. Aierken, Y.; Sevik, C.; Gülseren, O.; Peeters, F. M.; Çakır, D., MXenes/graphene heterostructures for Li battery applications: a first principles study. *Journal of Materials Chemistry A* **2018,** *6* (5), 2337-2345.
52. Persson, I.; Näslund, L.-Å.; Halim, J.; Barsoum, M. W.; Darakchieva, V.; Palisaitis, J.; Rosen, J.; Persson, P. O. Å., On the organization and thermal behavior of functional groups on Ti3C2 MXene surfaces in vacuum. *2D Materials* **2017,** *5* (1), 015002.
53. Berdiyorov, G., Effect of surface functionalization on the electronic transport properties of Ti3C2 MXene. *EPL (Europhysics Letters)* **2015,** *111* (6), 67002.
54. Ji, X.; Xu, K.; Chen, C.; Zhang, B.; Ruan, Y.; Liu, J.; Miao, L.; Jiang, J., Probing the electrochemical capacitance of MXene nanosheets for high-performance pseudocapacitors. *Physical Chemistry Chemical Physics* **2016,** *18* (6), 4460-4467.

55. Ashton, M.; Mathew, K.; Hennig, R. G.; Sinnott, S. B., Predicted surface composition and thermodynamic stability of MXenes in solution. *The Journal of Physical Chemistry C* **2016,** *120* (6), 3550-3556.
56. Guo, L.; Wang, X.; Leong, Z. Y.; Mo, R.; Sun, L.; Yang, H. Y., Ar plasma modification of 2D MXene Ti3C2Tx nanosheets for efficient capacitive desalination. *FlatChem* **2018,** *8*, 17-24.
57. Lai, S.; Jeon, J.; Jang, S. K.; Xu, J.; Choi, Y. J.; Park, J.-H.; Hwang, E.; Lee, S., Surface group modification and carrier transport properties of layered transition metal carbides (Ti2CTx, T:–OH,–F and–O). *Nanoscale* **2015,** *7* (46), 19390-19396.
58. Liu, T.; Liu, X.; Graham, N.; Yu, W.; Sun, K., Two-dimensional MXene incorporated graphene oxide composite membrane with enhanced water purification performance. *Journal of Membrane Science* **2020,** *593*, 117431.
59. Wu, Y.; Ding, L.; Lu, Z.; Deng, J.; Wei, Y., Two-dimensional MXene membrane for ethanol dehydration. *Journal of Membrane Science* **2019,** *590*, 117300.
60. Xie, X.; Chen, C.; Zhang, N.; Tang, Z.-R.; Jiang, J.; Xu, Y.-J., Microstructure and surface control of MXene films for water purification. *Nature Sustainability* **2019,** *2* (9), 856-862.
61. Huang, S.; Mochalin, V. N., Hydrolysis of 2D transition-metal carbides (MXenes) in colloidal solutions. *Inorganic chemistry* **2019,** *58* (3), 1958-1966.
62. Seyedin, S.; Zhang, J.; Usman, K. A. S.; Qin, S.; Glushenkov, A. M.; Yanza, E. R. S.; Jones, R. T.; Razal, J. M., Facile Solution Processing of Stable MXene Dispersions towards Conductive Composite Fibers. *Global Challenges* **2019,** *3* (10), 1900037.
63. Maleski, K.; Mochalin, V. N.; Gogotsi, Y., Dispersions of two-dimensional titanium carbide MXene in organic solvents. *Chemistry of Materials* **2017,** *29* (4), 1632-1640.
64. Li, G.; Jiang, K.; Zaman, S.; Xuan, J.; Wang, Z.; Geng, F., Ti3C2 sheets with an adjustable surface and feature sizes to regulate the chemical stability. *Inorganic chemistry* **2019,** *58* (14), 9397-9403.
65. Natu, V.; Hart, J. L.; Sokol, M.; Chiang, H.; Taheri, M. L.; Barsoum, M. W., Edge Capping of 2D-MXene Sheets with Polyanionic Salts To Mitigate Oxidation in Aqueous Colloidal Suspensions. *Angewandte Chemie International Edition* **2019,** *58* (36), 12655-12660.
66. Mathis, T.; Maleski, M.; Goad, A.; Sarycheva, A.; Anayee, M.; Foucher, A. C.; Hantanasirisakul, K.; Stach, E.; Gogotsi, Y., Modified MAX Phase Synthesis for Environmentally Stable and Highly Conductive Ti3C2 MXene. *ChemRxiv* **2020**.
67. Kim, J.; Yoon, Y.; Kim, S. K.; Park, S.; Song, W.; Myung, S.; Jung, H. K.; Lee, S. S.; Yoon, D. H.; An, K. S., Chemically Stabilized and Functionalized 2D-MXene with Deep Eutectic Solvents as Versatile Dispersion Medium. *Advanced Functional Materials* **2021**, 2008722.
68. Habib, T.; Zhao, X.; Shah, S. A.; Chen, Y.; Sun, W.; An, H.; Lutkenhaus, J. L.; Radovic, M.; Green, M. J., Oxidation stability of Ti 3 C 2 T x MXene nanosheets in solvents and composite films. *npj 2D Materials and Applications* **2019,** *3* (1), 1-6.
69. Liao, H.; Guo, X.; Wan, P.; Yu, G., Conductive MXene Nanocomposite Organohydrogel for Flexible, Healable, Low-Temperature Tolerant Strain Sensors. *Advanced Functional Materials* **2019,** *29* (39), 1904507.
70. Wen, J.; Zhang, X.; Gao, H., Role of the H-containing groups on the structural dynamics of Ti3C2Tx MXene. *Physica B: Condensed Matter* **2018,** *537*, 155-161.
71. Ma, Y.; Liu, N.; Li, L.; Hu, X.; Zou, Z.; Wang, J.; Luo, S.; Gao, Y., A highly flexible and sensitive piezoresistive sensor based on MXene with greatly changed interlayer distances. *Nature communications* **2017,** *8* (1), 1207.
72. Wen, Y.; Rufford, T. E.; Chen, X.; Li, N.; Lyu, M.; Dai, L.; Wang, L., Nitrogen-doped Ti3C2Tx MXene electrodes for high-performance supercapacitors. *Nano Energy* **2017,** *38*, 368-376.

73. Hantanasirisakul, K.; Zhao, M. Q.; Urbankowski, P.; Halim, J.; Anasori, B.; Kota, S.; Ren, C. E.; Barsoum, M. W.; Gogotsi, Y., Fabrication of Ti3C2Tx MXene transparent thin films with tunable optoelectronic properties. *Advanced Electronic Materials* **2016,** *2* (6), 1600050.
74. Mashtalir, O.; Lukatskaya, M. R.; Kolesnikov, A. I.; Raymundo-Pinero, E.; Naguib, M.; Barsoum, M.; Gogotsi, Y., The effect of hydrazine intercalation on the structure and capacitance of 2D titanium carbide (MXene). *Nanoscale* **2016,** *8* (17), 9128-9133.
75. Come, J.; Black, J. M.; Lukatskaya, M. R.; Naguib, M.; Beidaghi, M.; Rondinone, A. J.; Kalinin, S. V.; Wesolowski, D. J.; Gogotsi, Y.; Balke, N., Controlling the actuation properties of MXene paper electrodes upon cation intercalation. *Nano Energy* **2015,** *17*, 27-35.
76. Kajiyama, S.; Szabova, L.; Sodeyama, K.; Iinuma, H.; Morita, R.; Gotoh, K.; Tateyama, Y.; Okubo, M.; Yamada, A., Sodium-ion intercalation mechanism in MXene nanosheets. *ACS nano* **2016,** *10* (3), 3334-3341.
77. Osti, N. C.; Naguib, M.; Ostadhossein, A.; Xie, Y.; Kent, P. R.; Dyatkin, B.; Rother, G.; Heller, W. T.; van Duin, A. C.; Gogotsi, Y., Effect of metal ion intercalation on the structure of MXene and water dynamics on its internal surfaces. *ACS applied materials & interfaces* **2016,** *8* (14), 8859-8863.
78. Okubo, M.; Sugahara, A.; Kajiyama, S.; Yamada, A., MXene as a charge storage host. *Accounts of chemical research* **2018,** *51* (3), 591-599.
79. Lu, M.; Han, W.; Li, H.; Shi, W.; Wang, J.; Zhang, B.; Zhou, Y.; Li, H.; Zhang, W.; Zheng, W., Tent-pitching-inspired high-valence period 3-cation pre-intercalation excels for anode of 2D titanium carbide (MXene) with high Li storage capacity. *Energy Storage Materials* **2019,** *16*, 163-168.
80. Ren, C. E.; Alhabeb, M.; Byles, B. W.; Zhao, M.-Q.; Anasori, B.; Pomerantseva, E.; Mahmoud, K. A.; Gogotsi, Y., Voltage-Gated Ions Sieving through 2D MXene Ti3C2T x Membranes. *ACS Applied Nano Materials* **2018,** *1* (7), 3644-3652.
81. Yan, J.; Ren, C. E.; Maleski, K.; Hatter, C. B.; Anasori, B.; Urbankowski, P.; Sarycheva, A.; Gogotsi, Y., Flexible MXene/graphene films for ultrafast supercapacitors with outstanding volumetric capacitance. *Advanced Functional Materials* **2017,** *27* (30), 1701264.
82. Riazi, H.; Anayee, M.; Hantanasirisakul, K.; Shamsabadi, A. A.; Anasori, B.; Gogotsi, Y.; Soroush, M., Surface Modification of a MXene by an Aminosilane Coupling Agent. *Advanced Materials Interfaces* **2020**, 1902008.
83. Sun, Y.; Li, S.; Zhuang, Y.; Liu, G.; Xing, W.; Jing, W., Adjustable interlayer spacing of ultrathin MXene-derived membranes for ion rejection. *Journal of Membrane Science* **2019,** *591*, 117350.
84. Lipatov, A.; Alhabeb, M.; Lukatskaya, M. R.; Boson, A.; Gogotsi, Y.; Sinitskii, A., Effect of synthesis on quality, electronic properties and environmental stability of individual monolayer Ti3C2 MXene flakes. *Advanced Electronic Materials* **2016,** *2* (12), 1600255.
85. Alhabeb, M.; Maleski, K.; Anasori, B.; Lelyukh, P.; Clark, L.; Sin, S.; Gogotsi, Y., Guidelines for synthesis and processing of two-dimensional titanium carbide (Ti3C2T x MXene). *Chemistry of Materials* **2017,** *29* (18), 7633-7644.
86. Shekhirev, M.; Shuck, C. E.; Sarycheva, A.; Gogotsi, Y., Characterization of MXenes at Every Step, from Their Precursors to Single Flakes and Assembled Films. *Progress in Materials Science* **2020**, 100757.
87. Wu, M.; He, M.; Hu, Q.; Wu, Q.; Sun, G.; Xie, L.; Zhang, Z.; Zhu, Z.; Zhou, A., Ti3C2 MXene-based sensors with high selectivity for NH3 detection at room temperature. *ACS sensors* **2019,** *4* (10), 2763-2770.
88. Verger, L.; Xu, C.; Natu, V.; Cheng, H.-M.; Ren, W.; Barsoum, M. W., Overview of the synthesis of MXenes and other ultrathin 2D transition metal carbides and nitrides. *Current Opinion in Solid State and Materials Science* **2019,** *23* (3), 149-163.

89. Seredych, M.; Shuck, C. E.; Pinto, D.; Alhabeb, M.; Precetti, E.; Deysher, G.; Anasori, B.; Kurra, N.; Gogotsi, Y., High-temperature behavior and surface chemistry of carbide MXenes studied by thermal analysis. *Chemistry of Materials* **2019,** *31* (9), 3324-3332.
90. Bian, R.; He, G.; Zhi, W.; Xiang, S.; Wang, T.; Cai, D., Ultralight MXene-based aerogels with high electromagnetic interference shielding performance. *Journal of Materials Chemistry C* **2019,** *7* (3), 474-478.
91. Shuck, C. E.; Sarycheva, A.; Anayee, M.; Levitt, A.; Zhu, Y.; Uzun, S.; Balitskiy, V.; Zahorodna, V.; Gogotsi, O.; Gogotsi, Y., Scalable Synthesis of Ti3C2Tx MXene. *Advanced Engineering Materials* **2020**.
92. Xu, C.; Wang, L.; Liu, Z.; Chen, L.; Guo, J.; Kang, N.; Ma, X.-L.; Cheng, H.-M.; Ren, W., Large-area high-quality 2D ultrathin Mo 2 C superconducting crystals. *Nature materials* **2015,** *14* (11), 1135-1141.
93. Zhang, F.; Zhang, Z.; Wang, H.; Chan, C. H.; Chan, N. Y.; Chen, X. X.; Dai, J.-Y., Plasma-enhanced pulsed-laser deposition of single-crystalline M o 2 C ultrathin superconducting films. *Physical Review Materials* **2017,** *1* (3), 034002.
94. Xiao, X.; Yu, H.; Jin, H.; Wu, M.; Fang, Y.; Sun, J.; Hu, Z.; Li, T.; Wu, J.; Huang, L., Salt-templated synthesis of 2D metallic MoN and other nitrides. *ACS nano* **2017,** *11* (2), 2180-2186.
95. Jia, J.; Xiong, T.; Zhao, L.; Wang, F.; Liu, H.; Hu, R.; Zhou, J.; Zhou, W.; Chen, S., Ultrathin N-doped Mo2C nanosheets with exposed active sites as efficient electrocatalyst for hydrogen evolution reactions. *ACS nano* **2017,** *11* (12), 12509-12518.
96. Awasthi, G. P.; Maharjan, B.; Shrestha, S.; Bhattarai, D. P.; Yoon, D.; Park, C. H.; Kim, C. S., Synthesis, characterizations, and biocompatibility evaluation of polycaprolactone–MXene electrospun fibers. *Colloids and Surfaces A: Physicochemical and Engineering Aspects* **2020,** *586*, 124282.
97. Si, J.-Y.; Tawiah, B.; Sun, W.-L.; Lin, B.; Wang, C.; Yuen, A. C. Y.; Yu, B.; Li, A.; Yang, W.; Lu, H.-D., Functionalization of MXene nanosheets for polystyrene towards high thermal stability and flame retardant properties. *Polymers* **2019,** *11* (6), 976.
98. Huang, Y.; Jiang, S.; Liang, R.; Sun, P.; Hai, Y.; Zhang, L., Thermal-triggered insulating fireproof layers: A novel fire-extinguishing MXene composites coating. *Chemical Engineering Journal* **2019**, 123621.
99. Zhang, Q.; Yi, G.; Fu, Z.; Yu, H.; Chen, S.; Quan, X., Vertically Aligned Janus MXene-Based Aerogels for Solar Desalination with High Efficiency and Salt Resistance. *ACS nano* **2019,** *13* (11), 13196-13207.
100. Tao, N.; Zhang, D.; Li, X.; Lou, D.; Sun, X.; Wei, C.; Li, J.; Yang, J.; Liu, Y.-N., Near-infrared light-responsive hydrogels via peroxide-decorated MXene-initiated polymerization. *Chemical Science* **2019,** *10* (46), 10765-10771.
101. Enyashin, A. N.; Ivanovskii, A. L., Structural and electronic properties and stability of MX enes Ti2C and Ti3C2 functionalized by methoxy groups. *The Journal of Physical Chemistry C* **2013,** *117* (26), 13637-13643.
102. Zhang, J.; Liu, Y.; Lv, Z.; Zhao, T.; Li, P.; Sun, Y.; Wang, J., Sulfonated Ti3C2Tx to construct proton transfer pathways in polymer electrolyte membrane for enhanced conduction. *Solid State Ionics* **2017,** *310*, 100-111.
103. Lim, S.; Park, H.; Yang, J.; Kwak, C.; Lee, J., Stable colloidal dispersion of octylated Ti3C2-MXenes in a nonpolar solvent. *Colloids and Surfaces A: Physicochemical and Engineering Aspects* **2019,** *579*, 123648.
104. Chen, J.; Chen, K.; Tong, D.; Huang, Y.; Zhang, J.; Xue, J.; Huang, Q.; Chen, T., CO 2 and temperature dual responsive "Smart" MXene phases. *Chemical Communications* **2015,** *51* (2), 314-317.
105. Sheng, X.; Zhao, Y.; Zhang, L.; Lu, X., Properties of two-dimensional Ti3C2 MXene/thermoplastic polyurethane nanocomposites with effective reinforcement via melt blending. *Composites Science and Technology* **2019,** *181*, 107710.

106. Fu, J.; Yun, J.; Wu, S.; Li, L.; Yu, L.; Kim, K. H., Architecturally Robust Graphene-Encapsulated MXene Ti2CT x@ Polyaniline Composite for High-Performance Pouch-Type Asymmetric Supercapacitor. *ACS applied materials & interfaces* **2018,** *10* (40), 34212-34221.
107. Pandey, R. P.; Rasool, K.; Madhavan, V. E.; Aïssa, B.; Gogotsi, Y.; Mahmoud, K. A., Ultrahigh-flux and fouling-resistant membranes based on layered silver/MXene (Ti 3 C 2 T x) nanosheets. *Journal of Materials Chemistry A* **2018,** *6* (8), 3522-3533.
108. Fan, X.; Ding, Y.; Liu, Y.; Liang, J.; Chen, Y., Plasmonic Ti3C2T x MXene Enables Highly Efficient Photothermal Conversion for Healable and Transparent Wearable Device. *ACS nano* **2019,** *13* (7), 8124-8134.
109. Vatankhah-Varnoosfaderani, M.; Ina, M.; Adelnia, H.; Li, Q.; Zhushma, A. P.; Hall, L. J.; Sheiko, S. S., Well-defined zwitterionic microgels: synthesis and application as acid-resistant microreactors. *Macromolecules* **2016,** *49* (19), 7204-7210.
110. Vatankhah-Varnosfaderani, M.; Hu, X.; Li, Q.; Adelnia, H.; Ina, M.; Sheiko, S. S., Universal coatings based on zwitterionic–dopamine copolymer microgels. *ACS applied materials & interfaces* **2018,** *10* (24), 20869-20875.
111. Adelnia, H.; Blakey, I.; Little, A.; Peter, J.; Ta, H. T., Hydrogels Based on Poly (aspartic acid): Synthesis and Applications. *Frontiers in Chemistry* **2019,** *7*, 755.
112. Zhou, B.; zhang, z.; li, y.; han, g.; Feng, Y.; Wang, B.; zhang, d.; Ma, J.; Liu, C., Flexible, Robust and Multifunctional Electromagnetic Interference Shielding Film with Alternating Cellulose Nanofiber and MXene Layers. *ACS Applied Materials & Interfaces* **2020**.
113. Wu, X.; Liao, H.; Ma, D.; Chao, M.; Wang, Y.; Jia, X.; Wan, P.; Zhang, L., A wearable, self-adhesive, long-lastingly moist and healable epidermal sensor assembled from conductive MXene nanocomposites. *Journal of Materials Chemistry C* **2020**.
114. Xing, C.; Chen, S.; Liang, X.; Liu, Q.; Qu, M.; Zou, Q.; Li, J.; Tan, H.; Liu, L.; Fan, D., Two-dimensional MXene (Ti3C2)-integrated cellulose hydrogels: toward smart three-dimensional network nanoplatforms exhibiting light-induced swelling and bimodal photothermal/chemotherapy anticancer activity. *ACS applied materials & interfaces* **2018,** *10* (33), 27631-27643.
115. Liu, J.; Zhang, H. B.; Sun, R.; Liu, Y.; Liu, Z.; Zhou, A.; Yu, Z. Z., Hydrophobic, flexible, and lightweight MXene foams for high-performance electromagnetic-interference shielding. *Advanced Materials* **2017,** *29* (38), 1702367.
116. Wu, X.; Han, B.; Zhang, H.-B.; Xie, X.; Tu, T.; Zhang, Y.; Dai, Y.; Yang, R.; Yu, Z.-Z., Compressible, durable and conductive polydimethylsiloxane-coated MXene foams for high-performance electromagnetic interference shielding. *Chemical Engineering Journal* **2020,** *381*, 122622.
117. Wang, D.; Lin, Y.; Hu, D.; Jiang, P.; Huang, X., Multifunctional 3D-MXene/PDMS nanocomposites for electrical, thermal and triboelectric applications. *Composites Part A: Applied Science and Manufacturing* **2020,** *130*, 105754.
118. Xu, H.; Yin, X.; Li, X.; Li, M.; Liang, S.; Zhang, L.; Cheng, L., Lightweight Ti2CT x MXene/Poly (vinyl alcohol) Composite Foams for Electromagnetic Wave Shielding with Absorption-Dominated Feature. *ACS applied materials & interfaces* **2019,** *11* (10), 10198-10207.
119. Liu, J.; Zhang, H. B.; Xie, X.; Yang, R.; Liu, Z.; Liu, Y.; Yu, Z. Z., Multifunctional, superelastic, and lightweight MXene/polyimide aerogels. *Small* **2018,** *14* (45), 1802479.
120. Zhang, P.; Yang, X.-J.; Li, P.; Zhao, Y.; Niu, Q. J., Fabrication of novel MXene (Ti 3 C 2)/polyacrylamide nanocomposite hydrogels with enhanced mechanical and drug release properties. *Soft matter* **2020,** *16* (1), 162-169.
121. Anasori, B.; Gogotsi, Y., *2D Metal Carbides and Nitrides (MXenes)*. Springer: 2019.
122. Aziz, F.; Ismail, A., Spray coating methods for polymer solar cells fabrication: A review. *Materials Science in Semiconductor Processing* **2015,** *39*, 416-425.

123. Krebs, F. C., Fabrication and processing of polymer solar cells: A review of printing and coating techniques. *Solar energy materials and solar cells* **2009,** *93* (4), 394-412.
124. Mirkhani, S. A.; Shayesteh Zeraati, A.; Aliabadian, E.; Naguib, M.; Sundararaj, U., High Dielectric Constant and Low Dielectric Loss via Poly (vinyl alcohol)/Ti3C2T x MXene Nanocomposites. *ACS applied materials & interfaces* **2019,** *11* (20), 18599-18608.
125. Akuzum, B.; Maleski, K.; Anasori, B.; Lelyukh, P.; Alvarez, N. J.; Kumbur, E. C.; Gogotsi, Y., Rheological characteristics of 2D titanium carbide (MXene) dispersions: a guide for processing MXenes. *ACS nano* **2018,** *12* (3), 2685-2694.
126. Tanvir, A.; Sobolčiak, P.; Popelka, A.; Mrlik, M.; Spitalsky, Z.; Micusik, M.; Prokes, J.; Krupa, I., Electrically conductive, transparent polymeric nanocomposites modified by 2D Ti3C2Tx (MXene). *Polymers* **2019,** *11* (8), 1272.
127. Shao, J.; Wang, J.-W.; Liu, D.-N.; Wei, L.; Wu, S.-Q.; Ren, H., A novel high permittivity percolative composite with modified MXene. *Polymer* **2019,** *174*, 86-95.
128. Jin, X.; Wang, J.; Dai, L.; Liu, X.; Li, L.; Yang, Y.; Cao, Y.; Wang, W.; Wu, H.; Guo, S., Flame-retardant poly (vinyl alcohol)/MXene multilayered films with outstanding electromagnetic interference shielding and thermal conductive performances. *Chemical Engineering Journal* **2020,** *380*, 122475.
129. Shahzad, F.; Alhabeb, M.; Hatter, C. B.; Anasori, B.; Hong, S. M.; Koo, C. M.; Gogotsi, Y., Electromagnetic interference shielding with 2D transition metal carbides (MXenes). *Science* **2016,** *353* (6304), 1137-1140.
130. Ling, Z.; Ren, C. E.; Zhao, M.-Q.; Yang, J.; Giammarco, J. M.; Qiu, J.; Barsoum, M. W.; Gogotsi, Y., Flexible and conductive MXene films and nanocomposites with high capacitance. *Proceedings of the National Academy of Sciences* **2014,** *111* (47), 16676-16681.
131. Huang, X.; Wang, R.; Jiao, T.; Zou, G.; Zhan, F.; Yin, J.; Zhang, L.; Zhou, J.; Peng, Q., Facile preparation of hierarchical AgNP-loaded MXene/Fe3O4/polymer nanocomposites by electrospinning with enhanced catalytic performance for wastewater treatment. *ACS omega* **2019,** *4* (1), 1897-1906.
132. Cao, W.-T.; Chen, F.-F.; Zhu, Y.-J.; Zhang, Y.-G.; Jiang, Y.-Y.; Ma, M.-G.; Chen, F., Binary strengthening and toughening of MXene/cellulose nanofiber composite paper with nacre-inspired structure and superior electromagnetic interference shielding properties. *ACS nano* **2018,** *12* (5), 4583-4593.
133. Liu, R.; Miao, M.; Li, Y.; Zhang, J.; Cao, S.; Feng, X., Ultrathin Biomimetic Polymeric Ti3C2T x MXene Composite Films for Electromagnetic Interference Shielding. *ACS applied materials & interfaces* **2018,** *10* (51), 44787-44795.
134. Peng, Y.-Y.; Akuzum, B.; Kurra, N.; Zhao, M.-Q.; Alhabeb, M.; Anasori, B.; Kumbur, E. C.; Alshareef, H. N.; Ger, M.-D.; Gogotsi, Y., All-MXene (2D titanium carbide) solid-state microsupercapacitors for on-chip energy storage. *Energy & Environmental Science* **2016,** *9* (9), 2847-2854.
135. Dillon, A. D.; Ghidiu, M. J.; Krick, A. L.; Griggs, J.; May, S. J.; Gogotsi, Y.; Barsoum, M. W.; Fafarman, A. T., Highly conductive optical quality solution-processed films of 2D titanium carbide. *Advanced Functional Materials* **2016,** *26* (23), 4162-4168.
136. Ying, G.; Dillon, A. D.; Fafarman, A. T.; Barsoum, M. W., Transparent, conductive solution processed spincast 2d ti2ct x (mxene) films. *Materials Research Letters* **2017,** *5* (6), 391-398.
137. Wu, X.; Huang, B.; Lv, R.; Wang, Q.; Wang, Y., Highly flexible and low capacitance loss supercapacitor electrode based on hybridizing decentralized conjugated polymer chains with MXene. *Chemical Engineering Journal* **2019,** *378*, 122246.
138. Mao, H.; Gu, C.; Yan, S.; Xin, Q.; Cheng, S.; Tan, P.; Wang, X.; Xiu, F.; Liu, X.; Liu, J., MXene Quantum Dot/Polymer Hybrid Structures with Tunable Electrical Conductance and Resistive Switching for Nonvolatile Memory Devices. *Advanced Electronic Materials* **2019**, 1900493.

139. Anasori, B.; Sarycheva, A.; Buondonno, S.; Zhou, Z.; Yang, S.; Gogotsi, Y., 2D metal carbides (MXenes) in fibers. *Materials Today* **2017,** *20* (8), 481-482.
140. Wang, Q. W.; Zhang, H. B.; Liu, J.; Zhao, S.; Xie, X.; Liu, L.; Yang, R.; Koratkar, N.; Yu, Z. Z., Multifunctional and Water-Resistant MXene-Decorated Polyester Textiles with Outstanding Electromagnetic Interference Shielding and Joule Heating Performances. *Advanced Functional Materials* **2019,** *29* (7), 1806819.
141. Li, L.; Liu, X.; Wang, J.; Yang, Y.; Cao, Y.; Wang, W., New application of MXene in polymer composites toward remarkable anti-dripping performance for flame retardancy. *Composites Part A: Applied Science and Manufacturing* **2019,** *127*, 105649.
142. An, H.; Habib, T.; Shah, S.; Gao, H.; Patel, A.; Echols, I.; Zhao, X.; Radovic, M.; Green, M. J.; Lutkenhaus, J. L., Water sorption in MXene/polyelectrolyte multilayers for ultrafast humidity sensing. *ACS Applied Nano Materials* **2019,** *2* (2), 948-955.
143. Lin, B.; Yuen, A. C. Y.; Li, A.; Zhang, Y.; Chen, T. B. Y.; Yu, B.; Lee, E. W. M.; Peng, S.; Yang, W.; Lu, H.-D., MXene/chitosan nanocoating for flexible polyurethane foam towards remarkable fire hazards reductions. *Journal of hazardous materials* **2020,** *381*, 120952.
144. Uzun, S.; Seyedin, S.; Stoltzfus, A. L.; Levitt, A. S.; Alhabeb, M.; Anayee, M.; Strobel, C. J.; Razal, J. M.; Dion, G.; Gogotsi, Y., Knittable and Washable Multifunctional MXene-Coated Cellulose Yarns. *Advanced Functional Materials* **2019,** *29* (45), 1905015.
145. Adelnia, H.; Gavgani, J. N.; Riazi, H.; Bidsorkhi, H. C., Transition behavior, surface characteristics and film formation of functionalized poly (methyl methacrylate-co-butyl acrylate) particles. *Progress in Organic Coatings* **2014,** *77* (11), 1826-1833.
146. Riazi, H.; Jalali-Arani, A.; Taromi, F. A., In situ synthesis of silica/polyacrylate nanocomposite particles simultaneously bearing carboxylate and sulfonate functionalities via soap-free seeded emulsion polymerization. *Materials Chemistry and Physics* **2018,** *207*, 470-478.
147. Luo, J.-Q.; Zhao, S.; Zhang, H.-B.; Deng, Z.; Li, L.; Yu, Z.-Z., Flexible, stretchable and electrically conductive MXene/natural rubber nanocomposite films for efficient electromagnetic interference shielding. *Composites Science and Technology* **2019,** *182*, 107754.
148. Sun, R.; Zhang, H. B.; Liu, J.; Xie, X.; Yang, R.; Li, Y.; Hong, S.; Yu, Z. Z., Highly conductive transition metal carbide/carbonitride (MXene)@ polystyrene nanocomposites fabricated by electrostatic assembly for highly efficient electromagnetic interference shielding. *Advanced Functional Materials* **2017,** *27* (45), 1702807.
149. Xu, Z.; Gao, C., Graphene fiber: a new trend in carbon fibers. *Materials Today* **2015,** *18* (9), 480-492.
150. Levitt, A. S.; Alhabeb, M.; Hatter, C. B.; Sarycheva, A.; Dion, G.; Gogotsi, Y., Electrospun MXene/carbon nanofibers as supercapacitor electrodes. *Journal of Materials Chemistry A* **2019,** *7* (1), 269-277.
151. Mayerberger, E. A.; Urbanek, O.; McDaniel, R. M.; Street, R. M.; Barsoum, M. W.; Schauer, C. L., Preparation and characterization of polymer-Ti3C2Tx (MXene) composite nanofibers produced via electrospinning. *Journal of Applied Polymer Science* **2017,** *134* (37), 45295.
152. Shao, W.; Tebyetekerwa, M.; Marriam, I.; Li, W.; Wu, Y.; Peng, S.; Ramakrishna, S.; Yang, S.; Zhu, M., Polyester@ MXene nanofibers-based yarn electrodes. *Journal of Power Sources* **2018,** *396*, 683-690.
153. Sobolčiak, P.; Ali, A.; Hassan, M. K.; Helal, M. I.; Tanvir, A.; Popelka, A.; Al-Maadeed, M. A.; Krupa, I.; Mahmoud, K. A., 2D Ti3C2Tx (MXene)-reinforced polyvinyl alcohol (PVA) nanofibers with enhanced mechanical and electrical properties. *PloS one* **2017,** *12* (8), e0183705.
154. Zhang, H.; Wang, L.; Chen, Q.; Li, P.; Zhou, A.; Cao, X.; Hu, Q., Preparation, mechanical and anti-friction performance of MXene/polymer composites. *Materials & Design* **2016,** *92*, 682-689.

155. Rajavel, K.; Luo, S.; Wan, Y.; Yu, X.; Hu, Y.; Zhu, P.; Sun, R.; Wong, C., 2D Ti3C2Tx MXene/polyvinylidene fluoride (PVDF) nanocomposites for attenuation of electromagnetic radiation with excellent heat dissipation. *Composites Part A: Applied Science and Manufacturing* **2020,** *129*, 105693.
156. Cao, X.; Wu, M.; Zhou, A.; Wang, Y.; He, X.; Wang, L., Non-isothermal crystallization and thermal degradation kinetics of MXene/linear low-density polyethylene nanocomposites. *e-Polymers* **2017,** *17* (5), 373-381.
157. Samandari-Masouleh, L.; Mostoufi, N.; Khodadadi, A.; Mortazavi, Y.; Maghrebi, M., Modeling the growth of carbon nanotubes in a floating catalyst reactor. *Industrial & engineering chemistry research* **2012,** *51* (3), 1143-1149.
158. Zhang, X.; Wang, X.; Lei, Z.; Wang, L.; Tian, M.; Zhu, S.; Xiao, H.; Tang, X.; Qu, L., A Flexible MXene-Decorated Fabric with Interwoven Conductive Networks for Integrated Joule Heating, Electromagnetic Interference Shielding and Strain Sensing Performances. *ACS Applied Materials & Interfaces* **2020**.
159. Samandari-Masouleh, L.; Mostoufi, N.; Khodadadi, A.; Mortazavi, Y.; Maghrebi, M., Kinetic modeling of carbon nanotube production and minimization of amorphous carbon overlayer deposition in floating catalyst method. *International Journal of Chemical Reactor Engineering* **2012,** *10* (1).
160. Zhang, F.; Ju, P.; Pan, M.; Zhang, D.; Huang, Y.; Li, G.; Li, X., Self-healing mechanisms in smart protective coatings: A review. *Corrosion Science* **2018,** *144*, 74-88.
161. Zhai, L.; Narkar, A.; Ahn, K., Self-healing polymers with nanomaterials and nanostructures. *Nano Today* **2019**, 100826.
162. Zhang, Y.-Z.; Lee, K. H.; Anjum, D. H.; Sougrat, R.; Jiang, Q.; Kim, H.; Alshareef, H. N., MXenes stretch hydrogel sensor performance to new limits. *Science advances* **2018,** *4* (6), eaat0098.
163. Zou, Y.; Fang, L.; Chen, T.; Sun, M.; Lu, C.; Xu, Z., Near-infrared light and solar light activated self-healing epoxy coating having enhanced properties using MXene flakes as multifunctional fillers. *Polymers* **2018,** *10* (5), 474.
164. Luo, F.; Wu, K.; Guo, H.; Zhao, Q.; Lu, M., Simultaneous reduction and surface functionalization of graphene oxide for enhancing flame retardancy and thermal conductivity of mesogenic epoxy composites. *Polymer International* **2017,** *66* (1), 98-107.
165. Huang, X.; Zhi, C.; Lin, Y.; Bao, H.; Wu, G.; Jiang, P.; Mai, Y.-W., Thermal conductivity of graphene-based polymer nanocomposites. *Materials Science and Engineering: R: Reports* **2020,** *142*, 100577.
166. Kang, R.; Zhang, Z.; Guo, L.; Cui, J.; Chen, Y.; Hou, X.; Wang, B.; Lin, C.-T.; Jiang, N.; Yu, J., Enhanced Thermal Conductivity of Epoxy Composites Filled with 2D Transition Metal Carbides (MXenes) with Ultralow Loading. *Scientific Reports* **2019,** *9* (1), 9135.
167. Zhang, J.; Kong, N.; Uzun, S.; Levitt, A.; Seyedin, S.; Lynch, P. A.; Qin, S.; Han, M.; Yang, W.; Liu, J.; Wang, X.; Gogotsi, Y.; Razal, J. M., Scalable Manufacturing of Free-Standing, Strong Ti3C2Tx MXene Films with Outstanding Conductivity. *Advanced Materials* **2020,** *32* (23), 2001093.
168. Yan, C.; Ji, C.; Zeng, X.; Sun, R.; Wong, C.-P. In *Interconnecting the Promising MXenes via Ag Nanowire in Epoxy Nanocomposites for High-Performance Thermal Management Applications*, 2018 19th International Conference on Electronic Packaging Technology (ICEPT), IEEE: 2018; pp 510-512.
169. Liu, R.; Li, W., High-Thermal-Stability and High-Thermal-Conductivity Ti3C2T x MXene/Poly (vinyl alcohol)(PVA) Composites. *ACS omega* **2018,** *3* (3), 2609-2617.
170. Shahnazari, M.; Ahmadi, Z.; Masooleh, L., Perturbation Analysis of Heat Transfer and a Novel Method for Changing the Third Kind Boundary Condition into the First Kind. *Journal of Porous Media* **2017,** *20* (5).

171. Gavgani, J. N.; Adelnia, H.; Gudarzi, M. M., Intumescent flame retardant polyurethane/reduced graphene oxide composites with improved mechanical, thermal, and barrier properties. *Journal of Materials Science* **2014,** *49* (1), 243-254.
172. Bidsorkhi, H. C.; Soheilmoghaddam, M.; Pour, R. H.; Adelnia, H.; Mohamad, Z., Mechanical, thermal and flammability properties of ethylene-vinyl acetate (EVA)/sepiolite nanocomposites. *Polymer Testing* **2014,** *37*, 117-122.
173. Gavgani, J. N.; Adelnia, H.; Mir Mohamad Sadeghi, G.; Zafari, F., Intumescent flame retardant polyurethane/starch composites: thermal, mechanical, and rheological properties. *Journal of Applied Polymer Science* **2014,** *131* (23).
174. Wang, Y.; Jow, J.; Su, K.; Zhang, J., Dripping behavior of burning polymers under UL94 vertical test conditions. *Journal of fire sciences* **2012,** *30* (6), 477-501.
175. Pan, Y.; Fu, L.; Zhou, Q.; Wen, Z.; Lin, C. T.; Yu, J.; Wang, W.; Zhao, H., Flammability, thermal stability and mechanical properties of polyvinyl alcohol nanocomposites reinforced with delaminated Ti3C2Tx (MXene). *Polymer Composites* **2019**.
176. Naguib, M.; Saito, T.; Lai, S.; Rager, M. S.; Aytug, T.; Paranthaman, M. P.; Zhao, M.-Q.; Gogotsi, Y., Ti 3 C 2 T x (MXene)–polyacrylamide nanocomposite films. *RSC Advances* **2016,** *6* (76), 72069-72073.
177. Wang, L.; Qiu, H.; Song, P.; Zhang, Y.; Lu, Y.; Liang, C.; Kong, J.; Chen, L.; Gu, J., 3D Ti3C2Tx MXene/C hybrid foam/epoxy nanocomposites with superior electromagnetic interference shielding performances and robust mechanical properties. *Composites Part A: Applied Science and Manufacturing* **2019,** *123*, 293-300.
178. Zhang, J.; Kong, N.; Uzun, S.; Levitt, A.; Seyedin, S.; Lynch, P. A.; Qin, S.; Han, M.; Yang, W.; Liu, J., Scalable Manufacturing of Free-Standing, Strong Ti3C2Tx MXene Films with Outstanding Conductivity. *Advanced Materials* **2020**, 2001093.
179. Masooleh, L. S.; Arbogast, J. E.; Oktem, U.; Seider, W. D.; Soroush, M. In *A Method of Community Detection in Complex Weighted Networks*, 2020 Virtual AIChE Annual Meeting, AIChE: 2020.
180. Masooleh, L. S.; Oktem, U.; Seider, W. D.; Arbogast, J. E.; Soroush, M. In *Robust Large-Scale State-Estimate Prediction*, 2020 Virtual AIChE Annual Meeting, AIChE: 2020.
181. Zhou, L.; Zhang, X.; Ma, L.; Gao, J.; Jiang, Y., Acetylcholinesterase/chitosan-transition metal carbides nanocomposites-based biosensor for the organophosphate pesticides detection. *Biochemical Engineering Journal* **2017,** *128*, 243-249.
182. Liu, J.; Jiang, X.; Zhang, R.; Zhang, Y.; Wu, L.; Lu, W.; Li, J.; Li, Y.; Zhang, H., MXene-Enabled Electrochemical Microfluidic Biosensor: Applications toward Multicomponent Continuous Monitoring in Whole Blood. *Advanced Functional Materials* **2019,** *29* (6), 1807326.
183. Soheilmoghaddam, M.; Adelnia, H.; Bidsorkhi, H. C.; Sharifzadeh, G.; Wahit, M. U.; Akos, N. I.; Yussuf, A. A., Development of ethylene-vinyl acetate composites reinforced with graphene platelets. *Macromolecular Materials and Engineering* **2017,** *302* (2), 1600260.
184. Riazi, H.; A. Shamsabadi, A.; Grady, M. C.; Rappe, A. M.; Soroush, M., Experimental and theoretical study of the self-initiation reaction of methyl acrylate in free-radical polymerization. *Industrial & Engineering Chemistry Research* **2018,** *57* (2), 532-539.
185. Riazi, H.; Shamsabadi, A. A.; Corcoran, P.; Grady, M. C.; Rappe, A. M.; Soroush, M., On the thermal self-initiation reaction of n-butyl acrylate in free-radical polymerization. *Processes* **2018,** *6* (1), 3.
186. Laki, S.; A. Shamsabadi, A.; Riazi, H.; Grady, M. C.; Rappe, A. M.; Soroush, M., Experimental and Mechanistic Modeling Study of Self-Initiated High-Temperature Polymerization of Ethyl Acrylate. *Industrial & Engineering Chemistry Research* **2019**.
187. Kilikevičius, S.; Kvietkaitė, S.; Žukienė, K.; Omastová, M.; Aniskevich, A.; Zeleniakienė, D., Numerical investigation of the mechanical properties of a novel hybrid polymer composite reinforced with graphene and MXene nanosheets. *Computational Materials Science* **2020,** *174*, 109497.

188. Huang, Z.; Wang, S.; Kota, S.; Pan, Q.; Barsoum, M. W.; Li, C. Y., Structure and crystallization behavior of poly (ethylene oxide)/Ti3C2Tx MXene nanocomposites. *Polymer* **2016,** *102*, 119-126.
189. Yan, H.; Li, W.; Li, H.; Fan, X.; Zhu, M., Ti3C2 MXene nanosheets toward high-performance corrosion inhibitor for epoxy coating. *Progress in Organic Coatings* **2019,** *135*, 156-167.
190. Gavgani, J. N.; Adelnia, H.; Zaarei, D.; Gudarzi, M. M., Lightweight flexible polyurethane/reduced ultralarge graphene oxide composite foams for electromagnetic interference shielding. *RSC advances* **2016,** *6* (33), 27517-27527.
191. Raagulan, K.; Braveenth, R.; Kim, B. M.; Lim, K. J.; Lee, S. B.; Kim, M.; Chai, K. Y., An effective utilization of MXene and its effect on electromagnetic interference shielding: flexible, free-standing and thermally conductive composite from MXene–PAT–poly (p-aminophenol)–polyaniline co-polymer. *RSC Advances* **2020,** *10* (3), 1613-1633.
192. Qing, Y.; Zhou, W.; Luo, F.; Zhu, D., Titanium carbide (MXene) nanosheets as promising microwave absorbers. *Ceramics International* **2016,** *42* (14), 16412-16416.
193. Yang, H.; Dai, J.; Liu, X.; Lin, Y.; Wang, J.; Wang, L.; Wang, F., Layered PVB/Ba3Co2Fe24O41/Ti3C2 Mxene composite: enhanced electromagnetic wave absorption properties with high impedance match in a wide frequency range. *Materials Chemistry and Physics* **2017,** *200*, 179-186.
194. Bora, P. J.; Anil, A. G.; Ramamurthy, P. C.; Tan, D. Q., MXene interlayered crosslinked conducting polymer film for highly specific absorption and electromagnetic interference shielding. *Materials Advances* **2020**.
195. Wei, H.; Dong, J.; Fang, X.; Zheng, W.; Sun, Y.; Qian, Y.; Jiang, Z.; Huang, Y., Ti3C2Tx MXene/polyaniline (PANI) sandwich intercalation structure composites constructed for microwave absorption. *Composites Science and Technology* **2019,** *169*, 52-59.
196. Raagulan, K.; Kim, B. M.; Chai, K. Y., Recent Advancement of Electromagnetic Interference (EMI) Shielding of Two Dimensional (2D) MXene and Graphene Aerogel Composites. *Nanomaterials* **2020,** *10* (4), 702.
197. Jan, R.; Habib, A.; Akram, M. A.; Ahmad, I.; Shah, A.; Sadiq, M.; Hussain, A., Flexible, thin films of graphene–polymer composites for EMI shielding. *Materials Research Express* **2017,** *4* (3), 035605.
198. Iqbal, A.; Shahzad, F.; Hantanasirisakul, K.; Kim, M.-K.; Kwon, J.; Hong, J.; Kim, H.; Kim, D.; Gogotsi, Y.; Koo, C. M., Anomalous absorption of electromagnetic waves by 2D transition metal carbonitride Ti3CNTx (MXene). *Science* **2020,** *369* (6502), 446-450.
199. Liu, G.; Jin, W.; Xu, N., Two-dimensional-material membranes: a new family of high-performance separation membranes. *Angewandte Chemie International Edition* **2016,** *55* (43), 13384-13397.
200. Chen, D.; Ying, W.; Guo, Y.; Ying, Y.; Peng, X., Enhanced gas separation through Nanoconfined ionic liquid in laminated MoS2 membrane. *ACS applied materials & interfaces* **2017,** *9* (50), 44251-44257.
201. Moghadam, F.; Park, H. B., Two-dimensional materials: an emerging platform for gas separation membranes. *Current opinion in chemical engineering* **2018,** *20*, 28-38.
202. Cheng, W.; Lu, X.; Kaneda, M.; Zhang, W.; Bernstein, R.; Ma, J.; Elimelech, M., Graphene Oxide-Functionalized Membranes: The Importance of Nanosheet Surface Exposure for Biofouling Resistance. *Environmental Science & Technology* **2019,** *54* (1), 517-526.
203. Hong, S.; Ming, F.; Shi, Y.; Li, R.; Kim, I. S.; Tang, C. Y.; Alshareef, H. N.; Wang, P., Two-Dimensional Ti3C2T x MXene Membranes as Nanofluidic Osmotic Power Generators. *ACS nano* **2019,** *13* (8), 8917-8925.
204. Koltonow, A. R.; Huang, J., Two-dimensional nanofluidics. *Science* **2016,** *351* (6280), 1395.

205. Wang, S.; Wu, Y.; Zhang, N.; He, G.; Xin, Q.; Wu, X.; Wu, H.; Cao, X.; Guiver, M. D.; Jiang, Z., A highly permeable graphene oxide membrane with fast and selective transport nanochannels for efficient carbon capture. *Energy & Environmental Science* **2016,** *9* (10), 3107-3112.
206. Caffrey, N. M., Effect of mixed surface terminations on the structural and electrochemical properties of two-dimensional Ti3C2T2 and V2CT2 MXenes multilayers. *Nanoscale* **2018,** *10* (28), 13520-13530.
207. Ding, L.; Wei, Y.; Wang, Y.; Chen, H.; Caro, J.; Wang, H., A two-dimensional lamellar membrane: MXene nanosheet stacks. *Angewandte Chemie* **2017,** *129* (7), 1851-1855.
208. Li, L.; Zhang, T.; Duan, Y.; Wei, Y.; Dong, C.; Ding, L.; Qiao, Z.; Wang, H., Selective gas diffusion in two-dimensional MXene lamellar membranes: insights from molecular dynamics simulations. *Journal of Materials Chemistry A* **2018,** *6* (25), 11734-11742.
209. Karahan, H. E.; Goh, K.; Zhang, C.; Yang, E.; Yıldırım, C.; Chuah, C. Y.; Ahunbay, M. G.; Lee, J.; Tantekin-Ersolmaz, Ş. B.; Chen, Y.; Bae, T.-H., MXene Materials for Designing Advanced Separation Membranes. *Advanced Materials* **2020,** *32* (29), 1906697.
210. Ding, L.; Wei, Y.; Li, L.; Zhang, T.; Wang, H.; Xue, J.; Ding, L.-X.; Wang, S.; Caro, J.; Gogotsi, Y., MXene molecular sieving membranes for highly efficient gas separation. *Nature Communications* **2018,** *9* (1), 155.
211. Tavasoli, E.; Sadeghi, M.; Riazi, H.; Shamsabadi, A. A.; Soroush, M., Gas Separation Polysulfone Membranes Modified by Cadmium-based Nanoparticles. *Fibers and Polymers* **2018,** *19* (10), 2049-2055.
212. Shamsabadi, A. A.; Riazi, H.; Soroush, M., Mixed Matrix Membranes for CO2 Separations: Membrane Preparation, Properties, and Separation Performance Evaluation. In *Current Trends and Future Developments on (Bio-) Membranes*, Elsevier: 2018; pp 103-153.
213. Shamsabadi, A. A.; Isfahani, A. P.; Salestan, S. K.; Rahimpour, A.; Ghalei, B.; Sivaniah, E.; Soroush, M., Pushing Rubbery Polymer Membranes To Be Economic for CO2 Separation: Embedment with Ti3C2Tx MXene Nanosheets. *ACS Applied Materials & Interfaces* **2020,** *12* (3), 3984-3992.
214. Shen, J.; Liu, G.; Ji, Y.; Liu, Q.; Cheng, L.; Guan, K.; Zhang, M.; Liu, G.; Xiong, J.; Yang, J.; Jin, W., 2D MXene Nanofilms with Tunable Gas Transport Channels. *Advanced Functional Materials* **2018,** *28* (31), 1801511.
215. Ghanbari, M.; Emadzadeh, D.; Lau, W.; Riazi, H.; Almasi, D.; Ismail, A., Minimizing structural parameter of thin film composite forward osmosis membranes using polysulfone/halloysite nanotubes as membrane substrates. *Desalination* **2016,** *377*, 152-162.
216. Bidsorkhi, H. C.; Riazi, H.; Emadzadeh, D.; Ghanbari, M.; Matsuura, T.; Lau, W.; Ismail, A., Preparation and characterization of a novel highly hydrophilic and antifouling polysulfone/nanoporous TiO2 nanocomposite membrane. *Nanotechnology* **2016,** *27* (41), 415706.
217. Han, R.; Ma, X.; Xie, Y.; Teng, D.; Zhang, S., Preparation of a new 2D MXene/PES composite membrane with excellent hydrophilicity and high flux. *Rsc Advances* **2017,** *7* (89), 56204-56210.
218. Tang, Y.; Dubbeldam, D.; Tanase, S., Water–Ethanol and Methanol–Ethanol Separations Using in Situ Confined Polymer Chains in a Metal–Organic Framework. *ACS applied materials & interfaces* **2019,** *11* (44), 41383-41393.
219. Shin, Y.; Taufique, M. F. N.; Devanathan, R.; Cutsforth, E. C.; Lee, J.; Liu, W.; Fifield, L. S.; Gotthold, D. W., Highly selective supported Graphene oxide Membranes for Water-ethanol separation. *Scientific reports* **2019,** *9* (1), 1-11.
220. Wu, X.; Hao, L.; Zhang, J.; Zhang, X.; Wang, J.; Liu, J., Polymer-Ti3C2Tx composite membranes to overcome the trade-off in solvent resistant nanofiltration for alcohol-based system. *Journal of membrane science* **2016,** *515*, 175-188.
221. Zha, X.-J.; Zhao, X.; Pu, J.-H.; Tang, L.-S.; Ke, K.; Bao, R.-Y.; Bai, L.; Liu, Z.-Y.; Yang, M.-B.; Yang, W., Flexible anti-biofouling MXene/cellulose fibrous membrane for sustainable solar-driven water purification. *ACS applied materials & interfaces* **2019,** *11* (40), 36589-36597.

222. Gund, G. S.; Park, J. H.; Harpalsinh, R.; Kota, M.; Shin, J. H.; Kim, T.-i.; Gogotsi, Y.; Park, H. S., MXene/polymer hybrid materials for flexible AC-filtering electrochemical capacitors. *Joule* **2019,** *3* (1), 164-176.
223. Qin, L.; Tao, Q.; Liu, X.; Fahlman, M.; Halim, J.; Persson, P. O.; Rosen, J.; Zhang, F., Polymer-MXene composite films formed by MXene-facilitated electrochemical polymerization for flexible solid-state microsupercapacitors. *Nano Energy* **2019,** *60*, 734-742.
224. Zhu, M.; Huang, Y.; Deng, Q.; Zhou, J.; Pei, Z.; Xue, Q.; Huang, Y.; Wang, Z.; Li, H.; Huang, Q., Highly flexible, freestanding supercapacitor electrode with enhanced performance obtained by hybridizing polypyrrole chains with MXene. *Advanced Energy Materials* **2016,** *6* (21), 1600969.
225. Zhou, Y.; Zou, Y.; Peng, Z.; Yu, C.; Zhong, W., Arbitrary deformable and high-strength electroactive polymer/MXene anti-exfoliative composite films assembled into high performance, flexible all-solid-state supercapacitors. *Nanoscale* **2020,** *12* (40), 20797-20810.
226. Li, K.; Wang, X.; Li, S.; Urbankowski, P.; Li, J.; Xu, Y.; Gogotsi, Y., An ultrafast conducting polymer@ MXene positive electrode with high volumetric capacitance for advanced asymmetric supercapacitors. *Small* **2020,** *16* (4), 1906851.
227. Hu, M.; Zhang, H.; Hu, T.; Fan, B.; Wang, X.; Li, Z., Emerging 2D MXenes for supercapacitors: status, challenges and prospects. *Chemical Society Reviews* **2020,** *49* (18), 6666-6693.
228. Zhao, Y.; Zhao, J., Functional group-dependent anchoring effect of titanium carbide-based MXenes for lithium-sulfur batteries: A computational study. *Applied Surface Science* **2017,** *412*, 591-598.
229. Huang, H.; He, J.; Wang, Z.; Zhang, H.; Jin, L.; Chen, N.; Xie, Y.; Chu, X.; Gu, B.; Deng, W., Scalable, and low-cost treating-cutting-coating manufacture platform for MXene-based on-chip micro-supercapacitors. *Nano Energy* **2020,** *69*, 104431.
230. Yang, J.; Bao, W.; Jaumaux, P.; Zhang, S.; Wang, C.; Wang, G., MXene-Based Composites: Synthesis and Applications in Rechargeable Batteries and Supercapacitors. *Advanced Materials Interfaces* **2019,** *6* (8), 1802004.
231. Tu, S.; Jiang, Q.; Zhang, X.; Alshareef, H. N., Large dielectric constant enhancement in MXene percolative polymer composites. *ACS nano* **2018,** *12* (4), 3369-3377.
232. Umrao, S.; Tabassian, R.; Kim, J.; Zhou, Q.; Nam, S.; Oh, I.-K., MXene artificial muscles based on ionically cross-linked Ti3C2Tx electrode for kinetic soft robotics. *Science Robotics* **2019,** *4* (33), eaaw7797.
233. Liang, J.; Xu, Y.; Huang, Y.; Zhang, L.; Wang, Y.; Ma, Y.; Li, F.; Guo, T.; Chen, Y., Infrared-triggered actuators from graphene-based nanocomposites. *The Journal of Physical Chemistry C* **2009,** *113* (22), 9921-9927.
234. Liu, S.; Liu, Y.; Cebeci, H.; De Villoria, R. G.; Lin, J. H.; Wardle, B. L.; Zhang, Q., High electromechanical response of ionic polymer actuators with controlled-morphology aligned carbon nanotube/nafion nanocomposite electrodes. *Advanced functional materials* **2010,** *20* (19), 3266-3271.
235. Soleymaniha, M.; Shahbazi, M. A.; Rafieerad, A. R.; Maleki, A.; Amiri, A., Promoting role of MXene nanosheets in biomedical sciences: Therapeutic and biosensing innovations. *Advanced healthcare materials* **2019,** *8* (1), 1801137.
236. George, S. M.; Kandasubramanian, B., Advancements in MXene-Polymer composites for various biomedical applications. *Ceramics International* **2019**.
237. Golabdar, A.; Adelnia, H.; Moshtzan, N.; Nasrollah Gavgani, J.; Izadi-Vasafi, H., Anti-bacterial poly (vinyl alcohol) nanocomposite hydrogels reinforced with in situ synthesized silver nanoparticles. *Polymer Composites* **2019,** *40* (4), 1322-1328.
238. Tao, W.; Kong, N.; Ji, X.; Zhang, Y.; Sharma, A.; Ouyang, J.; Qi, B.; Wang, J.; Xie, N.; Kang, C., Emerging two-dimensional monoelemental materials (Xenes) for biomedical applications. *Chemical Society Reviews* **2019,** *48* (11), 2891-2912.

239. Rohaizad, N.; Mayorga-Martinez, C. C.; Fojtů, M.; Latiff, N. M.; Pumera, M., Two-dimensional materials in biomedical, biosensing and sensing applications. *Chemical Society Reviews* **2020**.
240. Chen, S.; Xing, C.; Huang, D.; Zhou, C.; Ding, B.; Guo, Z.; Peng, Z.; Wang, D.; Zhu, X.; Liu, S., Eradication of tumor growth by delivering novel photothermal selenium-coated tellurium nanoheterojunctions. *Science Advances* **2020,** *6* (15), eaay6825.
241. Tao, W.; Ji, X.; Zhu, X.; Li, L.; Wang, J.; Zhang, Y.; Saw, P. E.; Li, W.; Kong, N.; Islam, M. A., Two-dimensional antimonene-based photonic nanomedicine for cancer theranostics. *Advanced materials* **2018,** *30* (38), 1802061.
242. Rasool, K.; Mahmoud, K. A.; Johnson, D. J.; Helal, M.; Berdiyorov, G. R.; Gogotsi, Y., Efficient antibacterial membrane based on two-dimensional Ti 3 C 2 T x (MXene) nanosheets. *Scientific reports* **2017,** *7* (1), 1-11.
243. Zong, L.; Wu, H.; Lin, H.; Chen, Y., A polyoxometalate-functionalized two-dimensional titanium carbide composite MXene for effective cancer theranostics. *Nano Research* **2018,** *11* (8), 4149-4168.
244. Soroush, M.; Masooleh, L. S.; Seider, W. D.; Oktem, U.; Arbogast, J. E., Model-predictive safety optimal actions to detect and handle process operation hazards. *AIChE Journal* **2020,** *66* (6), e16932.
245. Lakhe, P.; Prehn, E. M.; Habib, T.; Lutkenhaus, J. L.; Radovic, M.; Mannan, M. S.; Green, M. J., Process Safety Analysis for Ti3C2T x MXene Synthesis and Processing. *Industrial & Engineering Chemistry Research* **2019,** *58* (4), 1570-1579.
246. Smagowska, B.; Pawlaczyk-Łuszczyńska, M., Effects of ultrasonic noise on the human body—a bibliographic review. *International Journal of Occupational Safety and Ergonomics* **2013,** *19* (2), 195-202.
247. Fadeel, B.; Bussy, C.; Merino, S.; Vázquez, E.; Flahaut, E.; Mouchet, F.; Evariste, L.; Gauthier, L.; Koivisto, A. J.; Vogel, U., Safety assessment of graphene-based materials: focus on human health and the environment. *ACS nano* **2018,** *12* (11), 10582-10620.